National Library of Canada
Bibliothèque nationale du Canada

Canadian Theses Service
Services des thèses canadiennes

Ottawa, Canada
K1A 0N4

CANADIAN THESES

THÈSES CANADIENNES

NOTICE

The quality of this microfiche is heavily dependent upon the quality of the original thesis submitted for microfilming. Every effort has been made to ensure the highest quality of reproduction possible.

If pages are missing, contact the university which granted the degree.

Some pages may have indistinct print especially if the original pages were typed with a poor typewriter ribbon or if the university sent us an inferior photocopy.

Previously copyrighted materials (journal articles, published tests, etc.) are not filmed.

Reproduction in full or in part of this film is governed by the Canadian Copyright Act, R.S.C. 1970, c. C-30. Please read the authorization forms which accompany this thesis.

AVIS

La qualité de cette microfiche dépend grandement de la qualité de la thèse soumise au microfilmage. Nous avons tout fait pour assurer une qualité supérieure de reproduction.

S'il manque des pages, veuillez communiquer avec l'université qui a conféré le grade.

La qualité d'impression de certaines pages peut laisser à désirer, surtout si les pages originales ont été dactylographiées à l'aide d'un ruban usé ou si l'université nous a fait parvenir une photocopie de qualité inférieure.

Les documents qui font déjà l'objet d'un droit d'auteur (articles de revue, examens publiés, etc.) ne sont pas microfilmés.

La reproduction, même partielle, de ce microfilm est soumise à la Loi canadienne sur le droit d'auteur, SRC 1970, c. C-30. Veuillez prendre connaissance des formules d'autorisation qui accompagnent cette thèse.

THIS DISSERTATION
HAS BEEN MICROFILMED
EXACTLY AS RECEIVED

LA THÈSE A ÉTÉ
MICROFILMÉE TELLE QUE
NOUS L'AVONS REÇUE

Canada

National Library of Canada
Bibliothèque nationale du Canada

Canadian Theses Division
Division des thèses canadiennes

Ottawa, Canada
K1A 0N4

0-315-24901-3

PERMISSION TO MICROFILM — AUTORISATION DE MICROFILMER

• Please print or type — Écrire en lettres moulées ou dactylographier

Full Name of Author — Nom complet de l'auteur

WOOD PHILIP

Date of Birth — Date de naissance	Country of Birth — Lieu de naissance
23rd MAY 1959	HONG KONG.

Permanent Address — Résidence fixe

246, TUNG CHOI STREET.
3rd FLOOR, MONG KOK
KOWLOON, HONG KONG

Title of Thesis — Titre de la thèse

A FAULT LOCATION ALGORITHM FOR POWER TRANSMISSION LINES USING CURVE FITTING

University — Université

THE UNIVERSITY OF ALBERTA

Degree for which thesis was presented — Grade pour lequel cette thèse fut présentée

M. Sc.

Year this degree conferred — Année d'obtention de ce grade	Name of Supervisor — Nom du directeur de thèse
1984	PROF. K. E. BOLLINGER

Permission is hereby granted to the NATIONAL LIBRARY OF CANADA to microfilm this thesis and to lend or sell copies of the film.

The author reserves other publication rights, and neither the thesis nor extensive extracts from it may be printed or otherwise reproduced without the author's written permission.

L'autorisation est, par la présente, accordée à la BIBLIOTHÈQUE NATIONALE DU CANADA de microfilmer cette thèse et de prêter ou de vendre des exemplaires du film.

L'auteur se réserve les autres droits de publication; ni la thèse ni de longs extraits de celle-ci ne doivent être imprimés ou autrement reproduits sans l'autorisation écrite de l'auteur.

Date	Signature
9th Oct. 1984	Philip Wood

NL-91 (4/77)

THE UNIVERSITY OF ALBERTA

A FAULT LOCATION ALGORITHM FOR POWER TRANSMISSION LINES USING CURVE FITTING

by

© PHILIP WOOD

A THESIS

SUBMITTED TO THE FACULTY OF GRADUATE STUDIES AND RESEARCH

IN PARTIAL FULFILMENT OF THE REQUIREMENTS FOR THE DEGREE

OF MASTER OF SCIENCE

DEPARTMENT OF ELECTRICAL ENGINEERING

EDMONTON, ALBERTA

FALL 1984

THE UNIVERSITY OF ALBERTA

RELEASE FORM

NAME OF AUTHOR PHILIP WOOD

TITLE OF THESIS A FAULT LOCATION ALGORITHM FOR POWER TRANSMISSION LINES USING CURVE FITTING

DEGREE FOR WHICH THESIS WAS PRESENTED MASTER OF SCIENCE

YEAR THIS DEGREE GRANTED FALL 1984

Permission is hereby granted to THE UNIVERSITY OF ALBERTA LIBRARY to reproduce single copies of this thesis and to lend or sell such copies for private, scholarly or scientific research purposes only.

The author reserves other publication rights, and neither the thesis nor extensive extracts from it may be printed or otherwise reproduced without the author's written permission.

(SIGNED) ..Philip Wood.....

PERMANENT ADDRESS:

..246, Tung Choi Street.....
..3rd Floor, Kowloon.....
...Hong Kong.....

DATED ....9th Oct.....1984

THE UNIVERSITY OF ALBERTA

FACULTY OF GRADUATE STUDIES AND RESEARCH

The undersigned certify that they have read, and recommend to the Faculty of Graduate Studies and Research, for acceptance, a thesis entitled A FAULT LOCATION ALGORITHM FOR POWER TRANSMISSION LINES USING CURVE FITTING submitted by PHILIP WOOD in partial fulfilment of the requirements for the degree of MASTER OF SCIENCE.

.....

Supervisor

.....

.....

Date....Oct. 9/81.....

To my beloved family

Abstract

High voltage power transmission lines are important elements in an electric power system. Unavoidable accidents often occur resulting in faults on these transmission lines. During the past few years, a considerable amount of studies and many research projects have been undertaken to develop a digital transmission line fault location algorithm.

A method involving curve fitting techniques for locating transmission line faults has been studied and tested in this project. The method is based on the least error squares approach which utilizes information of the first few cycles of post-fault data. The effects on the accuracy of the proposed fault location, due to the presence of line shunt reactance and fault resistance, have been investigated. Also, different order digital filters are employed in the testing to study the delay associated with each filter.

A digital computer program has been successfully developed and tested on locating faults of digitally simulated transmission lines. A fault detection routine is incorporated into the program to initialize the fault locating routine.

Acknowlegments

The author would like to express his greatest gratitude to Professor Ken. E. Bollinger, who supervised this work, for his valuable assistance and guidance throughout the project. His encouragement was essential for the completion of the work. He would also like to thank Mr. A. Huizinga for his support during the entire research work. Thanks are also given to Mr. D. Lee for proof-reading the thesis and Mr. V. Lai for the preparation of the figures. The author also like to express his sincere thanks to Dr. M. A. Abdelhalim and Mr. S. A. Soliman for their valuable advice and discussions.

Finally, the author would like to thank both the University of Alberta and his supervisor for their financial support throughout the course of this work.

Table of Contents

Chapter		Page
1.	Introduction	1
2.	A review of previously developed fault location algorithms	8
2.1	Introduction	8
2.2	Algorithms based on wave or telegraph equations	8
2.3	Newton-Raphson based algorithm	10
2.4	Reference model based algorithm	11
2.5	Algorithms employing the calculation of complex impedance	12
2.6	Conclusion	15
3.	Fault Location Algorithm	16
3.1	Introduction	16
3.2	Least error squares curve fitting technique and the pseudoinverse of a matrix	16
3.3	Development of the equation of condition for the fault location algorithm	25
3.4	Calculation of complex impedance and determination of fault distance	33
3.5	Special features in using least error squares curve fitting approach in fault location	36
3.6	Conclusion	37
4.	Testing the algorithm using simulated transmission lines	38
4.1	Introduction	38
4.2	Modelling of test system	38
4.2.1	Single-phase power system	39
4.2.2	Three-phase power system	43
4.3	Design of low-pass digital filters	49

4.4 Fault detection 55
4.5 Fault identification 56
4.6 Choice of data for locating fault 57
4.7 Discussion 59
5. Computer Implementation 61
5.1 Introduction 61
5.2 Program "model.c" 63
5.2.1 Transmission line model routine 63
5.2.2 Fault detection routine 64
5.2.3 Digital filter routine 68
5.3 Program "psedo.c" 68
5.4 Program "loc.c" 70
5.5 Conclusion 72
6. Performance of fault location algorithm 76
6.1 Introduction 76
6.2 Single-phase test model 78
6.3 Three-phase test model 85
6.4 Conclusion and General Discussion 101
7. Summary and Conclusion 104
References 107
Appendix A. Power System Parameters 112
Appendix B. Synthesizing Digital Filters 114

List of Tables

Table Page

3.1 Pseudoinverse of matrix A.....32

List of Figures

Figure		Page
1.1	On-line fault locator	5
4.1	Single-phase test system (pre-fault)	40
4.2	Equivalent circuit of the single-phase test system (pre-fault)	40
4.3	Single-phase test system (post-fault)	42
4.4	Equivalent circuit of the single-phase post-fault test system	42
4.5	One-line diagram of the three-phase system (pre-fault)	45
4.6	Single-phase equivalent circuit of the three-phase system (pre-fault)	45
4.7	Single-phase equivalent circuit of the test system (post-fault)	47
4.8	Single-phase equivalent circuit of the test system with fault resistance (post-fault)	47
4.9	Amplitude characteristic of an ideal low-pass digital filter	50
4.10	Unity step response of the three low-pass digital filters	54
5.1	Block diagram showing relationship between developed programs	62
5.2	General flow chart used to calculate both pre-fault and post-fault quantities	65
5.3	General flow chart of fault detection routine	66
5.4	General flow chart of low-pass filter routine	69
5.5	General flow chart of the program to calculate pseudoinverse matrix A^+	71
5.6	General flow chart of program "loc.c"	73
6.1	Time response of the pre-filtered and post-filtered current signal using 4th order filter - series model	79

6.2 Time response of the pre-filtered and post-filtered voltage signal using 4th order filter - series model.....79

6.3 Time response of the pre-filtered and post-filtered current signal using 8th order filter - series model.....80

6.4 Time response of the pre-filtered and post-filtered voltage signal using 8th order filter - series model.....80

6.5 Time response of the pre-filtered and post-filtered current signal using 10th order filter - series model.....81

6.6 Time response of the pre-filtered and post-filtered voltage signal using 10th order filter - series model.....81

6.7 Plot of fault location versus delay - series model and 4th order filter.....83

6.8 Plot of calculated impedances - series model and 4th order filter.....83

6.9 Plot of fault location versus delay - series model and 8th order filter.....84

6.10 Plot of calculated impedances - series model and 8th order filter.....84

6.11 Plot of fault location versus delay - series model and 10th order filter.....86

6.12 Plot of calculated impedances - series model and 10th order filter.....86

6.13 Time response of the pre-filtered and post-filtered current signal using 8th order filter - one pi faulted model.....88

6.14 Time response of the pre-filtered and post-filtered voltage signal using 8th order filter - one pi faulted model.....88

6.15 Time response of the pre-filtered and post-filtered current signal using 8th order filter - two pi faulted model.....89

6.16 Time response of the pre-filtered and post-filtered voltage signal using 8th order filter - two pi faulted model.....89

6.17 Time response of the pre-filtered and post-filtered current signal using 8th order filter - three pi faulted model.....90

6.18 Time response of the pre-filtered and post-filtered voltage signal using 8th order filter - three pi faulted model.....90

6.19 Plot of fault location versus delay - one pi faulted model and 4th order filter.....91

6.20 Plot of calculated impedances - one pi faulted model and 4th order filter.....91

6.21 Plot of fault location versus delay - one pi faulted model and 8th order filter.....92

6.22 Plot of calculated impedances - one pi faulted model and 8th order filter.....92

6.23 Plot of fault location versus delay - one pi faulted model and 10th order filter.....93

6.24 Plot of calculated impedances - one pi faulted model and 10th order filter.....93

6.25 Plot of fault location versus delay - two pi faulted model and 4th order filter.....95

6.26 Plot of calculated impedances - two pi faulted model and 4th order filter.....95

6.27 Plot of fault location versus delay - two pi faulted model and 8th order filter.....96

6.28 Plot of calculated impedances - two pi faulted model and 8th order filter.....96

6.29 Plot of fault location versus delay - two pi faulted model and 10th order filter.....97

6.30 Plot of calculated impedances - two pi faulted model and 10th order filter.....97

6.31 Plot of fault location versus delay - three pi faulted model and 4th order filter.....98

6.32 Plot of calculated impedances - three pi faulted model and 4th order filter.....98

6.33 Plot of fault location versus delay - three pi faulted model and 8th order filter.....99

6.34 Plot of calculated impedances - three pi faulted model and 8th order filter.....99

6.35 Plot of fault location versus delay - three pi faulted model and 10th order filter.....100

6.36 Plot of calculated impedances - three pi faulted model and 10th order filter.....100

6.37 Plots of fault location versus delay in the presence of different fault resistance - one pi faulted model and 8th order filter.....102

List of Abbreviations and Symbols

Abbreviations

Re	- real part of a complex quantity
KV	- kilovolt
MVA	- megavoltampere
fc	- cutoff frequency
dB	- decibel
s	- second
f1	- transition frequency
fs	- sampling frequency
MW	- megawatt
pf	- power factor

Symbols

R	- resistance in ohm
X	- reactance in ohm
Z	- impedance in ohm
r	- resistance of transmission line in ohm
l	- inductance of transmission line in Henry
c	- capacitance of transmission line in Farad
v	- instantaneous voltage
i	- instantaneous current
V	- voltage vector or phasor
I	- current vector or phasor
t	- time in second
y	- length in mile

A^+	- pseudoinverse of matrix A
A^{-1}	- inverse of matrix A
e	- error-symbol
Σ	- summation symbol
∂	- partial differentiation symbol
τ	- time constant
ω	- fundamental angular frequency in radian/second
α	- phase angle in radian
!	- factorial symbol
$\surd$	- square root

Superscripts

T	- transpose of matrix
i	- current quantity
v	- voltage quantity
0	- pre-fault quantity
f	- post-fault quantity

Subscripts

k	- kth component
p	- peak quantity
L	- line quantity
f	- fault quantity
t	- quantity corresponds to total number
l	- line parameter corresponds to length l

an - phase a to neutral quantity

bn - phase b to neutral quantity

cn - phase c to neutral quantity

CHAPTER I

Introduction

A modern electric power system is a complex interconnection of generators, transformers, transmission lines, static and rotating loads, protective relays, circuit breakers and various control elements. Power can be transmitted either by direct current, single-phase or poly-phase alternating current. In practice, three-phase sinusoidal alternating current has been adopted as the method of transmission due to its efficiency in generating power and in its transfer capacities.

Electrical energy is a fundamental essence to the human society. A continuous supply of electricity, irrespective of environmental conditions, is important to our daily lives. During the occurrence of faults, power utilities must be able to isolate the faulty section from the rest of the system to ensure the continuity of electric power supply. At the same time, a large current could result and flow through the network, which would cause severe damage to the system components. Damage to equipment and disruption of power could be minimised by the rapid disconnection of the faulty section by means of circuit breakers and protective relays. The type of relay or relays used in the protective scheme is mainly determined by the nature of the protected equipment.

Transmission lines form a major part of a power system. They are exposed to different environmental conditions and are spread over a large geographical area. As a result, lines experience more faults than other system components, and so a line protection scheme is essential to any electric power network. The types of line faults are mainly classified as short circuit and open circuit. Short circuit is mainly due to insulation failure, human error, lightning, wind damage and many others[1]. Open circuit may occur for a variety of reasons, including broken conductors and maloperation of circuit breakers. The detection, location and removal of line faults in the shortest time possible is of the utmost importance in the design of line protection.

The fast and accurate fault location of short-circuited transmission lines is always a prime concern of every power utility from economical and safety considerations. A good protection scheme will enhance the availability of a power system.

A comprehensive survey of various fault locating methods has been given by Stringfield, Marihart and Stevens[2]. In this reference, the authors have broadly classified the methods as travelling-visual-inspection type and measurement-at-a-fixed-reference-point type. The latter type is far superior to the former as less time and labor are required to locate a fault. Also, environmental conditions may affect the speed in locating the fault for

the former type. However, an example of the latter such as pulse-reflection type, needs a large amount of expensive hardware or well qualified operators to interpret fault oscillographic records.

Recent developments in digital technology have resulted in a decrease in cost and an increase in processing speed. It facilitates the introduction of on-line protection of electric power systems on a substation level. The use of micro/minicomputers in fault location offers greater flexibility and accuracy. In the past few years, new short-circuit fault location algorithms based on modern techniques have been developed. These methods employ measured electrical quantities at one or more points on the transmission line. Some of the methods make use of distributed-parameter line models, and the fault distance is determined by analysing the current and voltage travelling waves[3][4]. The accuracy of such an approach is affected by the system parameters and network configurations. The lumped-parameter model algorithm is often used in cases where the complex impedance between the faulty point and the measuring site is calculated. The location can thus be obtained by assuming that the line impedance is proportional to line length. This idea is popular in the field of digital distance relaying. However, the drawback of the lumped-parameter approach is that fault resistance and shunt capacitance of long transmission lines introduce error in the fault distance measurement. Dynamic parameter

estimation[5] has also been employed in algorithms for locating faults on power transmission lines. Using this algorithm, a set of non-linear equation is formed and solved through an iterative approach. In this approach, the configuration of the sequence reference model is determined by the type of fault present.

The block diagram shown in Figure 1.1 outlines the major components associated with an on-line fault locator. The current and potential transformers provide low level signals to the low-pass analog filter. These signals correspond to the transmission line currents and voltages. The low-pass filter prevents high harmonics and noise present in the signals from affecting the fault location algorithm. Alternatively, the analog low-pass filter can be replaced by a digital one which is incorporated into the fault location algorithm. This decreases the amount of hardware required by the fault locator. The analog to digital converter produces the corresponding digital information. Fault detection and identification routines can be incorporated into the fault distance measurement routine to increase the capability of the fault locator. The output of the locator provides information for the protective relaying system and for off-line fault analysis.

The object of this thesis is to implement and test an existing fault location algorithm based on current and voltage measurements at the sending end of a power

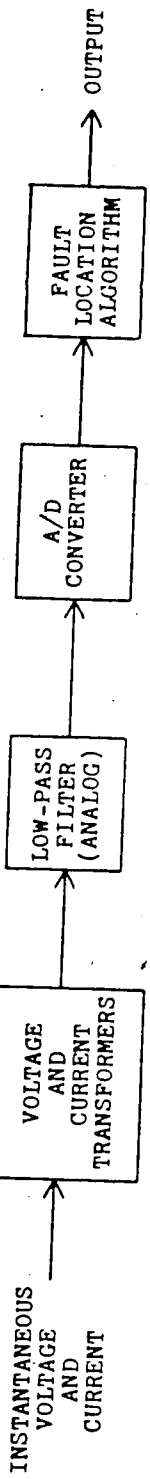

Figure 1.1 On-line fault locator.

transmission line. No special line coupling is required between the two ends of the line. The method employs least error squares curve fitting technique proposed by Sachdev and Baribeau[6]. The fault distance is determined by assuming that the line reactance is proportional to line length between the measuring and the fault points[7][8].

During the last few years, extensive research has been undertaken in the development of fault location algorithms using measurements of electrical quantities at some observation points. Chapter 2 discusses some of the algorithms proposed in the past.

Chapter 3 presents the algorithm suggested in Reference 6. The algorithm determines the fundamental current and voltage phasors of the post-fault transient waveforms. The waveforms include fundamental, third harmonic and decaying dc components. A complex impedance is calculated from the extracted fundamental phasors and fault distance is obtained based on the reactive component of the calculated impedance.

Digital simulations of transmission lines for testing the proposed algorithm are presented in Chapter 4. The models provide both pre-fault and post-fault information to the fault location algorithm in an off-line mode. The development of digital filters for suppressing unwanted high harmonics is also briefly discussed in this chapter. The cutoff frequencies for the filters are mainly determined by the equation of condition derived in Chapter 3.

Chapter 5 describes the implementation of the proposed algorithm using a PDP-11 microcomputer present in the Power Research Laboratory of the University of Alberta. The fault location algorithm is tested using transmission line models and digital filters which are presented in Chapter 4.

The performance of the proposed fault location algorithm is presented in Chapter 6. The time delay and accuracy of the algorithm are investigated using differennt order filters. The errors contributed by the presence of fault resistance and line shunt capacitance are discussed. Certain conclusions pertaining to the validity of the proposed fault location algorithm are put forward in the final chapter.

CHAPTER II

A review of previously developed fault location algorithms

2.1 Introduction

New digital fault location algorithms for power transmission lines have been developed in the past. Most of the algorithms are based on measured electrical quantities at some observation point on the line during the first few cycles of the fault occurrence. This approach can be subdivided into the following four major categories:

(i) Algorithms based on wave or telegraph equations.

(ii) Newton-Raphson based algorithms.

(iii) Reference model based algorithm.

(iv) Algorithms employing the calculation of complex impedance.

This chapter reviews some of the previously published fault distance measurement methods, which belong to one of the above four categories. The last category is often used in transmission line distance protection since the fault impedance loci can be determined based on electrical measurements at the relay location.

2.2 Algorithms based on wave or telegraph equations

The use of travelling wave phenomena for fault location has been presented in some previously published literature. With this approach, the fault location is deduced from the

post-fault current and voltage travelling waves. The waves are modelled either by the wave or the telegraph equations.

Kohlas[3] presented an accurate fault location algorithm for power transmission lines. In his approach, high frequency transients, due to the occurrence of short circuit fault, are incorporated into the distributed parameter mathematical model. The measured data from one end of the line enables the instantaneous profile of the line voltage to be obtained using the wave or telegraph equation. The fault location is determined from where either the voltage profile vanishes or its magnitude reaches a minimum. A major drawback of this approach is that the effect of a non-zero fault resistance is neglected. In addition, the complexity and accuracy of the solution to the travelling wave equation largely depends on the overall system configuration.

Another algorithm based on using wave equations, for line models, was suggested by Vitins[4]. In this method, the fault was located by determining the time delay between two quantities at the measurement site. These two measured quantities are associated with the travelling waves. The presence of the fault resistance has been taken into account in the development of the algorithm. However, a lossless transmission line has been assumed and computational effort is rather large in analysing the wave phenomenon.

2.3 Newton-Raphson based algorithm

A fault location problem can be formulated into a set of nonlinear equations which is solved using the Newton-Raphson technique. The Newton-Raphson method is a well known iterative method for solving nonlinear systems of equations and it has been successfully applied to many power system problems[9].

Westlin and Bubenko[10] proposed an iterative approach to fault location for power transmission lines based on sampled voltage and current at the sending end. A set of nonlinear equations is formulated by using a suitable Thevenin equivalent model for the receiving end of the line. Each type of fault results in a different set of equations. The fault distance, receiving end current and fault resistance can be determined from the solution of equations using the Newton-Raphson method. A low-pass filter is required to eliminate any high frequency component present in the post-fault transient waveforms. The algorithm is readily applied to situations where the fault resistance cannot be neglected. The disadvantage of this approach is that the Thévenin equivalent circuit at the receiving end of the line must be known prior to the calculation of the fault distance. Also, the iterative process is time consuming and hence extensive computational time is needed to locate the fault accurately.

A new type of fault location algorithm using the Fourier transformation method was developed by Takagi, Yamakoshi, Baba, Uemura and Sakaguchi[11]. In this approach, nonlinear algebraic equations, which contain the unknown variable corresponding to the fault distance, are formulated by applying the law of superposition to the faulted transmission line. Fourier analysis is used to extract the fundamental frequency components from the measurements available at the sending end of the line. The extracted components are required by the Newton-Raphson iterative program in solving the set of nonlinear equations. No communication channels are required between the two ends of the line, and the algorithm is able to locate the fault accurately without being affected by non-zero fault resistance. The disadvantage of this method is that an unrealistic lossless line is assumed. In addition, the type of source impedance at the sending and receiving end must be carefully studied to ensure the algorithm is applicable.

2.4 Reference model based algorithm

Recently, the fault location problem was treated as a dynamic system parameter estimation problem by Richards and Tan[5][12]. In their approach, a lumped-parameter mathematical model was introduced to compare its response with that of the real physical system during the occurrence of a fault. The fault location, fault resistance and transformer saturation parameters were computed by varying

the model's parameters until an adequate match is obtained between the real system and the model response. The presence of a fault resistance does not affect the accuracy of the algorithm. Due to the asymmetrical nature of a fault, a symmetrical component transformation[9] was used to formulate the reference mathematical model. Different types of fault result in different configurations of the reference model, which increases the complexity of the analysis. Also, the sequence reference model can be very complicated in the presence of simultaneous faults. In addition, a time consuming iterative approach is employed in estimating the parameters and hence the proposed algorithm is not suitable for on-line applications.

2.5 Algorithms employing the calculation of complex impedance

A digital distance relay used for line protection directly calculates complex impedance between some observation point to the faulted point. This concept of impedance calculation is easily applied to the fault location problem since the computed impedance provides the fault distance information.

Mann and Morrison[13] proposed an algorithm such that the peak magnitude of a sinusoid can be determined from its value and its rate of change at any arbitrary sampling instant. The impedance as seen from the measurement site is

equal to the ratio of the voltage and current sinusoidals at the measuring location. The values of the derivatives at any instant are approximated by the difference equations. The effects of the presence of a fault resistance and the decaying dc components alter the accuracy of the calculated impedance. Also, a very small sampling time is required to have an accurate approximation for the difference equations.

A slightly different approach was suggested by Gilcrest, Rockefeller and Urden[14]. In this approach, the authors used the first and second derivates to calculate the peak magnitude of the sinusoidal waveforms instead of using the instantaneous values and the first derivatives as shown in Reference 13. Three sets of sampled current and voltage values are required by the algorithm to determine th complex impedance of the faulted line. The benefit of this approach is that the decaying dc components present in the samples do not affect the accuracy of the algorithm. However, the high frequency components introduce errors into the final result and thus the fault location is subject to inaccuracies.

The truncated Fourier Series approach was also used by Phadka, Hlibka and Ibrahim[15] in digital relaying problems. The algorithm requires samples of current and voltage signals over one-half cycle of the fundamental frequency. The samples are then correlated with reference sine and cosine functions to extract the fundamental components in rectangular form. From these extracted voltage and current

components, the phasor impedance can be determined and hence the fault can be located. The response for this algorithm is fast due to its short data window, nevertheless its accuracy is not as good as could be since it is highly susceptible to high frequency components and decaying dc offsets.

The behaviour of a lumped-parameter transmission line model in which the shunt capacitance is neglected can be described by the following differential equation at any instant of time.

$$v = r \cdot i + l(di/dt) \qquad (2.1)$$

The above equation is valid for both pre-fault and post-fault conditions depending on the choice and combination of sampled voltages and currents (v and i). The numerical solution of equation (2.1) corresponds to the series resistance (r) and series inductance (l) of the given line. Breingan, Gallen and Chen[16] proposed an algorithm in which equation (2.1) is solved at three instances of time to calculate the two unknowns r and l. The advantage of this approach is that the decaying dc component is implicitly taken into account by the series R-L model of the transmission line. The validity of this method is only justified for short transmission lines in which the shunt capacitance can be neglected.

2.6 Conclusion

Previously published literature related to fault location problems has been briefly discussed in this chapter. The algorithm based on complex impedance calculation is readily adapted to the field of digital line protection. This approach is straightforward and requires the least amount of computational effort as compared to other algorithms. It is suitable for practical situations where the fast location of faults are desired. The major drawback of this approach is that its accuracy suffers from the presence of either fault resistance, decaying dc components, shunt capacitance or any combination of these factors.

CHAPTER III

Fault Location Algorithm

3.1 Introduction

Algorithms using different approaches in solving fault location problems have been briefly presented in the last chapter. The suitability and limitation of each algorithm have also been concisely discussed. The choice of a suitable algorithm that compromises between accuracy and speed is a difficult task.

In this chapter, a short-circuit fault location algorithm is presented. The method is based on the least error squares curves fitting technique proposed in Reference 6. This curve fitting technique, together with its relationship to the pseudoinverse of a matrix, is also discussed.

3.2 Least error squares curve fitting technique and the pseudoinverse of a matrix

Assuming a series of values "a" together with their corresponding values "r" are given, it is often required to find a functional relationship between the two variables r and a. Therefore, a set of unknown parameters, which describes the relationship between r and a, has to be calculated. The relationship can be of any function of a, including a straight line, a parabola or a circle. An

equation of condition, which describes the known nature of the relation or the curve to which the data has to be fitted, is formulated. Usually, the equation of condition is written in the form shown in equation (3.1)[6]:

$$r_i = a_{1i}x_1 + a_{2i}x_2 + \ldots + a_{n-1i}x_{n-1} + a_{ni}x_n \qquad (3.1)$$

where, $i = 1, 2, \ldots, n$

$a_{1i}, \ldots, a_{ni}, r_i$ are the known variables

$x_1, \ldots, x_n$ are the unknown parameters

Equation (3.1) consists of n unknowns x_1 to x_n. In general, at least n values of r together with the corresponding values of a are required to solve for the unknown parameters. If n values of r are given, n equations of the type (3.1) are obtained and they are shown as below:

$$\begin{aligned}
r_1 &= a_{11}x_1 + a_{12}x_2 + \ldots + a_{1n-1}x_{n-1} + a_{1n}x_n \\
r_2 &= a_{21}x_1 + a_{22}x_2 + \ldots + a_{2n-1}x_{n-1} + a_{2n}x_n \\
&\vdots \qquad\qquad\qquad\qquad\qquad\qquad \vdots \qquad (3.2) \\
r_{n-1} &= a_{n-11}x_1 + a_{n-12}x_2 + \ldots + a_{n-1n-1}x_{n-1} + a_{n-1n}x_n \\
r_n &= a_{n1}x_1 + a_{n2}x_2 + \ldots + a_{nn-1}x_{n-1} + a_{nn}x_n
\end{aligned}$$

The above n equations can be written in matrix form, thus:

$$\begin{bmatrix} r_1 \\ r_2 \\ \cdot \\ \cdot \\ \cdot \\ r_{n-1} \\ r_n \end{bmatrix} = \begin{bmatrix} a_{11} & a_{12} & \cdots & a_{1n-1} & a_{1n} \\ a_{21} & a_{22} & \cdots & a_{2n-1} & a_{2n} \\ \cdot & & & & \cdot \\ \cdot & & & & \cdot \\ \cdot & & & & \cdot \\ a_{n-11} & a_{n-12} & \cdots & a_{n-1n-1} & a_{n-1n} \\ a_{n1} & a_{n2} & \cdots & a_{nn-1} & a_{nn} \end{bmatrix} \begin{bmatrix} x_1 \\ x_2 \\ \cdot \\ \cdot \\ \cdot \\ x_{n-1} \\ x_n \end{bmatrix} \qquad (3.3)$$

or $$\acute{R} = \acute{A}X \qquad (3.4)$$

where, $\acute{R}$ is a n x 1 column vector

$\acute{A}$ is a n x n square matrix

X is a n x 1 column vector

If matrix $\acute{A}$ is non-singular, its inverse $\acute{A}^{-1}$ exists and the following equation is obtained:

$$(\acute{A})^{-1}\acute{R} = (\acute{A})^{-1}\acute{A}X$$

$$\Rightarrow \quad X = (\acute{A})^{-1}\acute{R} \qquad (3.5)$$

From equation (3.5), the unknown vector X is solved. Hence, the unknown parameters of the equation of condition, which describes the relationship between variables **r** and **a** are completely determined.

In practice, the number of known variables **r** is usually greater than the number of unknowns **x**. Under such circumstances, the number of equations in (3.2) is larger than n and the system of equations is said to be

overdetermined[17]. Equation (3.3) is modified as:

$$\begin{bmatrix} r_1 \\ r_2 \\ \cdot \\ \cdot \\ \cdot \\ r_{m-1} \\ r_m \end{bmatrix} = \begin{bmatrix} a_{11} & a_{12} & \cdots & a_{1n-1} & a_{1n} \\ a_{21} & a_{22} & \cdots & a_{2n-1} & a_{2n} \\ \cdot & & & & \cdot \\ \cdot & & & & \cdot \\ \cdot & & & & \cdot \\ a_{m-11} & a_{m-12} & \cdots & a_{m-1n-1} & a_{m-1n} \\ a_{m1} & a_{m2} & \cdots & a_{mn-1} & a_{mn} \end{bmatrix} \begin{bmatrix} x_1 \\ x_2 \\ \cdot \\ \cdot \\ \cdot \\ x_{n-1} \\ x_n \end{bmatrix}$$

or $$R = AX \qquad (3.6)$$

where, $m > n$

R is a m x 1 column vector

A is a rectangular matrix of order m x n

X is a n x 1 column vector

Equation (3.6) corresponds to an inconsistent system of linear algebraic equations. The inverse of A is not defined since A is not a square matrix. Normally, there is no exact solution for the vector X such that AX = R[17]. The least error squares technique has to be employed in solving the given curve fitting problem.

The following error-square expression is obtained for the i^{th} equation of matrix equation (3.6):

$$e_i^2 = (r_i - a_{i1}x_1 - a_{i2}x_2 - \ldots - a_{in-1}x_{n-1} - a_{in}x_n)^2 \qquad (3.7)$$

where, $i = 1, 2, \ldots, m$.

The sum of all the error squares becomes,

$$\sum_{i=1}^{m} e_i^2 = e_1^2 + e_2^2 + \ldots + e_{m-1}^2 + e_m^2$$

Hence it follows that,

$$\begin{aligned}\sum_{i=1}^{m} e_i^2 = {} & (r_1 - a_{11}x_1 - a_{12}x_2 - \ldots - a_{1n-1}x_{n-1} - a_{1n}x_n)^2 \\ & + (r_2 - a_{21}x_1 - a_{22}x_2 - \ldots - a_{2n-1}x_{n-1} - a_{2n}x_n)^2 \\ & + \ldots\ldots \\ & + (r_{m-1} - a_{m-11}x_1 - a_{m-12}x_2 - \ldots - a_{m-1n-1}x_{n-1} - \\ & a_{m-1n}x_n)^2 \\ & + (r_m - a_{m1}x_1 - a_{m2}x_2 - \ldots - a_{mn-1}x_{n-1} - a_{mn}x_n)^2 \end{aligned} \tag{3.8}$$

where e_i^2 is the error-square associated with the i^{th} equation of (3.6). Differentiating equation (3.8) with respect to x_1 yields the following equation,

$$\begin{aligned}\frac{\partial \sum_{i=1}^{m} e_i^2}{\partial x_1} = {} & 2(r_1 - a_{11}x_1 - a_{12}x_2 - \ldots - a_{1n-1}x_{n-1} - a_{1n}x_n)(-a_{11}) \\ & + 2(r_2 - a_{21}x_1 - a_{22}x_2 - \ldots - a_{2n-1}x_{n-1} - a_{2n}x_n)(-a_{21}) \\ & + \ldots\ldots \\ & + 2(r_{m-1} - a_{m-11}x_1 - a_{m-12}x_2 - \ldots - a_{m-1n-1}x_{n-1} - \\ & a_{m-1n}x_n)(-a_{m-11}) \\ & + 2(r_m - a_{m1}x_1 - a_{m2}x_2 - \ldots - a_{mn-1}x_{n-1} - a_{mn}x_n)(-a_{m1}) \end{aligned} \tag{3.9}$$

Equating equation (3.9) to zero yields,

$$\frac{\partial \sum_{i=1}^{m} e_i^2}{\partial x_1} = 0$$

$$\text{or,}\quad 2(r_1 - a_{11}x_1 - a_{12}x_2 - \ldots - a_{1n-1}x_{n-1} - a_{1n}x_n)(-a_{11})$$
$$+ 2(r_2 - a_{21}x_1 - a_{22}x_2 - \ldots - a_{2n-1}x_{n-1} - a_{2n}x_n)(-a_{21})$$
$$+ \ldots\ldots$$
$$+ 2(r_{m-1} - a_{m-11}x_1 - a_{m-12}x_2 - \ldots - a_{m-1n-1}x_{n-1} -$$
$$a_{m-1n}x_n)(-a_{m-11})$$
$$+ 2(r_m - a_{m1}x_1 - a_{m2}x_2 - \ldots - a_{mn-1}x_{n-1} - a_{mn}x_n)(-a_{m1})$$
$$= 0 \qquad (3.10)$$

Rearranging equation (3.10) gives the following normal equation[6],

$$\sum_{i=1}^{m} r_i a_{i1} = \sum_{i=1}^{m} a_{i1}^2 x_1 + \sum_{i=1}^{m} a_{i1}a_{i2}x_2 + \ldots\ldots$$
$$+ \sum_{i=1}^{m} a_{i1}a_{in-1}x_{n-1} + \sum_{i=1}^{m} a_{i1}a_{in}x_n \qquad (3.11)$$

If equation (3.8) is differentiated with respect to x_2 and the resulting equation equated to zero and the various terms rearranged, a second normal equation is formulated:

$$\sum_{i=1}^{m} r_i a_{i2} = \sum_{i=1}^{m} a_{i2}a_{i1}x_1 + \sum_{i=1}^{m} a_{i2}^2 x_2 + \ldots\ldots$$
$$+ \sum_{i=1}^{m} a_{i2}a_{in-1}x_{n-1} + \sum_{i=1}^{m} a_{i2}a_{in}x_n \qquad (3.12)$$

The above procedures are repeated for x_3 to x_n and thus n normal equations are derived. The n^{th} normal equation is shown in equation (3.13),

$$\sum_{i=1}^{m} r_i a_{in} = \sum_{i=1}^{m} a_{in}a_{i1}x_1 + \sum_{i=1}^{m} a_{in}a_{i2}x_2 + \ldots\ldots$$
$$+ \sum_{i=1}^{m} a_{in}a_{in-1}x_{n-1} + \sum_{i=1}^{m} a_{in}^2 x_n \qquad (3.13)$$

The least error squares approach yields n normal equations from the original m equations. From equations (3.11), (3.12) and (3.13), the n normal equations can be expressed in matrix form as:

$$\begin{bmatrix} \Sigma r_i a_{i1} \\ \Sigma r_i a_{i2} \\ \vdots \\ \Sigma r_i a_{in-1} \\ \Sigma r_i a_{in} \end{bmatrix} = \begin{bmatrix} \Sigma a_{i1}^2 & \Sigma a_{i1}a_{i2} & \cdots & \Sigma a_{i1}a_{in-1} & \Sigma a_{i1}a_{in} \\ \Sigma a_{i2}a_{i1} & \Sigma a_{i2}^2 & \cdots & \Sigma a_{i2}a_{in-1} & \Sigma a_{i2}a_{in} \\ \vdots & & & & \vdots \\ \Sigma a_{in-1}a_{i1} & \Sigma a_{in-1}a_{i2} & \cdots & \Sigma a_{in-1}^2 & \Sigma a_{in-1}a_{in} \\ \Sigma a_{in}a_{i1} & \Sigma a_{in}a_{i2} & \cdots & \Sigma a_{in}a_{in-1} & \Sigma a_{in}^2 \end{bmatrix} \begin{bmatrix} x_1 \\ x_2 \\ \vdots \\ x_{n-1} \\ x_n \end{bmatrix}$$

or $$\bar{R} = \bar{A}X \qquad (3.14)$$

where $\bar{R}$ is a n x 1 column vector

$\bar{A}$ is a n x n square matrix

X is a n x 1 column vector

all the summations are from i = 1 to m

The least error squares process can be summarized in the following steps:

(i) Obtain the error squared expression for each r.

(ii) Sum all the error square terms.

(iii) Differentiate the sum of error squares with respect to each unknown x.

(iv) Equate each result from step (iii) to zero and rearrange the resulting equation.

(v) Obtain the final matrix equation $\bar{R} = \bar{A}X$.

The definition of matrices A and R, and the product of the transpose of A and R gives the following result,

$$A^T R = \begin{bmatrix} a_{11} & a_{21} & \cdots & a_{m-1\,1} & a_{m1} \\ a_{12} & a_{22} & \cdots & a_{m-1\,2} & a_{m2} \\ \cdot & \cdot & & \cdot & \cdot \\ \cdot & \cdot & & \cdot & \cdot \\ \cdot & \cdot & & \cdot & \cdot \\ a_{1\,n-1} & a_{2\,n-1} & \cdots & a_{m-1\,n-1} & a_{m\,n-1} \\ a_{1n} & a_{2n} & \cdots & a_{m-1\,n} & a_{mn} \end{bmatrix} \begin{bmatrix} r_1 \\ r_2 \\ \cdot \\ \cdot \\ \cdot \\ r_{m-1} \\ r_m \end{bmatrix}$$

This can be written in compact form,

$$A^T R = \begin{bmatrix} \Sigma r_i a_{i1} \\ \Sigma r_i a_{i2} \\ \cdot \\ \cdot \\ \cdot \\ \Sigma r_i a_{i\,n-1} \\ \Sigma r_i a_{in} \end{bmatrix}$$

or, $$A^T R = \bar{R} \qquad (3.15)$$

where the summations are taken from i = 1 to m.

Substituting equation (3.15) into (3.14) yields,

$$\underset{(n\times m)(m\times 1)}{A^T R} = \underset{(n\times n)(n\times 1)}{\bar{A} X} \qquad (3.16)$$

Substituting equation (3.6) into (3.16) gives,

$$A^T A X = \bar{A} X$$

or, $$A^{T}A = \bar{A} \tag{3.17}$$

The least error squares curve fitting problem is now readily solved by substituting equations (3.15) and (3.17) into equation (3.14). The result is,

$$A^{T}R = A^{T}AX \tag{3.18}$$

The unknown vector X in equation (3.18) is solved by premultiplying both sides of equation (3.18) with the inverse of $A^{T}A$, provided that the inverse exists. The final equation is given by,

$$(A^{T}A)^{-1}A^{T}R = (A^{T}A)^{-1}A^{T}AX$$

or, $$X = (A^{T}A)^{-1}A^{T}R \tag{3.19}$$

$(A^{T}A)^{-1}A^{T}$ is the left pseudoinverse of matrix A[6]. Matrix A must have a rank equal to n to ensure that $A^{T}A$ is non-singular; $A^{T}A$ is invertible[18].

In summary, the least error squares curve fitting solution is obtained by first finding the pseudoinverse of the rectangular matrix A, then the matrix R is premultiplied by the pseudoinverse to determine the unknown vector X. As a result, the least error squares problem is resolved into a matrix algebraic problem involving the calculation of the pseudoinverse.

3.3 Developme of the equation of condition for the fault location algorithm

The least error squares curve fitting technique and its relationship with the pseudoinverse of a matrix have been presented in Section 3.2. This technique was suggested in Reference 6 as a tool for digital relaying of transmission lines. The same approach can also be applied to fault location problems. In order to apply the curve fitting approach, equations of condition for both the post-fault voltage and current waveforms have to be formulated.

In the presence of a short-circuit fault, current and voltage waveforms at the sending end of a transmission line are represented by equations (3.20) and (3.21) respectively:

$$i = K^{I} e^{-t/\tau} + \Sigma G_k^{I} \sin(k\omega t + \alpha_k^{I}) \qquad (3.20)$$

$$v = K^{V} e^{-t/\tau} + \Sigma G_k^{V} \sin(k\omega t + \alpha_k^{V}) \qquad (3.21)$$

where, i is the instantaneous current at time t

v is the instantaneous voltage at time t

τ is the time constant of the given system

K^{I} and K^{V} are the magnitudes of the dc offset of the current and voltage signals respectively

G_k^{I} and G_k^{V} are the magnitudes of the k^{th} harmonic of the current and voltage signals respectively

α_k^{I} and α_k^{V} are the phase angles of the k^{th} harmonic of the current and voltage signals respectively

ω is the fundamental frequency of the given system

It is assumed that all the fifth and higher harmonics present in the waveforms have been eliminated by either a low-pass analog or digital filter. Also, the post-fault current and voltage signals usually do not consist of even harmonic components. As a result, equation (3.20) is simplified and the resulting equation is shown as (3.22) by expanding the exponential term ($e^{-t/\tau}$) as a power series.

$$i = K'(1 - t/\tau + t^2/\tau^2 2! - t^3/\tau^3 3! + \ldots) + G_1' \sin(\omega t + \alpha_1') + G_3' \sin(3\omega t + \alpha_3') \qquad (3.22)$$

where ! denotes factorial

The two sinusoidal terms present in equation (3.22) can be expanded, thus yielding the following equations:

$$G_1' \sin(\omega t + \alpha_1') = G_1' \sin(\omega t)\cos(\alpha_1') + G_1' \cos(\omega t)\sin(\alpha_1') \qquad (3.23)$$

and

$$G_3' \sin(3\omega t + \alpha_3') = G_3' \sin(3\omega t)\cos(\alpha_3') + G_3' \cos(3\omega t)\sin(\alpha_3') \qquad (3.24)$$

Substituting equations (3.23) and (3.24) into equation (3.22) and approximating the power series of equation (3.22) by only the first three terms, equation (3.22) is modified into:

$$i = K' - K't/\tau + K't^2/2\tau^2 + G_1' \sin(\omega t)\cos(\alpha_1') + G_1' \cos(\omega t)\sin(\alpha_1') + G_3' \sin(3\omega t)\cos(\alpha_3') + G_3' \cos(3\omega t)\sin(\alpha_3') \qquad (3.25)$$

The above equation can be transferred into an equation of condition as shown in Reference 6 by using the substitutions given in equation (3.27). The resultant equation of condition for the current waveform is shown below:

$$i = a_1^i(t)x_1^i + a_2^i(t)x_2^i + a_3^i(t)x_3^i + a_4^i(t)x_4^i + a_5^i(t)x_5^i + a_6^i(t)x_6^i + a_7^i(t)x_7^i \qquad (3.26)$$

and

$$\begin{aligned} x_1^i &= K^i & a_1^i(t) &= 1 \\ x_2^i &= G_1^i\cos(\alpha_1^i) & a_2^i(t) &= \sin(\omega t) \\ x_3^i &= G_1^i\sin(\alpha_1^i) & a_3^i(t) &= \cos(\omega t) \\ x_4^i &= G_3^i\cos(\alpha_3^i) & a_4^i(t) &= \sin(3\omega t) \\ x_5^i &= G_3^i\sin(\alpha_3^i) & a_5^i(t) &= \cos(3\omega t) \\ x_6^i &= -K^i/\tau & a_6^i(t) &= t \\ x_7^i &= K^i/2\tau^2 & a_7^i(t) &= t^2 \end{aligned} \qquad (3.27)$$

The values of x's are unknown and a's are known since ω and t are predetermined.

Proceeding in the same manner, an equation of condition for the voltage waveform is obtained and is written as:

$$v = a_1^v(t)x_1^v + a_2^v(t)x_2^v + a_3^v(t)x_3^v + a_4^v(t)x_4^v + a_5^v(t)x_5^v + a_6^v(t)x_6^v + a_7^v(t)x_7^v \qquad (3.28)$$

where,

$$\begin{aligned} x_1^v &= K^v & a_1^v(t) &= 1 \\ x_2^v &= G_1^v\cos(\alpha_1^v) & a_2^v(t) &= \sin(\omega t) \\ x_3^v &= G_1^v\sin(\alpha_1^v) & a_3^v(t) &= \cos(\omega t) \\ x_4^v &= G_3^v\cos(\alpha_3^v) & a_4^v(t) &= \sin(3\omega t) \\ x_5^v &= G_3^v\sin(\alpha_3^v) & a_5^v(t) &= \cos(3\omega t) \end{aligned} \qquad (3.29)$$

$$x_6^v = -K^v/\tau \qquad a_6^v(t) = t$$

$$x_7^v = K^v/2\tau^2 \qquad a_7^v(t) = t^2$$

From equations (3.27) and (3.29) :

$$a_j^i(t) = a_j^v(t) \tag{3.30}$$

where j = 1, 2, ..., 7

For simplicity's sake, the superscripts associated with all the a's are left out in the subsequent analysis.

The analog current and voltage signals are converted into digital form as the input to the fault location algorithm. Each sample of data results in an equation of condition either in the form of equation (3.26) or (3.28). The number of unknowns, x, of each equation is seven, which implies that at least seven samples are required to compute the unknowns. In general, a larger number of samples can be used but each additional sample increases the window size and more time is required before the fault can be located.

At the d^{th} sampling instant, equations (3.26) and (3.28) are rewritten as the following two equations:

$$i = a_{d1}x_1^i + a_{d2}x_2^i + a_{d3}x_3^i + a_{d4}x_4^i + a_{d5}x_5^i + a_{d6}x_6^i + a_{d7}x_7^i \tag{3.31}$$

and

$$v = a_{d1}x_1^v + a_{d2}x_2^v + a_{d3}x_3^v + a_{d4}x_4^v + a_{d5}x_5^v + a_{d6}x_6^v + a_{d7}x_7^v \tag{3.32}$$

where the subscript d denotes the d^{th} sampling instant.

If m samples of current and voltage are acquired, m equations of (3.31) and (3.32) result and these are written in matrix form as:

$$AX^{I} = I \tag{3.33}$$

and

$$AX^{V} = V \tag{3.34}$$

where, A is a m x 7 matrix

X^{I} and X^{V} are 7 x 1 column vectors

I and V are m x 1 column vectors.

I and V are known column vectors since they are consist of input current and voltage samples. X^{I} and X^{V} are the unknown vectors which are solved from equations (3.33) and (3.34). A is specified since the fundamental frequency and sampling rate are predetermined.

Usually, the number of samples, m, is greater than seven. Under such circumstances, the matrix A becomes rectangular in nature. Equations (3.33) and (3.34) are solved by applying the concept of least error squares curve fitting which was briefly discussed in Section 3.2. The unknown values of x are obtained by premultiplying the equations with the pseudoinverse of A.

In the proposed algorithm, the matrix A is determined by the sampling rate, the time instant when t is equal to zero, and the fundamental frequency of the given system. In general, the fundamental frequency is fixed and the

remaining two parameters have to be arbitrarily chosen to obtain the desired matrix A.

The first parameter to be considered is the sampling rate. The highest frequencey present in the equation of condition determines the lower limit of the sampling rate. Theoretically, the sampling frequency must be at least twice the largest frequency present in the signal to avoid aliasing. From equations (3.26) and (3.28), the sampling rate has to be at least 360 Hz since the equations consist of up to third harmonic components (360 Hz). In practice, a sampling rate larger than 360 Hz is desired to ensure that the aliasing effect is totally eliminated from the digitized values. If the sampling rate is too high, the determinant of matrix A^TA becomes small and hence the inverse becomes large. A fast sampling rate is undesirable since the elements of the matrix $(A^TA)^{-1}$ have to be multiplied with the sampled values and any noise present in the signal would be amplified. The sampling rate is determined by considering the above factors.

Another parameter which has to be studied is the time reference[6] (the instant when t is equal to zero). Different time references result in different matrices A and these can affect the implementation of the algorithm. The authors of Reference 6 tried three different time references such that the time is set at zero at the instant of either the first, second or third sample.

In order to select the best equation of condition for relaying applications, different combinations of sampling rate, time reference and sampling window size have been studied in Reference 6. After considering the elements of the pseudoinverse of A, the authors decided to select the following parameters which result in the pseudoinverse matrix shown in Table 3.1:

Sampling rate = 720 Hz.

Total number of samples = 9.

Time reference = time set to zero at the instant of the second sample.

The above combination of parameters has the following advantages:

(i) The sampling rate is chosen at 720 Hz which is a multiple of the fundamental frequency. This eases the computational implementation of the algorithm.

(ii) Nine samples at 720 Hz sampling rate are required by the algorithm. This corresponds to three-quarters of a cycle at the fundamental frequency which is well within the operating time of a protection system (the time between the instant of fault inception and the time when the circuit breaker trips).

(iii) Considering the pseudoinverse matrix shown in Table 3.1, the values of the elements of the second and third rows are symmetrical with respect to the centre sample. Also, one element in the third row is repeated

0.809	0.274	-0.404	-0.269	0.065	0.157	0.473	0.699	-0.805
2.267	-4.950	1.669	1.613	-1.195	1.613	1.669	-4.950	2.267
-0.675	0.364	0.621	0.364	0	-0.364	-0.621	-0.364	0.675
0.080	-0.317	0.373	0.070	-0.414	0.070	0.373	-0.317	0.080
-0.100	0.230	-0.009	-0.270	0	0.270	0.009	-0.230	0.100
-1249.558	2072.809	-614.738	-530.720	671.787	-632.875	-825.174	1970.660	-862.190
126704.901	-242608.111	86394.722	69815.692	-80614.407	69815.692	86394.722	-242608.111	126704.901

Table 3.1 Pseudoinverse of matrix

four times and another element is zero.

These all contribute to the reduction of computation in the proposed fault location algorithm.

3.4 Calculation of complex impedance and determination of fault distance

As mentioned earlier, the unknown vectors X^I and X^V of equations (3.33) and (3.34) are solved by premultiplying both equations with the pseudoinverse of A. The resultant equations become:

$$\underset{(7\times m)(m\times 1)}{A^{+}} \underset{(7\times 1)}{I} = \underset{(7\times 1)}{X^{I}} \qquad (3.35)$$

and

$$\underset{(7\times m)(m\times 1)}{A^{+}} \underset{(7\times 1)}{V} = \underset{(7\times 1)}{X^{V}} \qquad (3.36)$$

where A^{+}[17] is the pseudoinverse of A and is defined as

$(A^{T}A)^{-1}A^{T}$

m is equal to nine.

The second and third elements of the unknown vectors X^I and X^V consist of information regarding the components of fundamental current and voltage phasors. By multiplying the elements of the second row of A^{+} with the nine samples of phase current, the component x_2^I is obtained. Similarly, x_3^I is solved by determining the products of the third row's elements of A^{+} with the nine sampled phase currents. The two unknowns x_2^V and x_3^V are solved in the same manner as x_2^I and x_3^I but the sampled values now correspond to phase to neutral voltage. As a result, the following four components are

obtained:

$$x_2^i = i_p \cos(\alpha_1^i) \tag{3.37}$$

$$x_3^i = i_p \sin(\alpha_1^i) \tag{3.38}$$

$$x_2^v = v_p \cos(\alpha_1^v) \tag{3.39}$$

$$x_3^v = v_p \sin(\alpha_1^v) \tag{3.40}$$

where, i_p is the peak value of the fundamental current component

α_1^i is the phase angle of the fundamental current component

v_p is the peak value of the fundamental voltage component

α_1^v is the phase angle of the fundamental voltage component

The resistive component R_L of the line apparent complex impedance as seen from the sending end of the line at any instant t can be expressed as:

$$R_L = Re\left[\frac{v}{i}\right] = \frac{v_p}{i_p}\cos(\alpha_1^v - \alpha_1^i)$$

$$R_L = \frac{v_p[\cos(\alpha_1^v)\cos(\alpha_1^i) + \sin(\alpha_1^v)\sin(\alpha_1^i)]}{i_p}$$

$$R_L = \frac{v_p\cos(\alpha_1^v)i_p\cos(\alpha_1^i) + v_p\sin(\alpha_1^v)i_p\sin(\alpha_1^i)}{i_p^2}$$

$$R_L = \frac{v_p\cos(\alpha_1^v)i_p\cos(\alpha_1^i) + v_p\sin(\alpha_1^v)i_p\sin(\alpha_1^i)}{i_p^2\cos^2(\alpha_1^i) + i_p^2\sin^2(\alpha_1^i)} \tag{3.41}$$

Substituting equations (3.37) to (3.40) into equation (3.41) yields the final expression of R_L [6],

$$R_L = \frac{X_2X_2' + X_3X_3'}{X_2'X_2' + X_3'X_3'} \qquad (3.42)$$

Applying a similar procedure, the reactive component X of the apparent impedance is shown to be:

$$X_L = \frac{X_3X_2' - X_2X_3'}{X_2'X_2' + X_3'X_3'} \qquad (3.43)$$

The calculated R_L and X_L from equations (3.42) and (3.43) correspond to the resistive and reactive components of the apparent impedance of the transmission line respectively. In the presence of zero-resistance short-circuit fault, the calculated R_L is exactly equal to the line resistance seen from the fault location algorithm to the faulted point. However, fault resistance is incorporated into the final R_L if the fault resistance cannot be neglected.

Assuming line length is proportional to the line reactance, the calculated reactive component of the apparent impedance using equation (3.43) is used to locate the short-circuit fault. Fault distance y_f is determined by the following relationship:

$$y_f = \frac{X_f y_t}{X_t} \qquad (3.44)$$

where, y_f is the distance from the sending end of the line to the faulted point

y_t is the total length of the line

X_f is the apparent line reactance from the sending

end to the faulted point

X_t is the total reactance of the line.

y_t and X_t are known values, y_f can be determined once X_f is calculated. The fault is located using the reactance ratio as shown in equation (3.44), and the presence of ground resistance does not affect the final fault distance measurement. However, the accuracy of the algorithm is affected by line shunt capacitance and this effect will be studied in Chapter 6.

3.5 Special features in using least error squares curve fitting approach in fault location

In the last two sections, the development of the proposed fault location algorithm using least error squares curve fitting technique has been briefly discussed. Some of the advantages of the proposed method are summarized below:

(i) The freedom in choosing the equation of condition which results in the presence of decaying dc component and any desired harmonic component.

(ii) The flexibility in selecting the data window size.

(iii) Some allowance in choosing the sampling rate.

(iv) The pseudoinverse can be calculated in an off-line mode since the elements of matrix A are all known prior to the calculation of the fault distance.

(v) No iteration is required and hence results in less of a computational burden.

(vi) The effect of ground resistance to the accuracy of the fault location is minimized due to the fact that the fault distance measurement is based on the reactance ratio.

(vii) No prior knowledge of source impedance at either the sending or receiving end is required.

3.6 Conclusion

In this chapter, the least error squares curve fitting technique has been briefly studied. It has been shown that the pseudoinverse of a matrix provides the solution of the least error squares problem.

The fault location algorithm employing the least error squares curve fitting approach has been derived. This algorithm is readily implemented by digital computers and it has shown that it is well suited to on-line applications. The next chapter discusses the various mathematical models which are used in the testing of the developed algorithm.

CHAPTER IV

Testing the algorithm using simulated transmission lines

4.1 Introduction

A fault location algorithm has been presented in the previous chapter. Two simple power systems under both pre-fault and post-fault conditions were chosen for study. The systems, which were set up in an off-line mode, provide transient fault data to the proposed fault location algorithm and thus allow the performance of the algorithm to be evaluated under different system configurations.

As mentioned earlier, a low-pass filter is required by the algorithm to attenuate high frequency harmonics present in the post-fault waveforms. The design of the filter affects the performance of the algorithm to a large extent.

Detection and identification functions can be included digitally in the algorithm to increase the capability of the algorithm. These additional facilities remove the need for a communication link between the protective system and the fault locating system, thus increasing the portability of the fault location algorithm.

4.2 Modelling of test system

In testing the performance of the proposed fault location approach, two simple power sytems are used. The

systems are selected in order to represent practical situations. The first one is a single-phase system consisting of a short, aluminium-cable-steel-reinforced(ACSR)[19] overhead transmission line. The line is mathematically represented by a series equivalent R-L model. The second system is a three-phase network consisting of a medium length, copper-conductor type overhead transmission line. The transmission line is modelled by a three-pi equivalent circuit.[20]

4.2.1 Single-phase power system

A single-line diagram of the single-phase system is shown in Figure 4.1. The system, operating under normal condition, consists of a generator G1 feeding into a load L1 through transformers and transmission lines. li1 is the line monitored by the fault location algorithm. The data of the components is shown in Appendix A.

The components of the system are modelled using equivalent impedances. Using $126/\sqrt{3}$ KV as the base voltage and 100 MVA as the base power, the impedances are converted to per unit base. The steady-state equivalent circuit of the system, in all the impedances are in per unit values, is given in Figure 4.2. The transmission line li1 is modelled by a lumped series R-L network as shown in Figure 4.2.

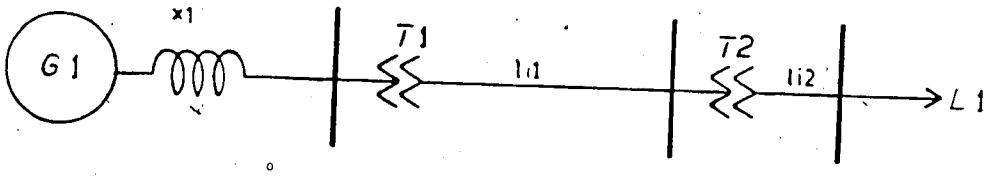

Figure 4.1 Single-phase test system (pre-fault).

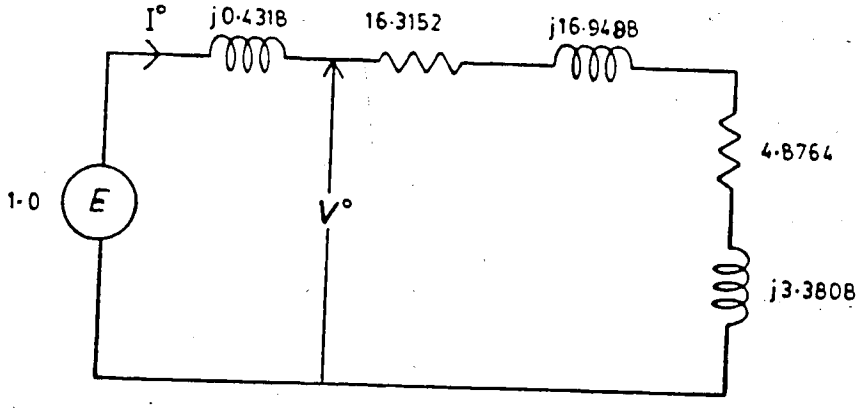

Figure 4.2 Equivalent circuit of the single-phase test system (pre-fault).

The steady-state pre-fault current and voltage phasors of the sending end of the line li1 are denoted by I° and V° respectively. From Figure 4.2, the expression of I° and V° are written as:

$$I^\circ = \frac{1.0}{j0.4318 + 16.3152 + j16.9488 + 4.8764 + j3.3808} \quad (4.1)$$

$$V^\circ = 1.0 - I^\circ \cdot j0.4318 \quad (4.2)$$

The presence of a short-circuit ground fault on the line li1 yields the faulted system shown in Figure 4.3. The parameter y_f corresponds to the distance measured from the sending end of the line li1 to the faulted point. The equivalent circuit of the faulted system is shown in Figure 4.4. The circuit is used to solve for the transient response of both i_1^f and v^f immediately after the fault has occurred.

In Figure 4.4, i_1^f and v^f correspond to the instantaneous values. r_1^f and l_1^f are the sending resistance and inductance respectively of the faulted line between the sending end and the faulted point. Their values are dependant upon the fault location since they are directly proportional to the line length. e is the generated emf and is a sinusoidal function.

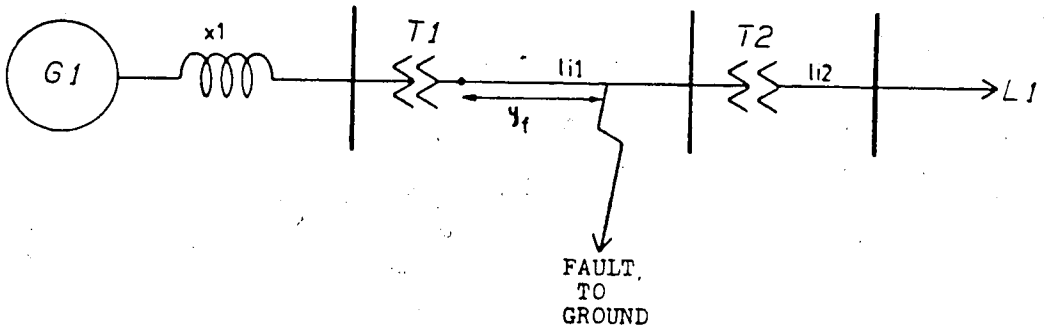

Figure 4.3 Single-phase test system (post-fault).

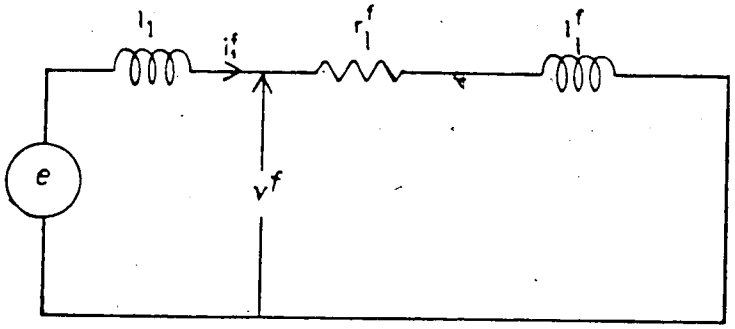

Figure 4.4 Equivalent circuit of the single-phase post-fault test system.

The following time domain differential equations are written by considering the equivalent model shown in Figure 4.4.

$$e = l_1 \frac{di_1^f}{dt} + r_1^f i_1^f + l_1^f \frac{di_1^f}{dt}$$

i.e. $$\frac{di_1^f}{dt} = \frac{e - r_1^f i_1^f}{l_1 + l_1^f} \qquad (4.3)$$

and, $$v^f = r_1^f i_1^f + l_1^f \frac{di_1^f}{dt} \qquad (4.4)$$

From equations (4.3) and (4.4), the unknowns i_1^f and v^f are solved numerically for each small time step using Euler's integration method. The quantities e, l_1, r_1^f and l_1^f are all known prior to the calculation. Initial conditions for i_1^f and v^f are given by the pre-fault steady-state values of I° and V° respectively.

4.2.2 Three-phase power system

The second test system is almost identical to the system described in Section 4.2.1 except now each element consists of three components, the a-, b- and c-phase. Line li1 is replaced by a three-phase 133.5 mile-long overhead copper conductor transmission line. The three conductors are spaced 15.8 feet apart. Transmission line li2 is a three-phase 5 mile-long overhead copper conductor line with conductors spaced 4 feet apart. For simplicity, no mutual coupling is assumed between the three phases.

In the normal operating mode, the system can be assumed to be in a balanced three-phase state. Figure 4.5 is the one-line diagram of the balanced system.

The single-phase equivalent circuit of the three-phase system is shown in Figure 4.6. The various components are modelled by their equivalent impedances. The values given in Figure 4.6 are in per unit with $126/\sqrt{3}$ KV and 100 MVA chosen as the base voltage and base power respectively.

The transmission line li1, which is monitored by the fault location algorithm, is represented by three "pi" sections. Each "pi" section corresponds to a 44.5 mile-long transmission line, and its line parameters are given by equations (4.5) and (4.6) with operating frequency of 60 Hz.

$$Z_{\pi}(\text{series impedance}) = 0.06 + j0.2355 \text{ pu} \qquad (4.5)$$

$$Z'_{\pi}(\text{shunt reactance}) = -j55.7 \text{ pu} \qquad (4.6)$$

The single-phase equivalent model is used to analyse the balanced three-phase system. The distribution of currents and voltages is calculated from the network equations. Hence, the pre-fault current (I°) and pre-fault voltage (V°) are solved.

If a three-phase ground fault occurs accidentally on the line li1, a single-phase post-fault mathematical model

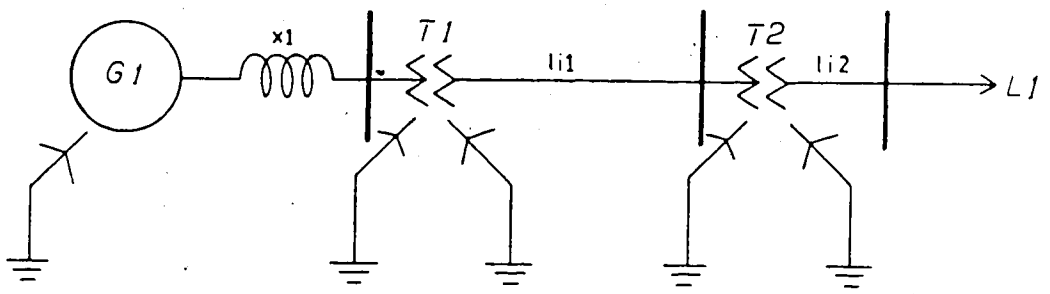

Figure 4.5 One-line diagram of the three-phase system (pre-fault).

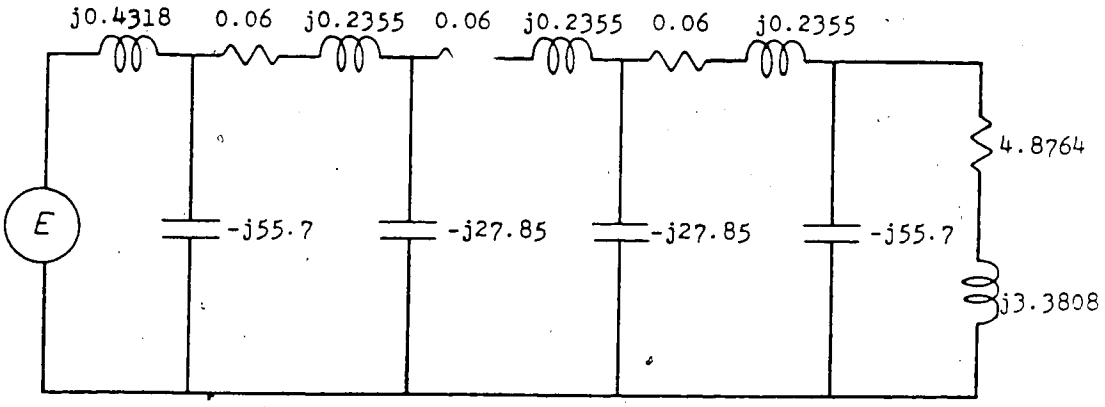

Figure 4.6 Single-phase equivalent circuit of the three-phase system (pre-fault).

is used to report the condition. This is shown in Figure 4.7. The fault exists at a location 44.5 miles from the sending terminal of the line. The use of the single-phase equivalent circuit to study the post-fault system is possible since the fault is a balanced three-phase type.

Using Kirchhoff's current and voltage laws, the following circuit equations can be written from the post-fault single-phase equivalent circuit (Figure 4.7) immediately after the occurrence of the fault:

$$e - v^f = l_1^f \frac{di_1^f}{dt}$$

i.e.

$$\frac{di_1^f}{dt} = \frac{e - v^f}{l_1^f} \qquad (4.7)$$

and,

$$v^f = r_1^f i_2^f + l_1^f \frac{di_2^f}{dt}$$

i.e.

$$\frac{di_2^f}{dt} = \frac{v^f - r_1^f i_2^f}{l_1^f} \qquad (4.8)$$

and,

$$i_1^f = C_1^f \frac{dv^f}{dt} + i_2^f$$

i.e.

$$\frac{dv^f}{dt} = \frac{i_1^f - i_2^f}{C_1^f} \qquad (4.9)$$

The single-phase equivalent circuit is modified and the resultant network is shown in Figure 4.8 if the three-phase ground fault involves fault resistance r_f. The faulted network is simplified by assuming no load current and current i_2^f flows into ground completely through the fault resistance.

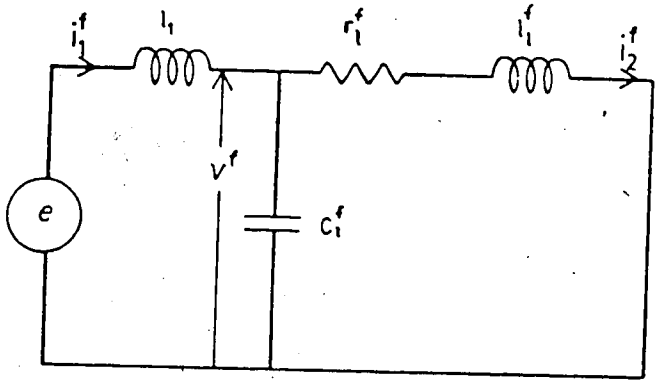

Figure 4.7 Single-phase equivalent circuit of the test system (post-fault).

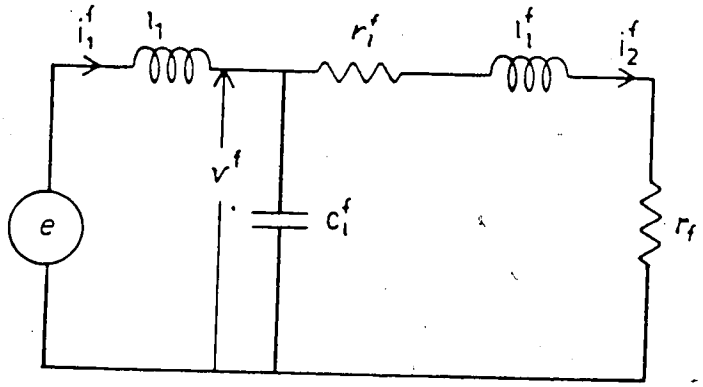

Figure 4.8 Single-phase equivalent circuit of the test system with fault resistance (post-fault).

In analysing the circuit shown in Figure 4.8, the following equations are obtained:

$$e - v^f = l_1 \frac{di_1^f}{dt}$$

$$\rightarrow \quad \frac{di_1^f}{dt} = \frac{e - v^f}{l_1} \qquad (4.10)$$

and, $$v^f = r_1^f i_2^f + l_1^f \frac{di_2^f}{dt} + r_f i_2^f$$

$$\rightarrow \quad \frac{di_2^f}{dt} = \frac{v^f - r_1^f i_2^f - r_f i_2^f}{l} \qquad (4.11)$$

and, $$i_1^f = c_1^f \frac{dv^f}{dt} + i_2^f$$

$$\rightarrow \quad \frac{dv^f}{dt} = \frac{i_1^f - i_2^f}{c_1^f} \qquad (4.12)$$

Comparing equations (4.7) to (4.9) and equations (4.10) to (4.12), it is observed that the two sets of equations are almost identical except for a slight difference between equations (4.8) and (4.11). This similarity between the two systems eases the computer implementation in simulating the two faulted networks.

Euler's method is employed to solve the differential equations (4.7) to (4.9) or equations (4.10) to (4.12) for the unknowns i_1^f and v^f in discrete time intervals. The initial conditions for the faulted network is obtained from the pre-fault model.

Proceeding in a similar manner as in the 44.5 mile-fault case, the transient response immediately after

the presence of fault is obtained for three-phase ground fault occurring at a location 89 miles or 133.5 miles from the sending end of the line. Therefore, the proposed algorithm can be tested in conditions under which line shunt capacitance is present and fault location is varied.

In analysing the faulted system in the presence of an asymmetrical fault, the single-phase-equivalent-circuit approach is not applicable. Under such circumstances, all the three phases have to be considered in order to derive the transient response. This analysis becomes very complicated if mutual coupling exists between the three phases..

4.3 Design of low-pass digital filters

The amplitude characteristic of an ideal low-pass digital filter with cutoff frequency fc is shown in Figure 4.9. The characteristic has a "brick wall" shape[21].

Methods used in the design of digital filter have been developed in the past. The text "Introduction to digital filtering"[22] edited by Bogner and Constantinides provides a good description of the various design methods. One of the methods is the "Direct synthesis of digital filters" which is used to design recursive low-pass digital filters. This technique is employed in this thesis to develop filters for the fault location algorithm. The method has a special feature such that the Bilinear Transformation[23], which is

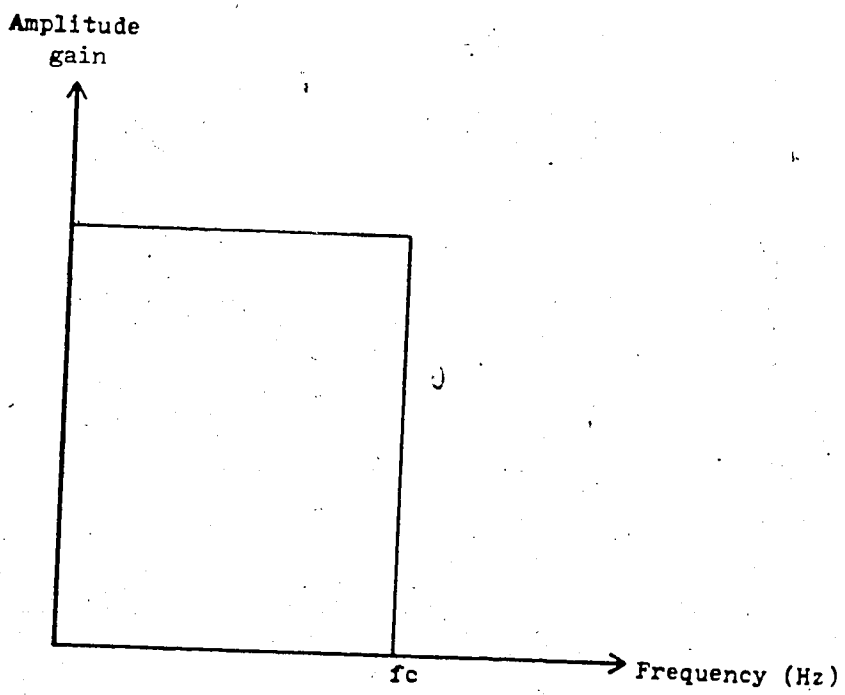

Figure 4.9 Amplitude characteristic of an ideal low-pass digital filter.

required to transform transfer functions from s-domain to z-domain, has been implicitly taken into account. The design problem is resolved into finding a particular function to approximate the ideal "brick wall" characteristic when using the direct design method.

Depending on the degree of approximation, different particular functions are required in the design analysis. One such function is to simulate a low-pass digital filter corresponding to that of a Butterworth-type low-pass analog filter. This function has a magnitude spectrum which decreases monotonically in both passband and stopband. Also, the magnitude is decreased by 3 dB at the cutoff frequency fc. The design procedures of the direct approach is shown below[22]:

(i) The order of the digital filter (N) is chosen from the given design specifications.

(ii) The pole locations are determined on the z^{-1}-plane and are selected those that lie outside the unit circle to ensure that a stable filter results. Alternatively, the poles can be obtained from the z-plane by choosing those that lie within the unit circle.

(iii) An N^{th} order zero exists and is at location $z^{-1} = -1$.

(iv) A transfer function in terms of the z^{-1}- or z-domain is constructed from the located poles and zeros.

A low-pass filter has to be included in the proposed fault location algorithm as shown is Chapter 3. According to the equations of condition given in equations (3.26) and (3.28), the following specifications have to be satisfied in the design of any desired digital filter:

(i) Fifth and higher harmonic components present in the post-fault transient waveforms are attenuated.

(ii) The sampling rate of the filter has to be at lea twice the third harmonic frequency (180 Hz).

Based on the direct approach as described above, three different ordered digital filters of the Butterworth-type have been designed. The details of each filter is described in the following. Appendix B gives the design procedures for each derived filter.

(a) 4th order low-pass filter:

Cutoff frequency = 203 Hz

Transition frequency = 285 Hz

Sampling frequency = 720 Hz

Attenuation at transition frequency better than 30 dB

Transfer function ($G(z^{-1})$) is,

$$G(z^{-1}) = \frac{6.078(1 + z^{-1})^4}{(z^{-2} + 0.638z^{-1} + 2.2)(z^{-2} + 4.212z^{-1} + 20.127)} \qquad (4.13)$$

(b) 8th order low-pass filter:

Cutoff frequency = 200 Hz

Transition frequency = 295 Hz

Sampling frequency = 1440 Hz

Attenuation at transition frequency better than 30 dB

$$G(z^{-1}) = \frac{0.023(1 + z^{-1})^8}{(z^{-2} - 1.512z^{-1} + 1.351)(z^{-2} - 2.238z^{-1} + 2.482)} \times \frac{1}{(z^{-2} - 3.541z^{-1} + 4.509)(z^{-2} - 5.170z^{-1} + 7.043)} \quad (4.14)$$

(c) 10th order low-pass filter:

Cutoff frequency = 218 Hz

Transition frequency = 290 Hz

Sampling frequency = 1440 Hz

Attenuation at transition frequency better than 30 dB

$$G(z^{-1}) = \frac{0.032}{(z^{-2} - 1.331z^{-1} + 1.292)(z^{-2} - 1.842z^{-1} + 2.173)} \times \frac{(1 + z^{-1})^{10}}{(z^{-2} - 2.737z^{-1} + 3.713)(z^{-2} - 4.230z^{-1} + 6.283)} \times \frac{1}{(z^{-2} - 5.928z^{-1} + 9.209)} \quad (4.15)$$

The unity step response of the three low-pass digital filters is given in Figure 4.10. It has been observed that a time delay is associated with each filter. The delay is longer for higher order filters. This increases the time required to locate the fault. The three designed filters are used in the proposed algorithm and the delay caused by each filter will be discussed in Chapter 6.

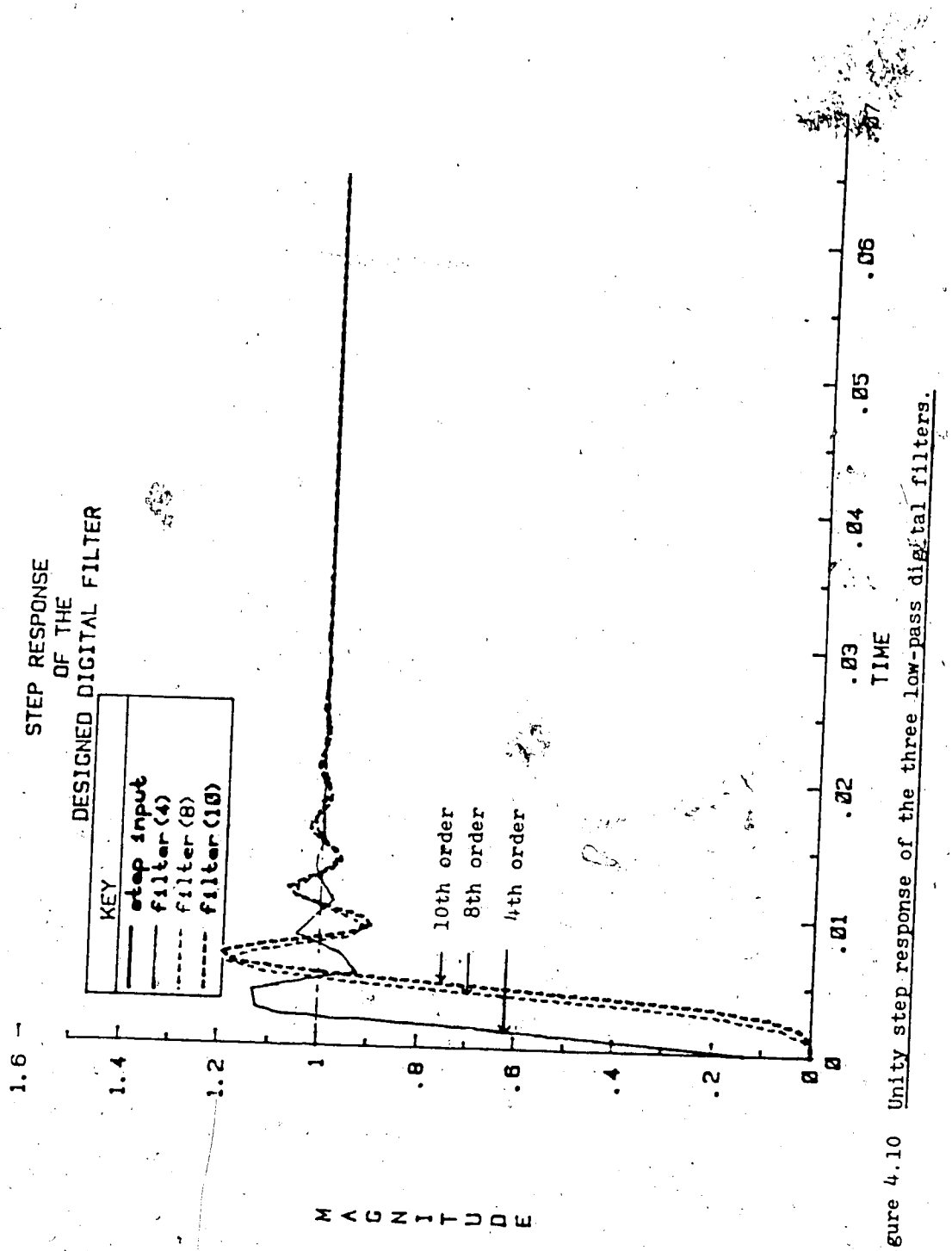

Figure 4.10 Unity step response of the three low-pass digital filters.

4.4 Fault detection

In the implementation of the fault location algorithm, two options are available at the start of the fault distance calculation. The first is to design a fault detection algorithm incorporated with the locating algorithm. The detection algorithm initiates the faulted point determination routine once the occurrence of a fault is detected. The second option is to attempt to locate a fault continuously. The latter option has the advantage that no detection algorithm is required. However, the disadvantage is that meaningless fault locations result from data collected from pre-fault state, or from data acquired partly between pre-fault and post-fault states. In addition, unnecessary calculations are needed during the pre-fault state since no distinction is made between the pre-fault and post-fault states. From the above considerations, a detection routine is developed and applied to the fault location algorithm.

The detection algorithm is based on comparing latest samples of electrical quantities of all the phases with the corresponding samples in the previous cycle. The algorithm is operated once a complete cycle of data has been received. The data can be either phase current or phase to neutral voltage or both. In order to increase the sensitivity of the routine, both current and voltage are used in the comparison. Also, three consecutive samples are employed in

each comparison to accommodate the possibility of spikes present in the current and voltage waveforms. Fault inception is only acknowledged if all the latest three consecutive samples differ from their corresponding one-cycle-ago samples by a value which exceeds the prespecified threshold tolerance. The tolerance is an input to the detection routine and can be altered by the choice of the user.

4.5 Fault identification

In the proposed fault location algorithm, a lot of multiplications and divisions are involved in the calculation of complex impedance. For a three-phase system, six impedances are calculated to locate all types of short-circuit faults. The six impedances are the phase-to-phase and phase-to-ground impedances. As a result, a lot of computational time is required. This greatly increases the time needed to locate a fault.

In order to increase the operating speed of the algorithm, it is necessary to reduce the number of impedance calculations. High speed is essential for on-line applications. One of the solutions is to include a fault identification algorithm. This additional routine is initiated by the detection algorithm and is used to determine the type of fault. Once the fault is identified, a suitable choice of current and voltage combination is

selected to calculate the appropriate impedance. From this calculated impedance, the faulted point is located. Moreover, the identification routine can provide a report regarding the type of fault for off-line analysis.

Fault identification algorithms were proposed in previously published articles. Reference 16 presents a method which belongs to this category.

4.6 Choice of data for locating fault

Once the fault type has been identified, a suitable combination of current and voltage is required to determine the impedance of the faulted phase or phases. For a single-phase-to-ground fault, a compensation technique is required to eliminate the sound-phase effect[24] in the calculation of impedance. In the case of phase fault, "delta"[16] current and voltage are used. Fault resistance is included in the impedance calculation if fault resistance cannot be neglected. This effect affects the accuracy of fault locating.

If phase "a" of a well-transposed line is subject to a single-phase-to-ground fault, equation (4.16)[24] is used to calculate the complex impedance. The equation has to be modified for the untransposed case[24].

$$Z_{al} = \frac{V_{an}}{I_{an} + K(I_{bn} + I_{cn})} \qquad (4.16)$$

where, V_{an} is the phase to neutral voltage of phase a at the sending end of the line

I_{an} is the phase current in phase a at the sending end of the line

I_{bn} is the phase current in phase b at the sending end of the line

I_{cn} is the phase current in phase c at the sending end of the line

K is equal to $|Z_m/Z_s|$

Z_s is the self-impedance of the line

Z_m is the mutual-impedance of the line

Z_{aL} is the faulty phase apparent self-impedance as seen from the sending end to the faulted point.

From equation (4.16), the faulted phase to neutral voltage and faulted phase current together with a correct proportion of non-faulted phase currents are used as the input signals for the fault location algorithm. The compensation scheme provides a higher accuracy in the final result. Equations similar to that of (4.16) are derived for a single-phase-to-ground fault on b- and c-phase.

The impedance of a phase-a-to-b fault, phase-a-to-b ground fault or three-phase fault is calculated by equation (4.17). Similar equations are used for phase faults occurring between b and c phases or between a and c phases.

$$Z_{+L} = \frac{V_{an} - V_{bn}}{I_{an} - I_{bn}} \qquad (4.17)$$

where, V_{an} is the phase to neutral voltage of phase a at the sending end of the line

V_{bn} is the phase to neutral voltage of phase b at the sending end of the line

I_{an} is the phase current in phase a at the sending end of the line

I_{bn} is the phase current in phase b at the sending end of the line

Z_{+L} is the apparent positive sequence line impedance between the sending end and the faulted point.

In considering equation (4.17), the appropriate choices of current difference and voltage difference are used for faults relating to two or three phases.

4.7 Discussion

Two simple power system models and three Butterworth-type low-pass digital filters, which are used in the testing of the proposed fault location algorithm, are presented in this chapter. It has been shown that the inclusion of fault detection and fault identification routines can increase the operating speed and the capability of the algorithm. Compensation by non-faulted phase currents reduces the effect due to mutual coupling and hence

the accuracy of the algorithm is improved.

In the implementation of the proposed algorithm, no compensation technique is employed in the testing program since the three-phase test model does not consist of any mutual coupling between the phases. Also no fault identification routine is included because the type of fault is already known during the stage when the faulted model is simulated. However, if the algorithm is applied to practical field data, the above two missing routines have to be incorporated with the location algorithm to complete the algorithm.

CHAPTER V

Computer Implementation

5.1 Introduction

In Chapter 3, it has been mentioned that the fault location algorithm involving pseudoinverse matrix is readily implemented into computer programs. Two programs have been developed using "C" programming language[25] based on this approach. The simple transmission line models, which were presented in Chapter 4, are used to test the proposed fault location algorithm. The relationship between the various developed programs are outlined in the block diagram as shown in Figure 5.1.

The programs are implemented on a PDP-11 microcomputer available in the Power Research Laboratory. The computer uses UNIX[26][27] as s operating system and supports high level languages such as C and FORTRAN 77. The attractive programming environment of the UNIX system and the powerful strength of C language ease the development of programs.

The developed programs, which are mentioned in Figure 5.1, are discussed in this chapter. The logic of each program is briefly presented in terms of general and detailed flow charts. The flow charts are essential in understanding the organisations of the programs.

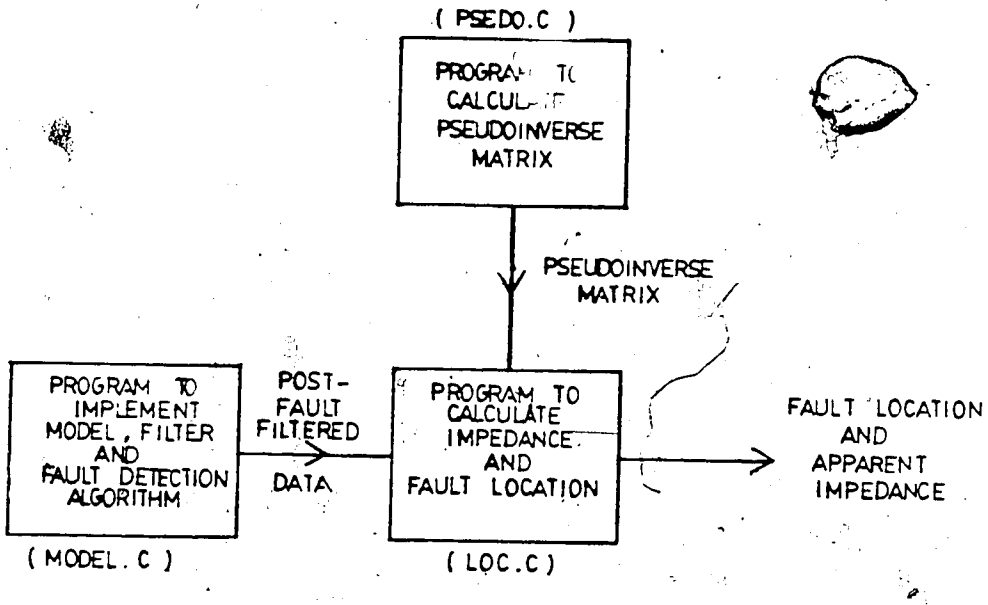

NOTE : The names in parenthesis correspond to the names of the appropriate programs .

Figure 5.1 Block diagram showing relationship between developed programs.

5.2 Program "model.c"

The program "model.c" is used to simulate the simple transmission line system under both pre-fault and post-fault conditions. The test model is either a single-phase or three-phase system. In both cases, a single-phase equivalent circuit is used to obtain the transient response of the faulted system as discussed in the previous chapter. This is feasible for the three-phase system since it is subject to symmetrical three-phase-to-ground fault. In addition to the model simulation, a fault detection routine and a low-pass digital filter are also implemented in the program.

5.2.1 Transmission line model routine

The program starts by declaring the dimensions of the various arrays and setting the system parameters. The strategy for detecting fault inception is an input to the program and is varied according to the user's choice. The pre-fault current and voltage phasors, which are obtained from the pre-fault steady state model, are required by the routine to calculate the instantaneous current and voltage prior to the occurrence of a fault.

The differential equations of the faulted system are formulated according to the location of the fault. For a non-zero resistance ground fault, the fault resistance has to be considered in deriving the differential equations as shown in Section 4.2. The equations are solved using Euler's

method for the unknown electrical quantities of the sending end of the transmission line. The pre-fault and post-fault instantaneous current and voltage were printed on a LA120 line printer and plotted on a HP7225 X-Y plotter. Figure 5.2 is the general flow chart of the routine which simulates the mathematical model of the test system.

5.2.2 Fault detection routine

Following the routine of the transmission line system, a fault detection routine is implemented into the program. The general flow chart of the detection routine is given in Figure 5.3. If the current sample lies within the first cycle of data, the routine compares the three latest successive samples with a maximum value to decide whether a fault has occurred. Otherwise, the routine compares the three latest consecutive samples with those of one cycle ago. In the latter case, the routine concludes a fault has occurred if all the three differences exceed a prespecified threshold value.

Immediately after a fault has been detected, one and three quarter cycles of pre-fault data and three cycles of post-fault data are stored. The pre-fault quantities are used to determine the type of fault if a fault identification routine is implemented into the program. Only three complete cycles of post-fault data are available to locate the fault. This simulates a practical situation in

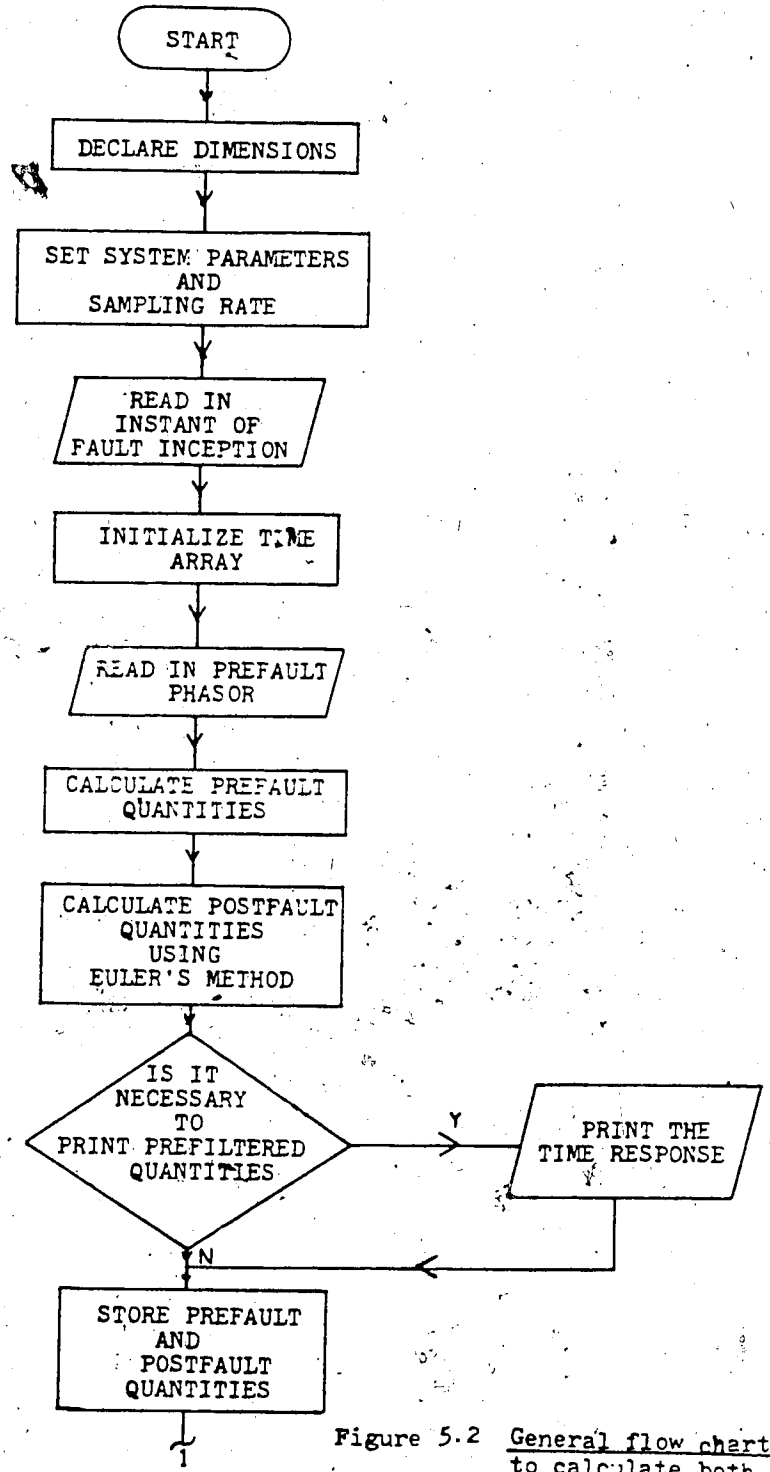

Figure 5.2 General flow chart used to calculate both pre-fault and post-fault quantities.

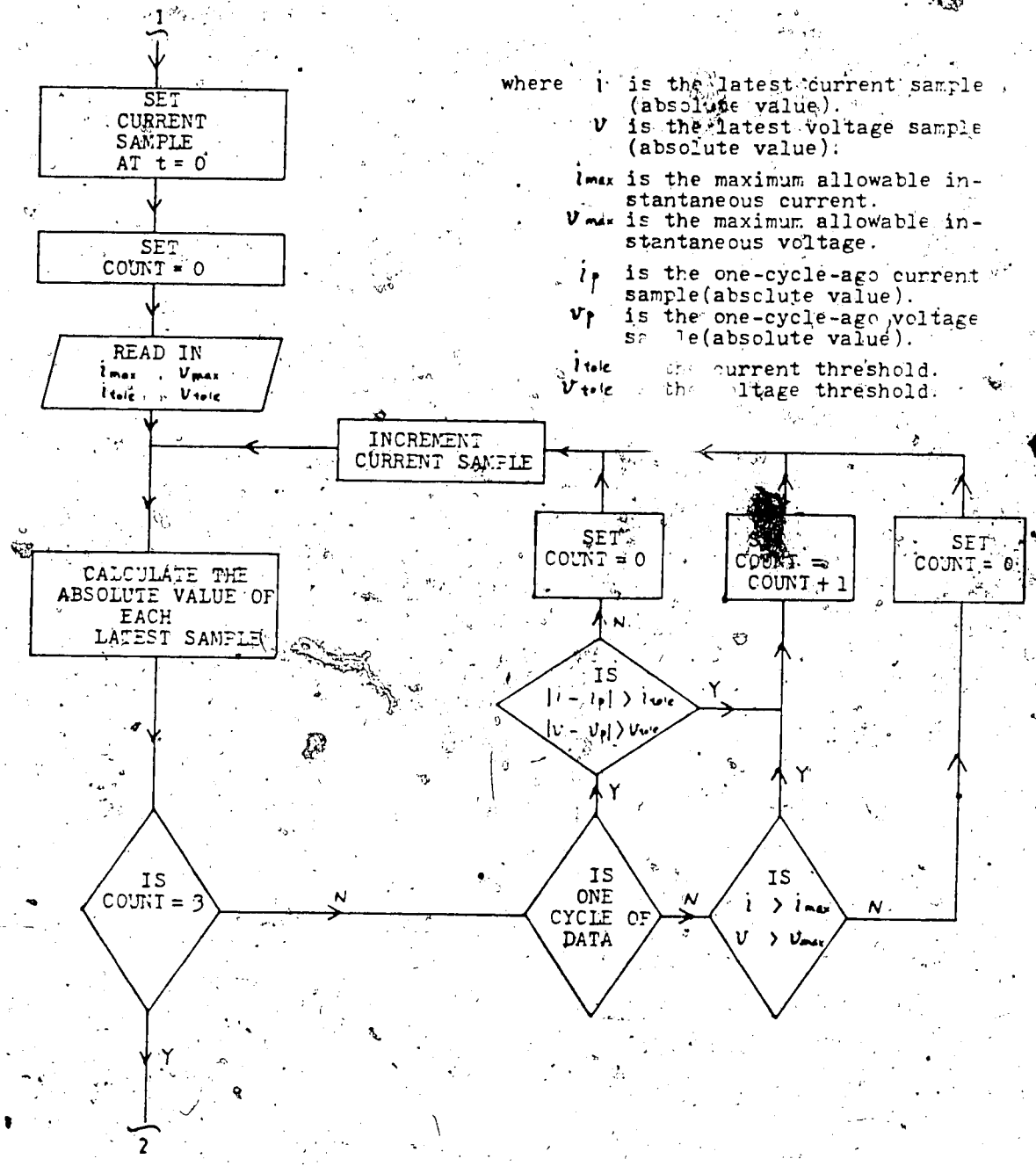

Figure 5.3 General flow chart of fault detection routine (con'd).

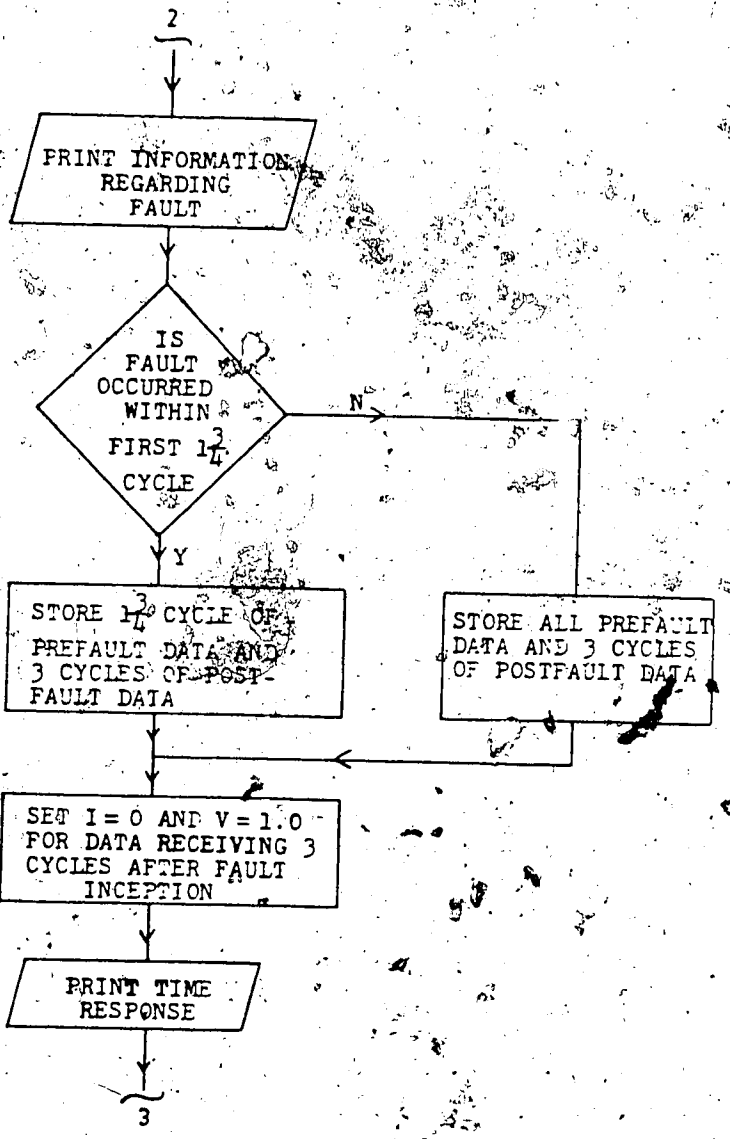

Figure 5.3 General flow chart of fault detection routine.

which the circuit breaker of the line begins to operate three cycles after the instant of fault inception. Once the breaker is tripped, the phase current vanishes and this is what the routine has simulated.

5.2.3 Digital filter routine

The low-pass digital filter routine, which is shown in Figure 5.4, is to suppress predetermined high harmonic components present in the digitally simulated line data. Difference equations of the three developed filters are formulated from their corresponding transfer functions. These transfer functions have been shown in Chapter 4. The difference equations are used to obtain the filtered response. The filtered post-fault values are stored in a data file which is read by the fault location program to determine the faulted point. If it is desired, the filtered response can be plotted on a plotter and is compared with the unfiltered response. From Figure 5.4, it has been noticed that a change of sampling frequency is required as the sampling rate is different between the transmission line simulation and the filter simulation.

5.3 Program "psedo.c"

In Chapter 3, it has been mentioned that the pseudoinverse of a matrix provides the solution of the fault location problem. The pseudoinverse A^+, which is present in

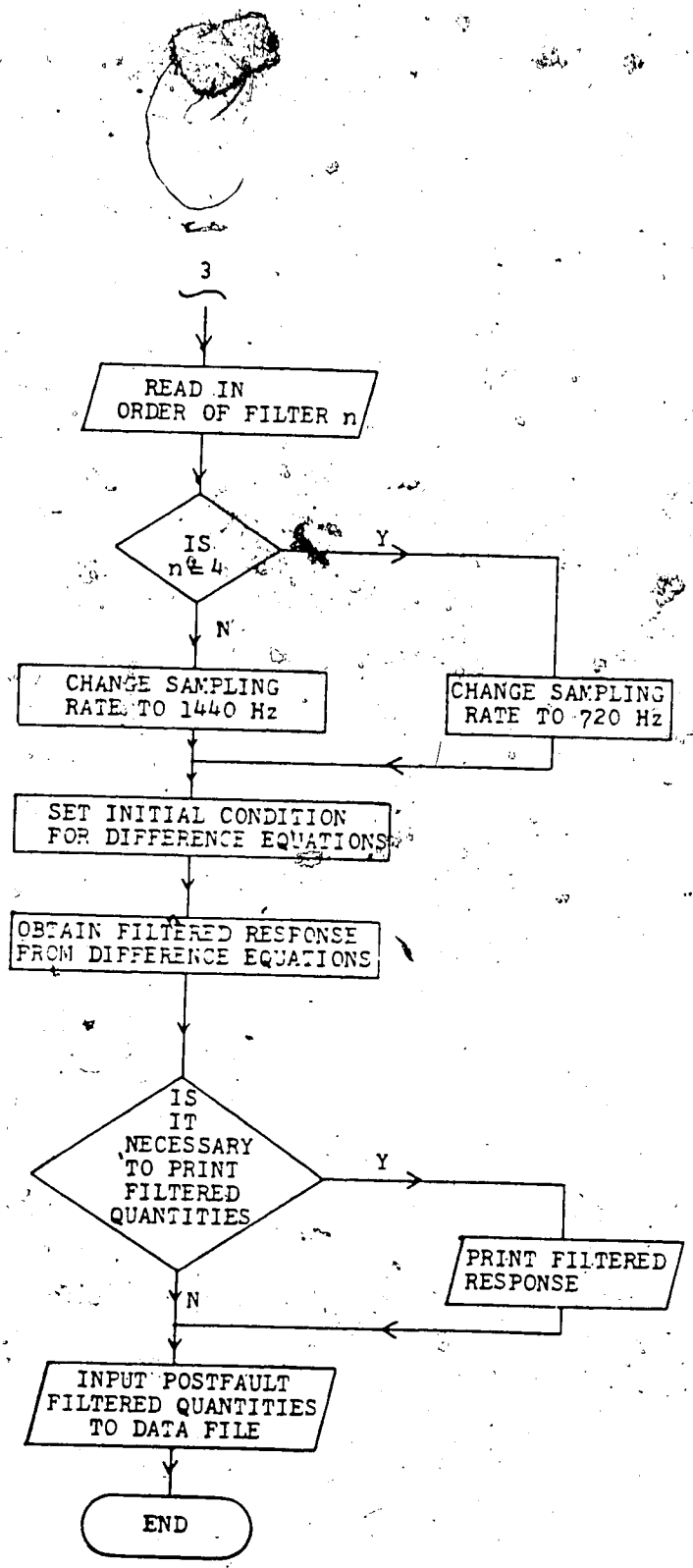

Figure 5.4 General flow chart of low-pass filte. utine.

equations (3.35) and (3.36), is calculated from the program "psedo.c". The resultant pseudoinverse matrix has already been shown in Table 3.1. The matrix is used by the program "loc.c" to calculate the post-fault current and voltage phasors. The general flow chart of the program "psedo.c" is given in Figure 5.5.

The program starts by formulating the matrix A. The elements of A are selected according to the desired combination of parameters given in Section 3.3. Matrix operators such as transpose, multiplication and inversion are all used in the program to calculate the pseudoinverse matrix $((A^TA)^{-1}A^T)$. The final solution is output to a file which is read by the program "loc.c". The advantage in using two different programs to implement the pseudoinverse calculating routine and the fault locating routine is that the former routine is only executed once and there is no need to execute it every time when the latter routine is called.

5.4 Program "loc.c"

The impedance calculating and fault distance measuring routines are implemented into the program "loc.c". The program is to locate the fault of the faulted model simulated by the program "model.c".

Immediately after the programs "model.c" and "psedo.c" have been executed, the program "loc.c" is ready to be

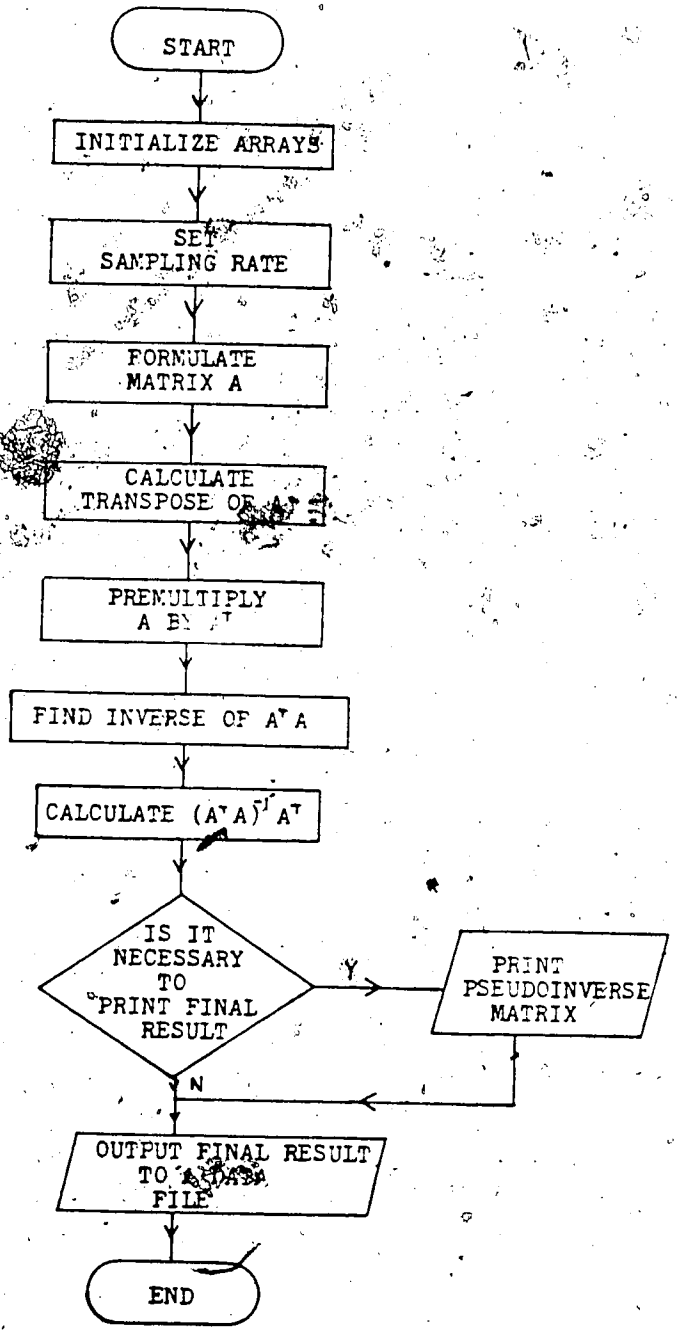

Figure 5.5 General flow chart of the program to calculate pseudoinverse matrix $A^{\dagger}$.

called. Figure 5.6 is the general flow chart of the program "loc.c". The inputs to the program are the pseudoinverse matrix, order of the employed filter, total line length, entire line impedance, and total number of post-fault samples along with the respective current and voltage values. Equations (3.42) and (3.43) are used to calculate the apparent impedance seen between the sending end of the line to the faulted point. The location of fault is then determined from the computed reactance ratio using equation (3.44). The final result is plotted on a X-Y plotter and if desired, printed on a line printer. From Figure 5.6, it has been observed that the program continuously locates the fault until the last set of nine samples has been employed. If a 4^{th} order filter is used in the program "model.c", nine successive samples are required for the impedance calculation. In the case of 8^{th} or 10^{th} order filter, every second sample is skipped to collect nine consecutive samples. This is necessary to simulate the sampling frequency of the fault location algorithm since its sampling frequency is half that of the digital filter.

5.5 Conclusion

This chapter has outlined the programs which have been developed in order to implement and test the proposed fault location algorithm. Flow charts are given to explain the details of the appropriate routines. The programs are programmed on a PDP-11 microcomputer to study the

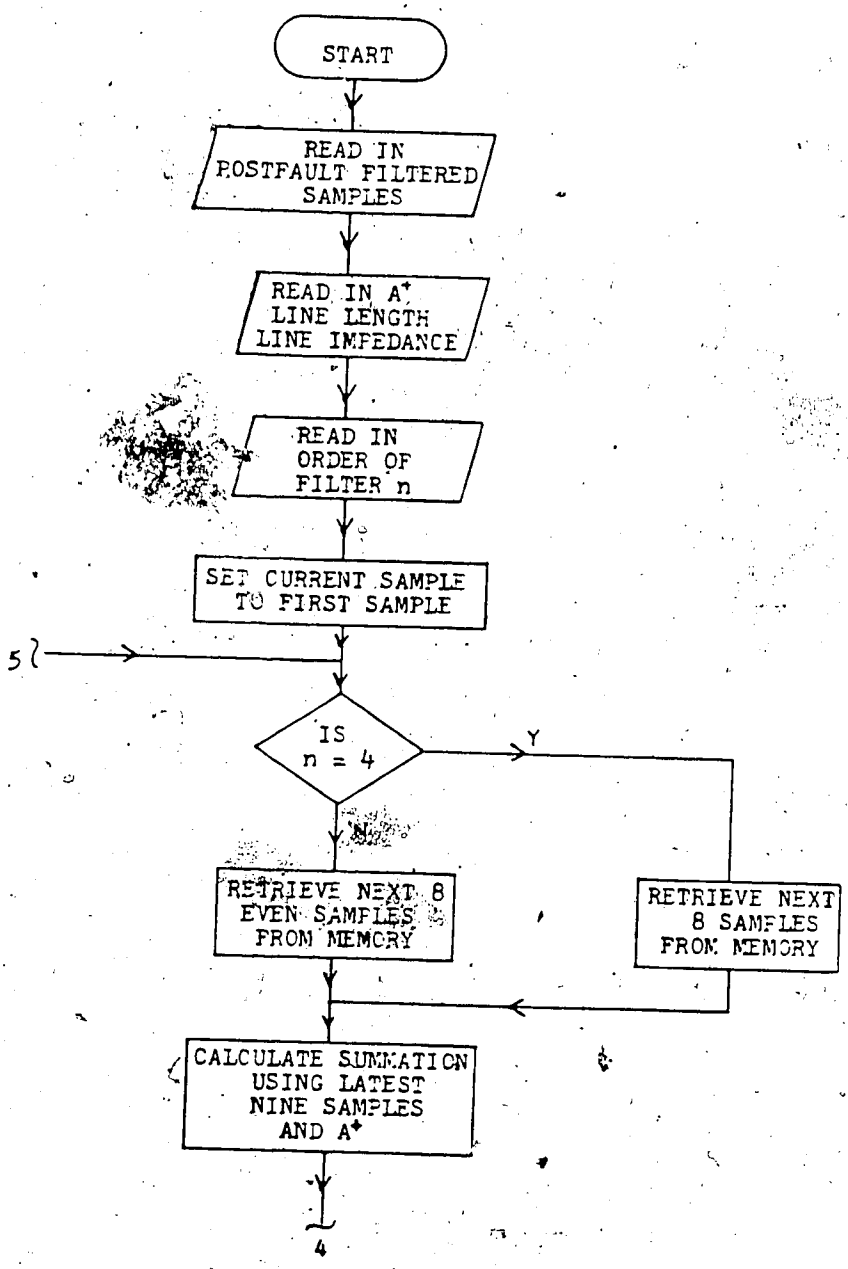

Figure 5.6 General flow chart of program "loc.c" (con'd).

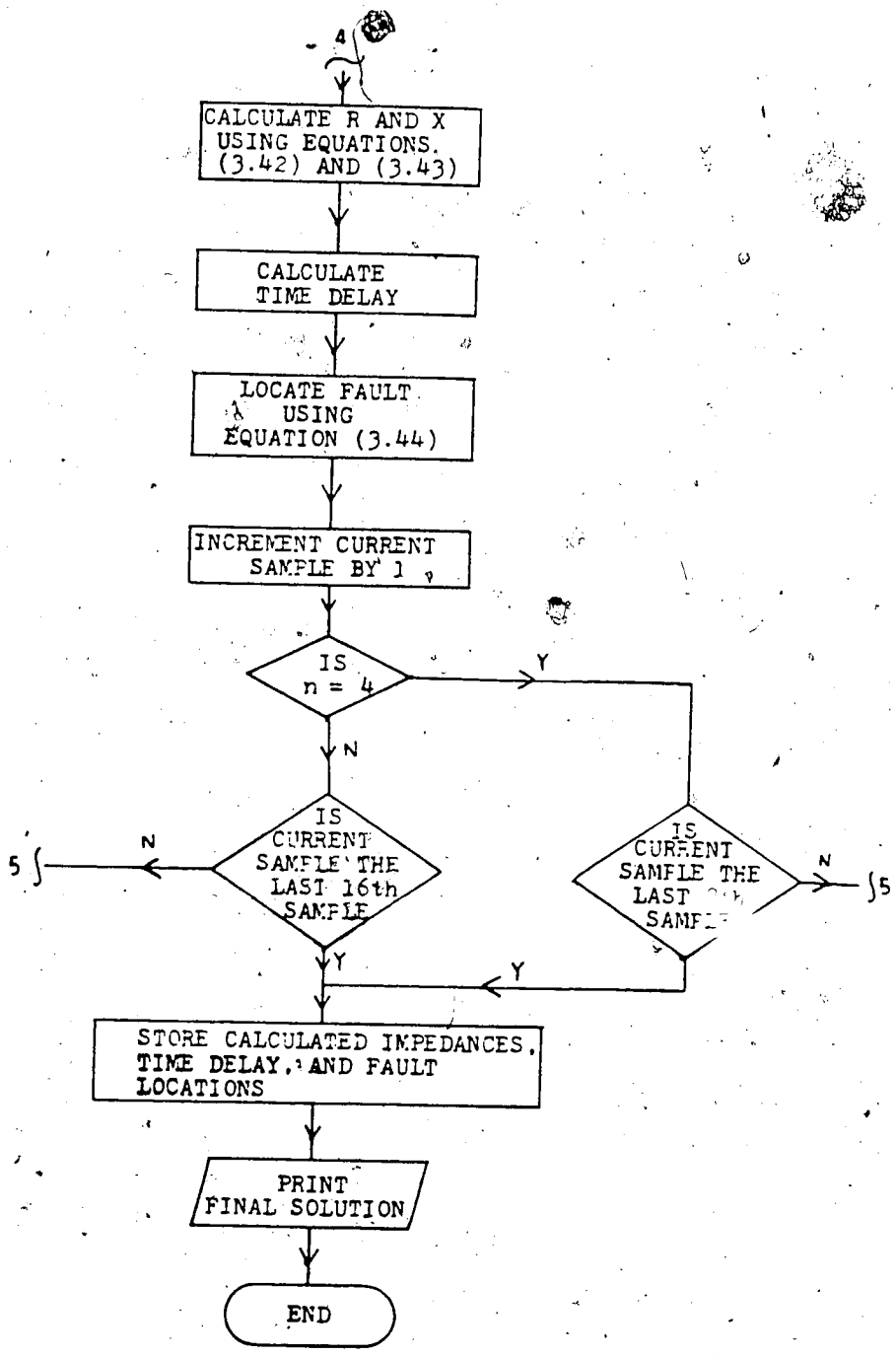

Figure 5.6 General flow chart of program "loc.c".

performance of the algorithm using differently ordered filters as applied to differently faulted systems. These studies will be presented in the next chapter.

CHAPTER VI

Performance of fault location algorithm

6.1 Introduction

The proposed fault location algorithm as described in the previous chapter was implemented using computer programs. Simple power transmission systems, which are outlined in Chapter 4, were simulated to obtain data for testing the fault location algorithms. The following sections in this chapter will present the performance of one of the algorithms under different conditions. These conditions include employment of different order low-pass filters, variation of fault location, presence of fault resistance and line shunt reactance in the faulted transmission line model.

The time response of the current and voltage signals, which are measured at the sending end of the studied power line, will also be given in this chapter. Once a fault occurs along the line, transients are produced in both the sending-end current and voltage. These transients are affected by both the location of fault and the instant of fault inception. In testing the algorithm, the fault is initiated at an instant such that the generated line to neutral voltage of the faulted phase has a phase angle of 240°. If necessary, the instant of fault inception can be easily varied by changing the appropriate input of the

program "model.c" as mentioned in Chapter 5.

Ideally, once a fault is initiated, both the collected current and voltage samples can be used in the calculations of impedance and fault distance. However, there is a delay of response associated with each filter and this causes a delay in acquiring samples by the fault location algorithm to perform the appropriate calculations. For example, if the third post-fault sample together with its eight successive samples are used as input data instead of using the first nine post-fault samples, a delay of two sampling intervals results for the corresponding fault distance estimation. This delay in locating a fault affects the performance of the algorithm to a great extent since a desired fault location algorithm has to locate the fault in the shortest possible time. In this chapter, the delay in acquiring data for calculating the fault location due to different order filters is studied. Figures of calculated fault distance versus delay are given. All these resulting distances are obtained from post-fault data with delay of at least 0.0125 s. If samples with a delay of less than 0.0125 s are used, the computed fault distances are very much different from the true distance and these meaningless results are not shown in the appropriate figures. Since the circuit breaker of the line is assumed to be tripped three cycles after the fault inception, the calculated locations shown in the figures of fault location versus delay are all based on samples collected within the first three post-fault cycles.

Calculated impedances under different testing conditions are also presented in this chapter. The impedances are plotted on R-X plots. In each plot, the impedances are calculated from different sets of samples by varying the delay in acquiring samples until the first three cycles of post-fault data have all been used. Similar to the estimated locations shown in the appropriate figures, the calculated impedances given in the R-X planes are all based on samples with not less than 0.0125 s of delay.

6.2 Single-phase test model

The single-phase power transmission system, which is outlined in Section 4.2.1, is used in studying the performance of the proposed algorithm. The algorithm is applied to a 30 mile-long overhead transmission line. A short-circuit ground fault is applied at a distance 10 miles from the sending end of the line. No resistance is involved in the short-circuit path. Theoretically, the impedance between the sending end and the faulted point is 5.44 + j 5.65 pu. Since there is no fault resistance and no line shunt reactance present in the faulted model, a high degree of accuracy is expected in the fault distance measurement.

The transient response of the faulted system before and after filtering are given in Figures 6.1 through 6.6. These figures are obtained by employing different ordered low-pass filters to suppress undesired harmonics from reaching the

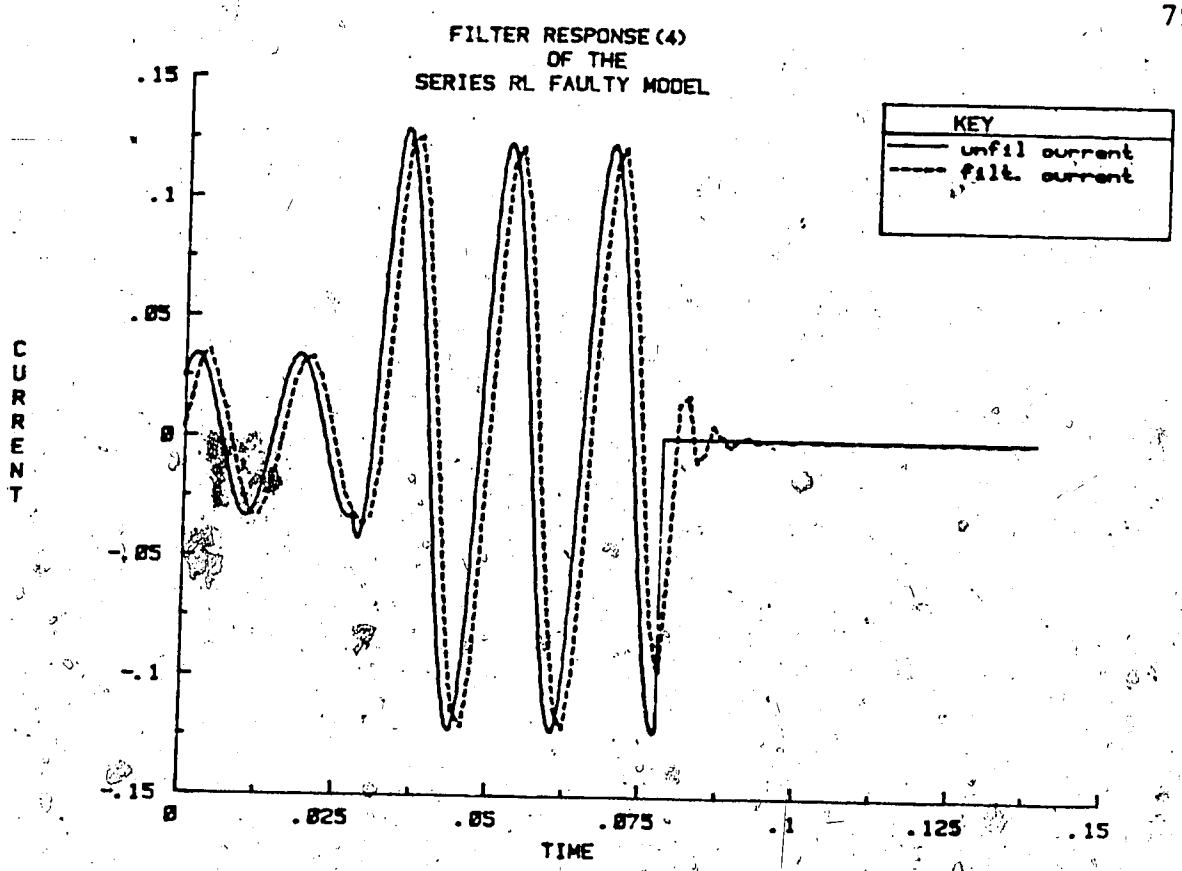

Figure 6.1 Time response of the pre-filtered and post-filtered current signal using 4th order filter - series model.

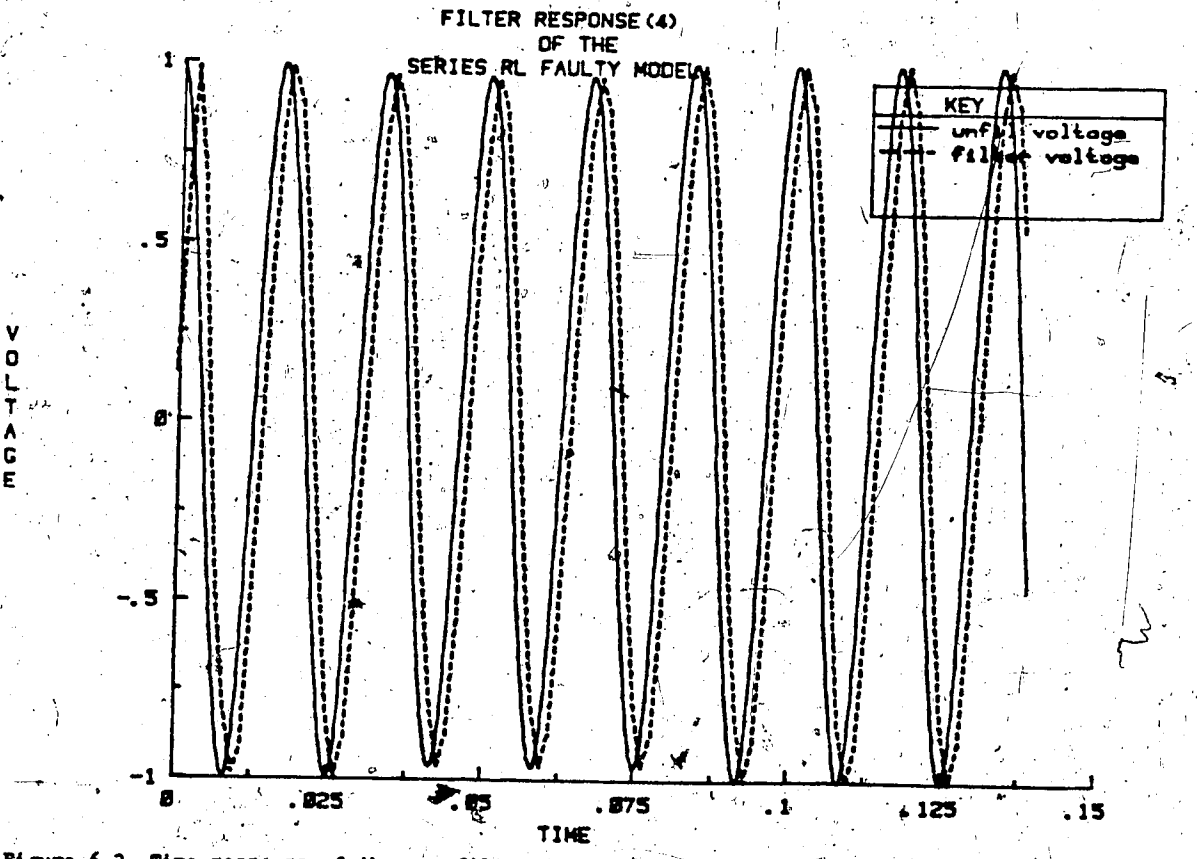

Figure 6.2 Time response of the pre-filtered and post-filtered voltage signal using 4th order filter - series model.

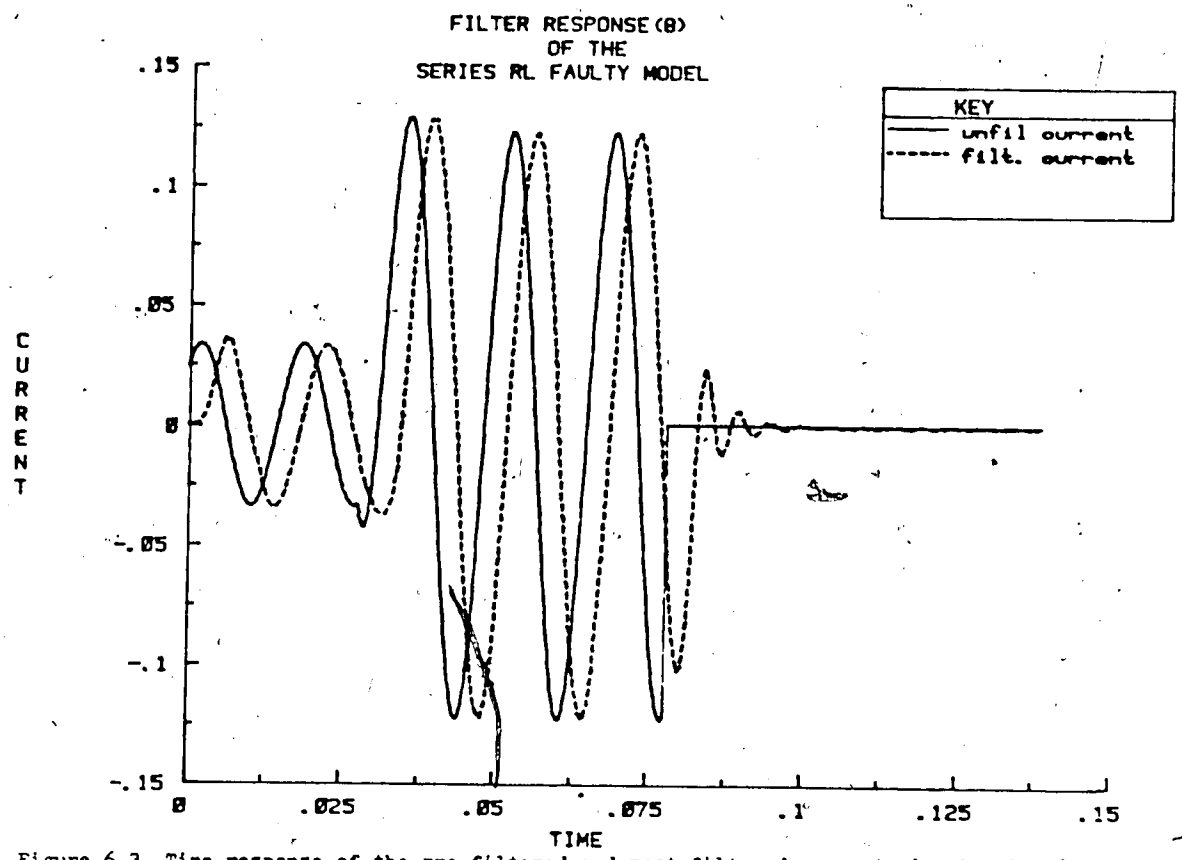

Figure 6.3 Time response of the pre-filtered and post-filtered current signal using 8th order filter - series model.

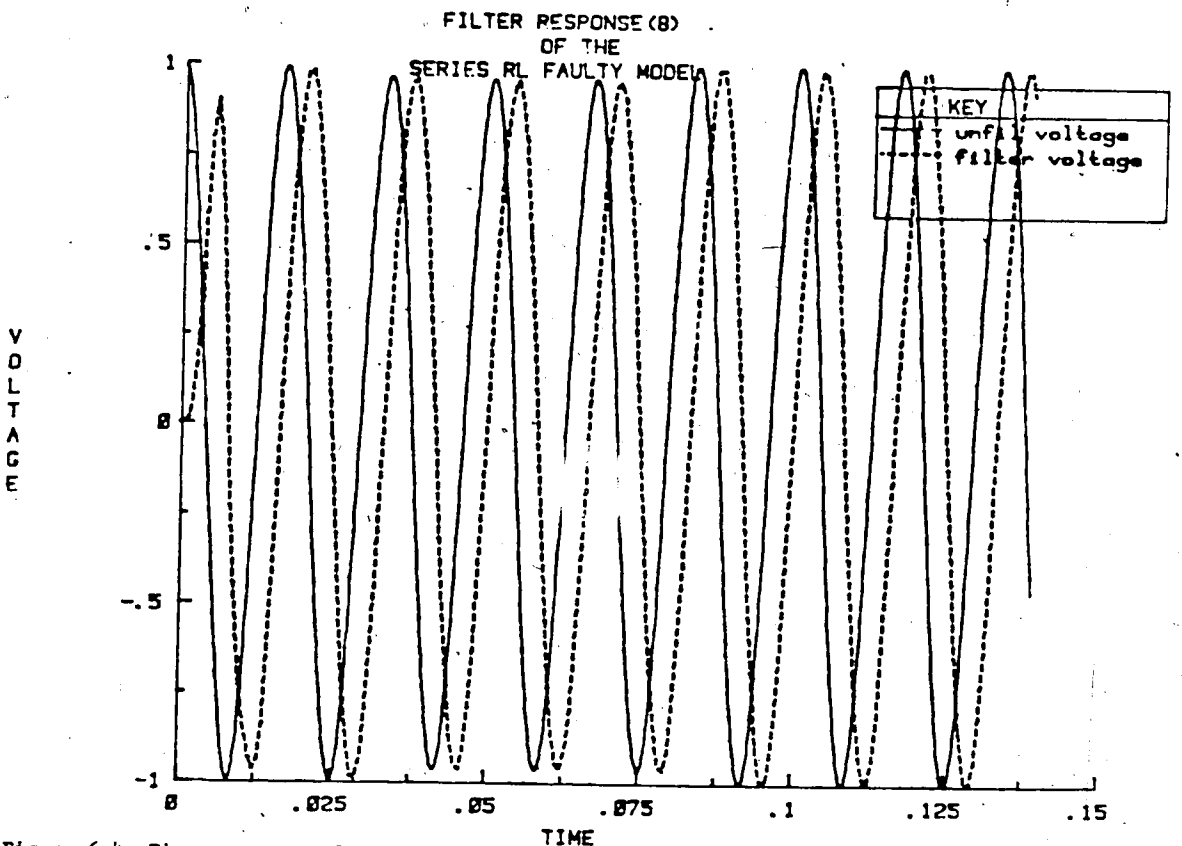

Figure 6.4 Time response of the pre-filtered and post-filtered voltage signal using 8 order filter - series model.

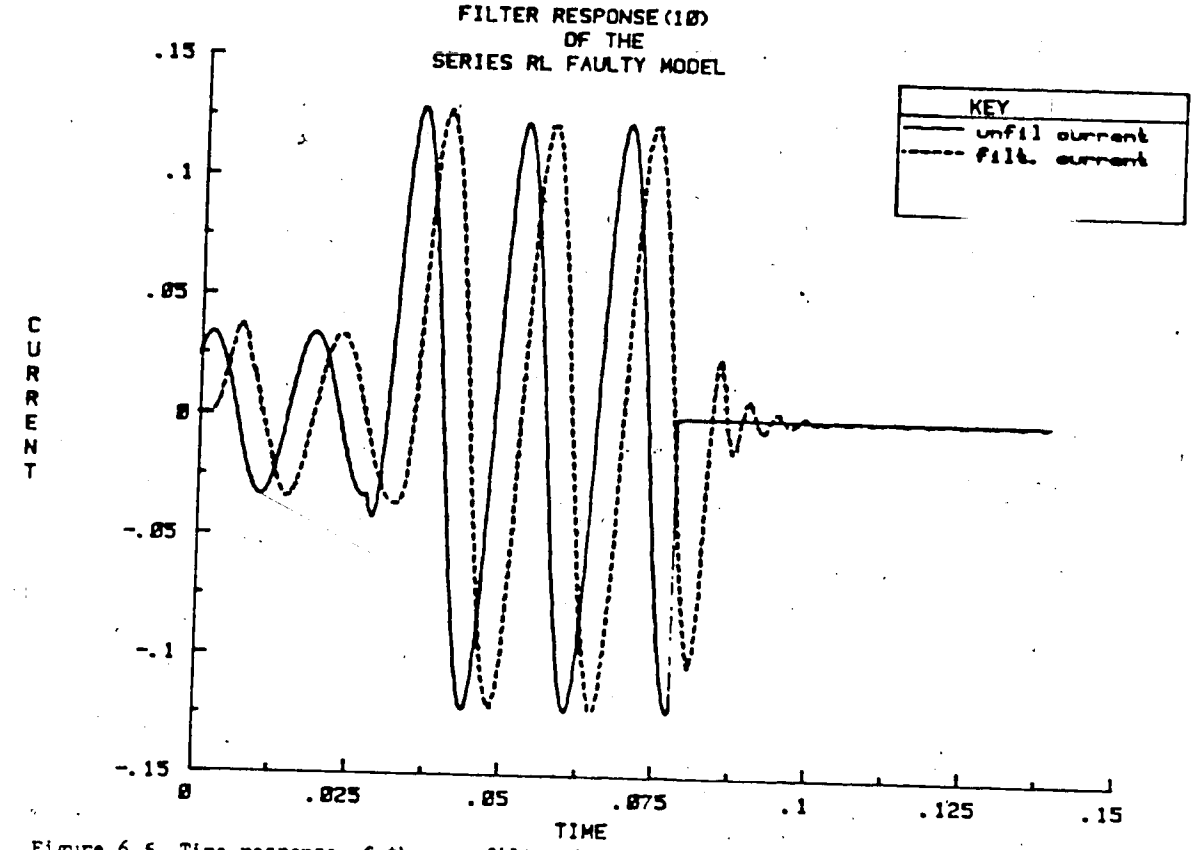

Figure 6.5 Time response of the pre-filtered and post-filtered current signal using 10th order filter - series model.

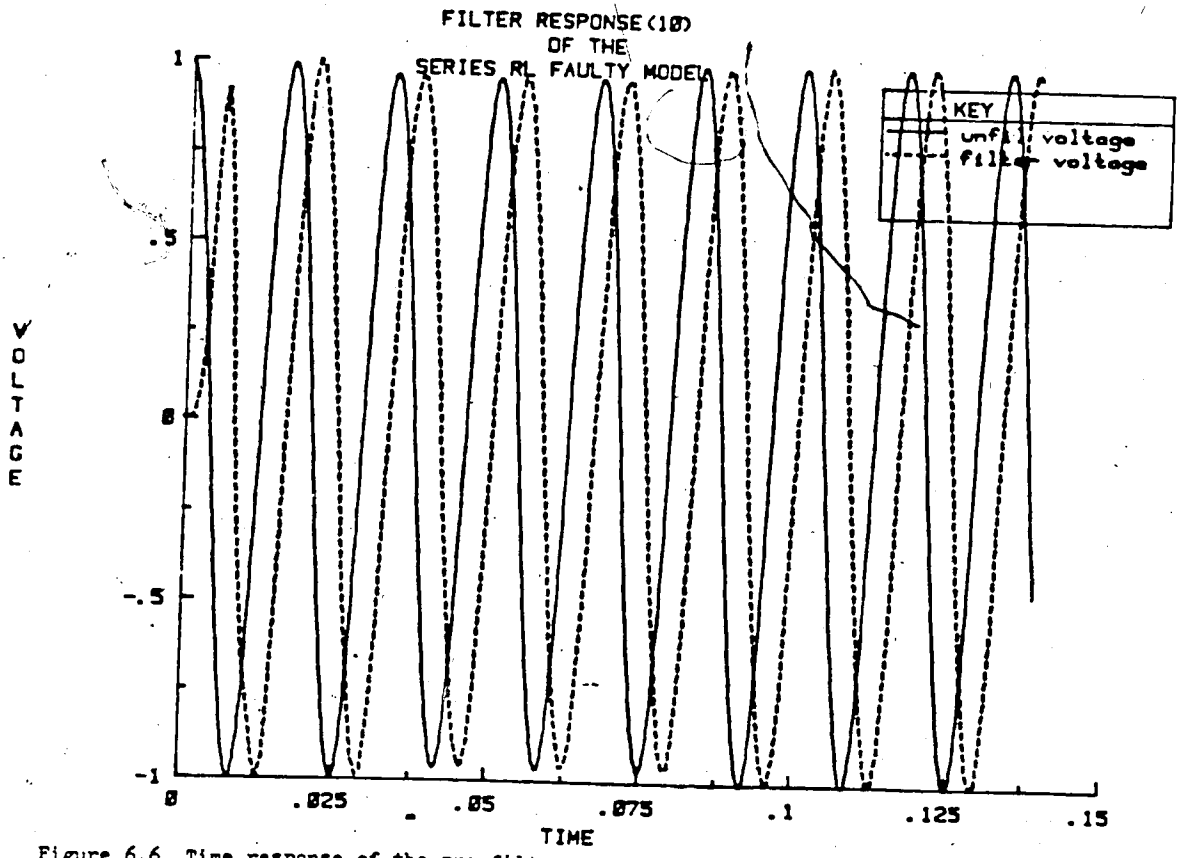

Figure 6.6 Time response of the pre-filtered and post-filtered voltage signal using 10th order filter - series model.

algorithm. From these figures, it has been observed that no high frequency component is present in the unfiltered post-fault waveform. In this special case, a low-pass filter is not necessary in testing the algorithm. However, a filter is still employed as an added safeguard. Considering the post-fault current response, the peak magnitude is almost three times that of the pre-fault value. This large current causes overheating to the system components if the fault is not cleared in the shortest possible time.

Figures 6.7 and 6.8 show graphs of calculated fault distance versus delay and the corresponding calculated impedances respectively when a 4th order filter is incorporated with the fault location algorithm. It has been observed that if samples with a delay of at least 0.0275 s are used, the corresponding estimated fault location is very close to the true value of 10 miles. Longer delay increases the accuracy of the final result. The calculated impedances converge to the true impedance of 5.44 + j 5.65 pu as shown in Figure 6.8 if longer delay is permitted.

The performance of the algorithm, when an 8th order filter is employed, is given in Figures 6.9 and 6.10. If a delay of at least 0.029 s is allowed in acquiring samples by the algorithm, both the calculated impedance and estimated fault distance are almost equal to their respective true values.

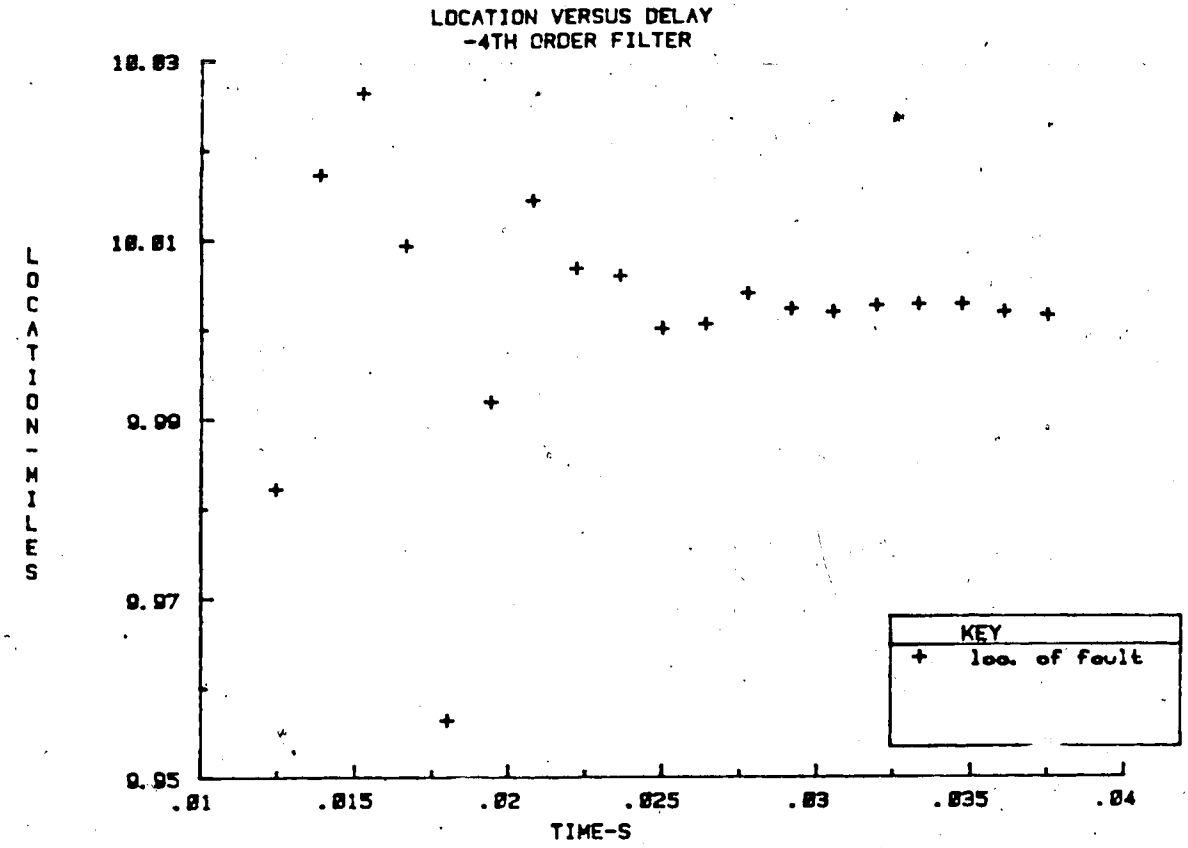

Figure 6.7 Plot of fault location versus delay - series model and 4th order filter.

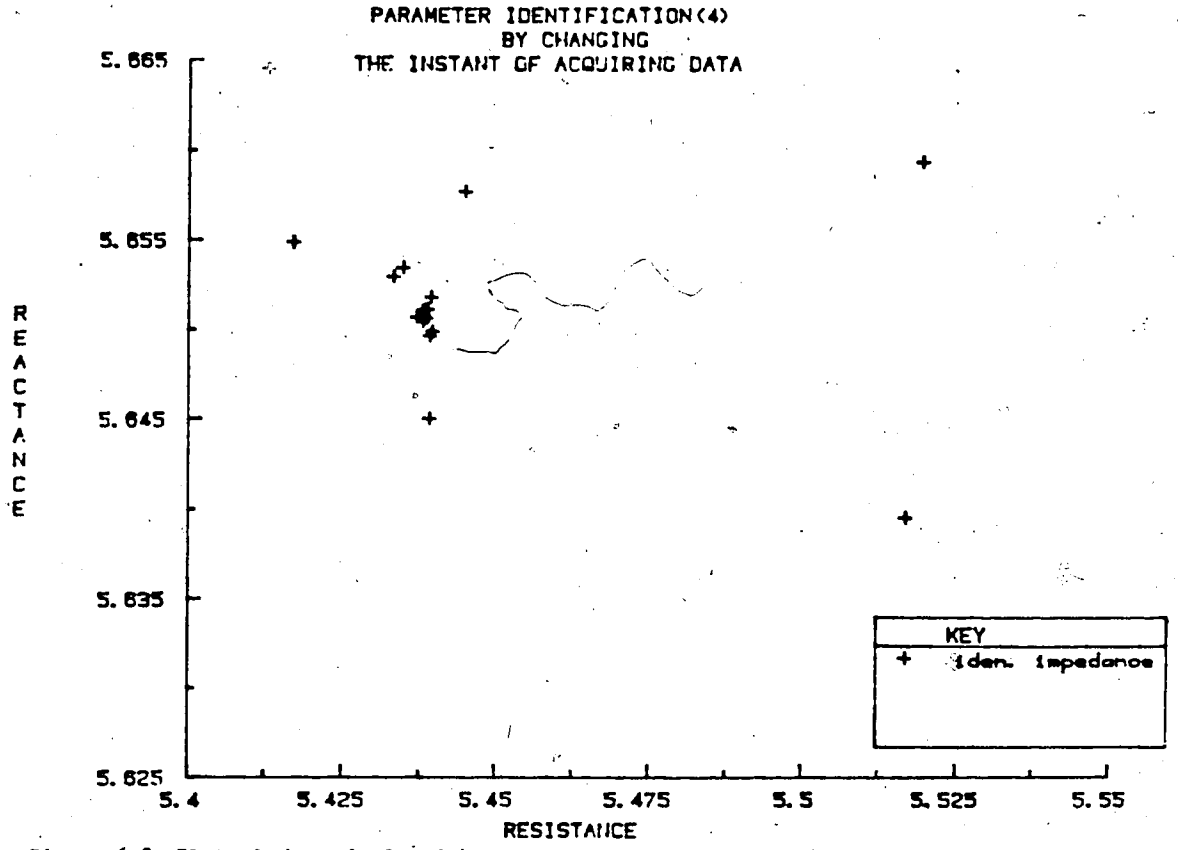

Figure 6.8 Plot of the calculated impedances - series model and 4th order filter.

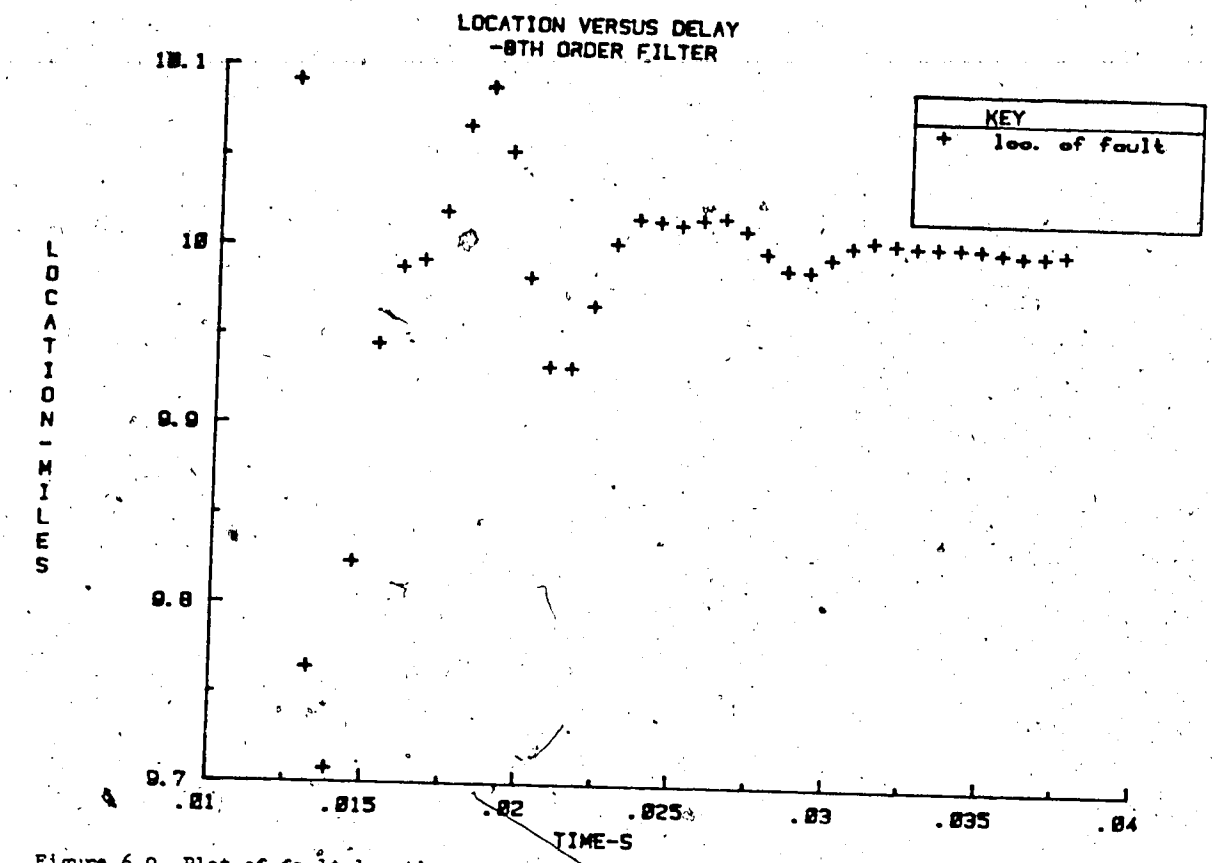

Figure 6.9 Plot of fault location versus delay - series model and 8th order filter.

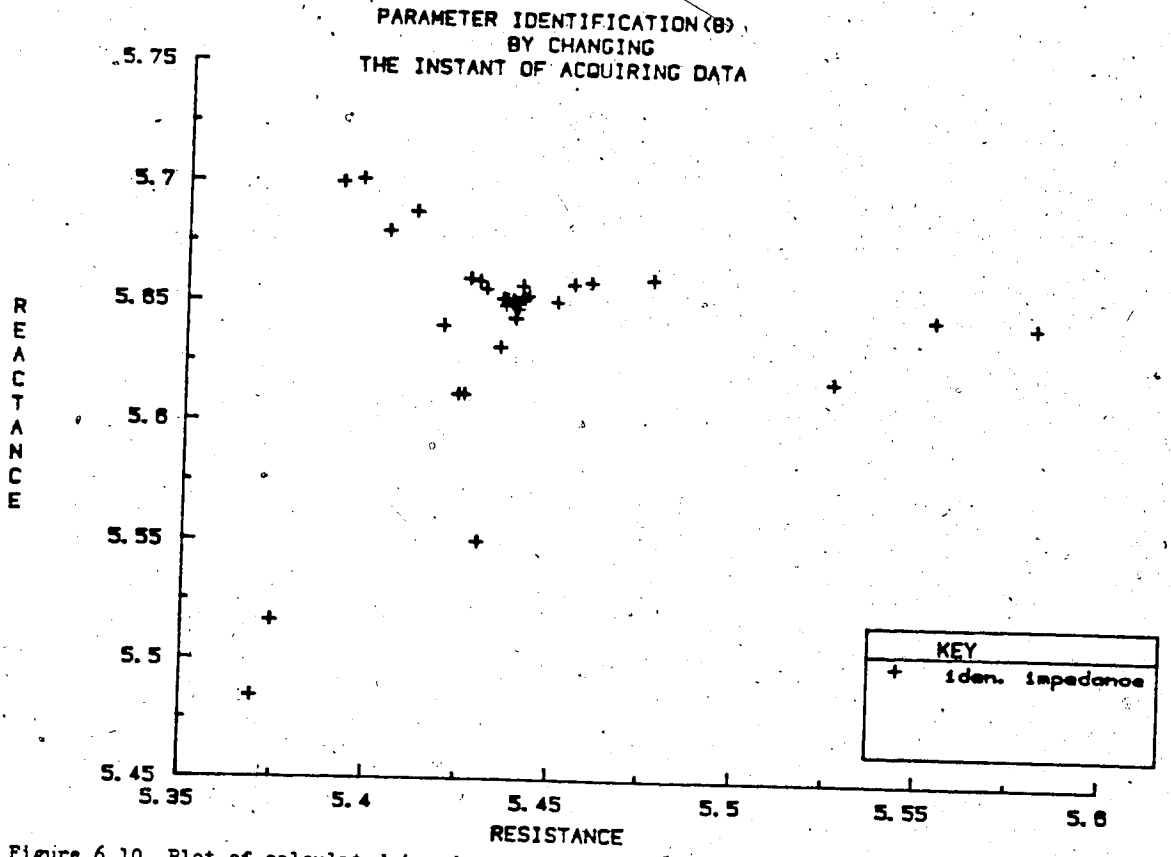

Figure 6.10 Plot of calculated impedances - series model and 8th order filter.

The solutions of the fault location and impedance calculations are plotted on Figures 6.11 and 6.12 respectively for the case when a 10th order filter is used in the testing. The simulated results compare well with the true values if the corresponding calculations are based on input samples collected at least 0.032 s after the occurrence of the fault. If samples acquired before 0.032 s are used, the algorithm is inaccurate and the resultant impedances are scattered over the R-X plane as seen in Figure 6.12.

6.3 Three-phase test model

In Section 4.2.2, mathematical models of a simple three-phase power transmission system under both pre-fault and post-fault conditions are developed. These models are used in testing the validity of the proposed fault location algorithm. A three-phase 133.5 mile-long overhead transmission line is monitored by the algorithm. The line is modelled by three sections of an equivalent "pi" circuit. Three-phase ground faults occur along the line at distances of 44.5 miles, 89 miles and 133.5 miles from the sending end of the line. The effect of non-zero fault resistance on the accuracy of the algorithm is also studied. This non-zero resistance ground fault occurs at a location 44.5 miles from the generating terminal of the line.

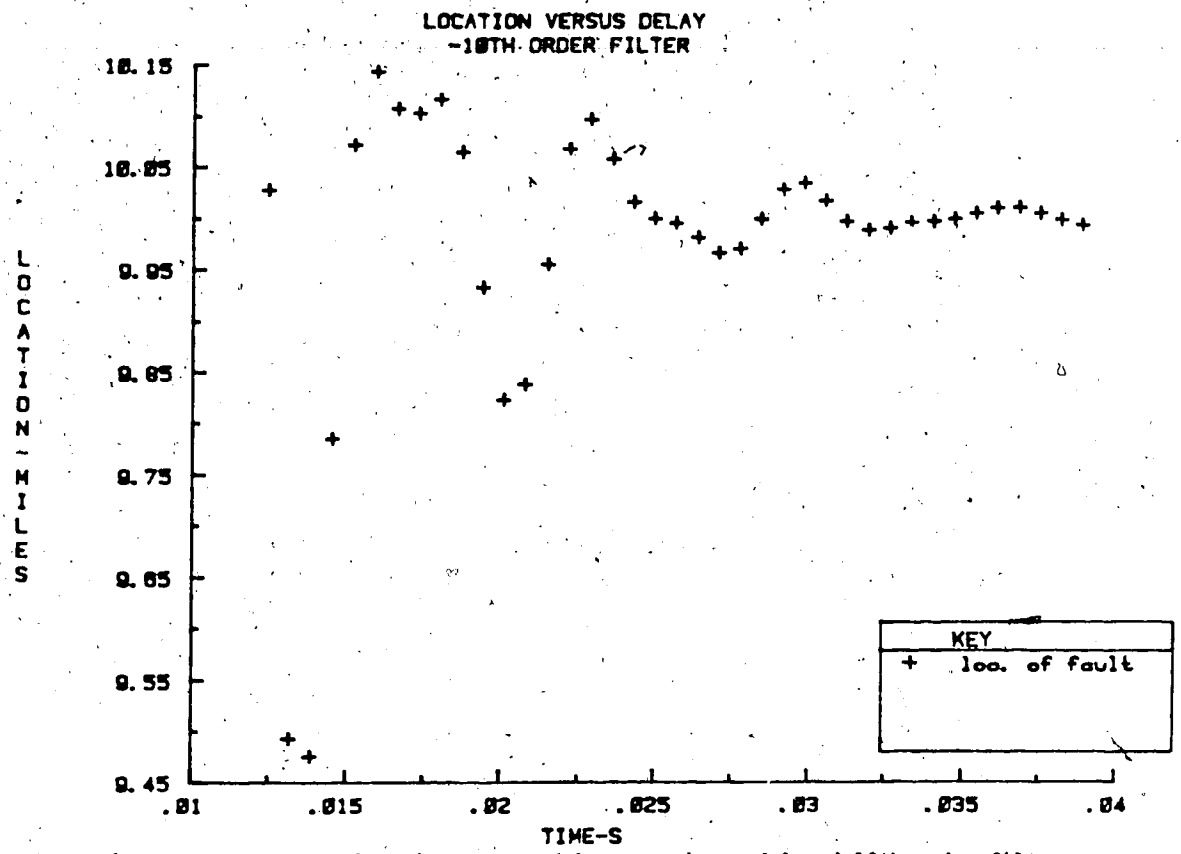

Figure 6.11 Plot of fault location versus delay - series model and 10th order filter.

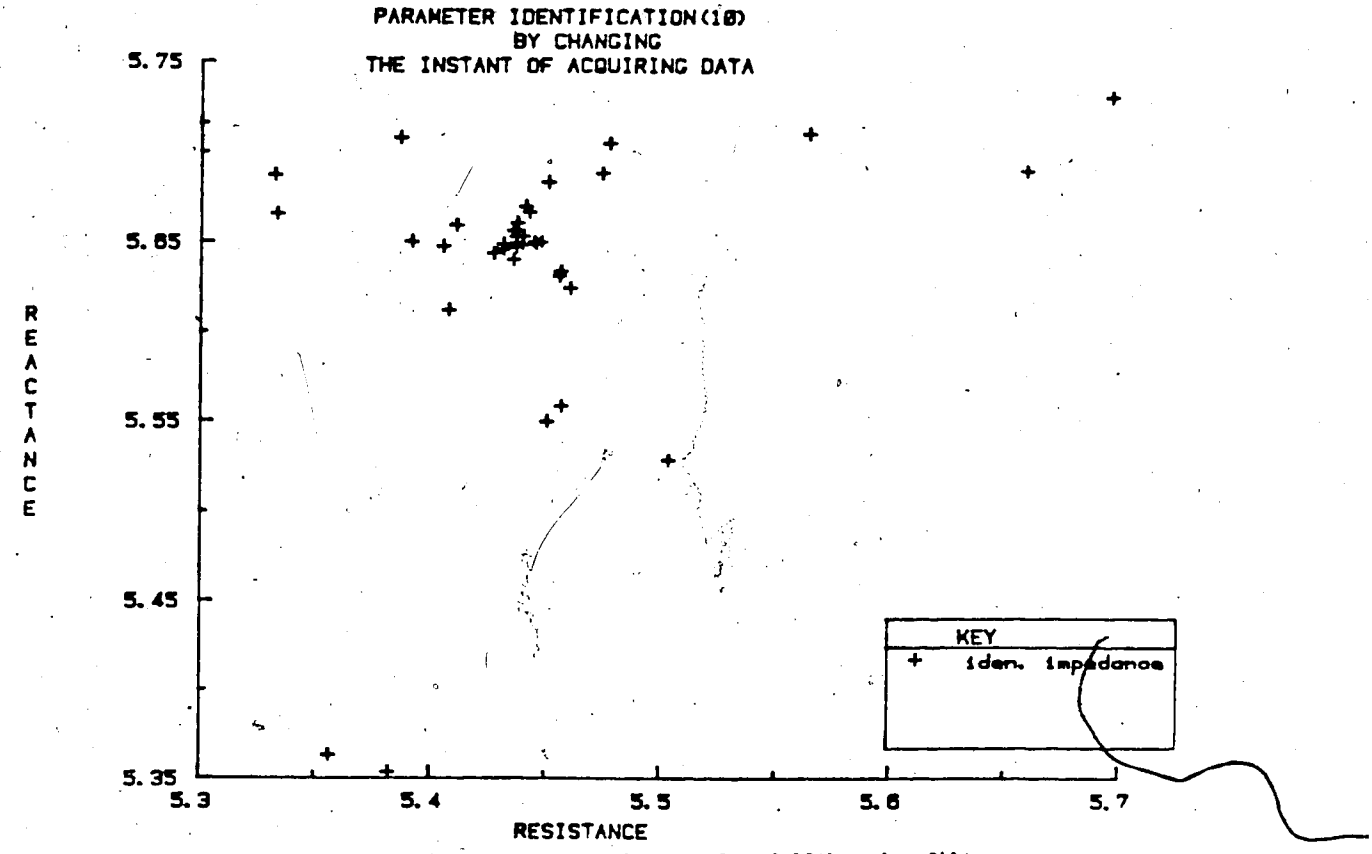

Figure 6.12 Plot of calculated impedances - series model and 10th order filter.

The unfiltered and filtered responses of the test system prior to and after the occurrence of a fault are given in Figures 6.13 through 6.18. The various Figures are obtained by varying the location of fault. The responses shown in these Figures correspond to the case when an 8^{th} order filter is employed for filtering purposes. Similar results are obtained using a 4^{th} order filter and a 10^{th} order filter, which are not given in this thesis. From Figures 6.13 through 6.18, it can be observed that both a decaying component and high frequency components are present in the pre-filtered post-fault transients. The high frequency components are especially noticeable in the voltage waveform when the line is subjected to a fault occurring at the sending end. The filtered responses, as shown in Figures 6.13 through 6.18, illustrate that the high frequency components have been suppressed. These indicate that the designed filter functions properly according to the design specifications.

The estimated locations and calculated impedances that result when using the proposed algorithm, together with different order filters, are given in Figures 6.19 through 6.24. These results are obtained when a fault is initiated at a distance 44.5 miles from the sending end of the monitored line. The measured distances agree favorably with the true fault location (44.5 miles) provided that a certain delay in acquiring data is permitted. The true impedance is 0.061 + j 0.236 pu and compares well with the calculated

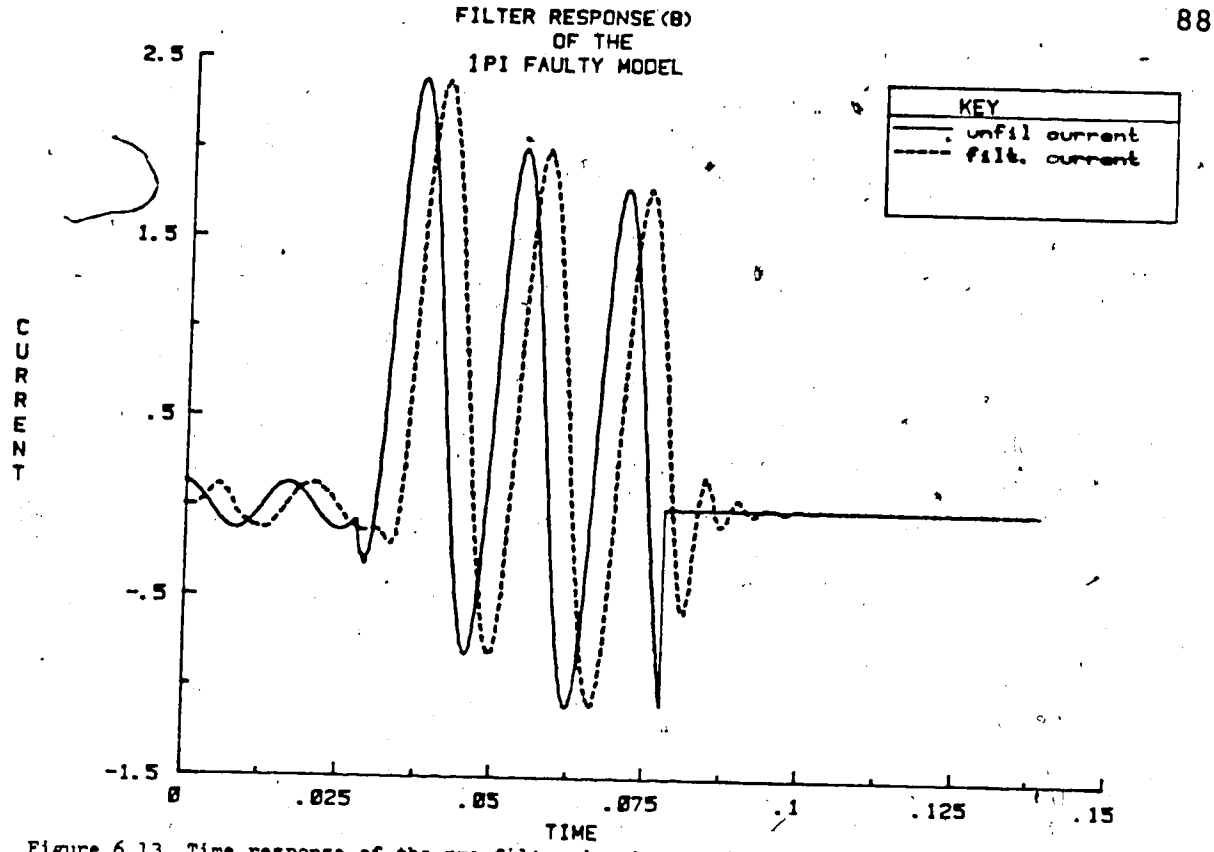

Figure 6.13 Time response of the pre-filtered and post-filtered current signal using 8th order filter - one pi faulted model.

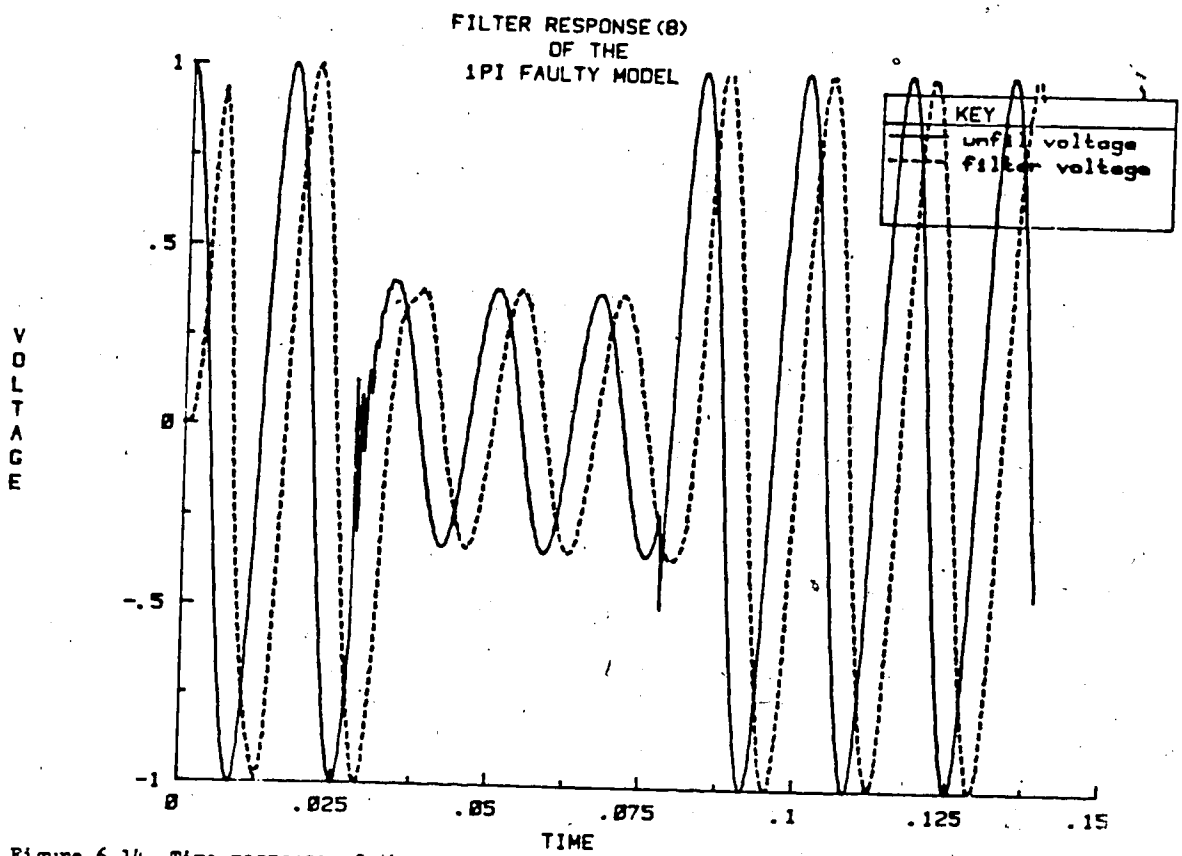

Figure 6.14 Time response of the pre-filtered and post-filtered voltage signal using 8th order filter - one pi faulted model.

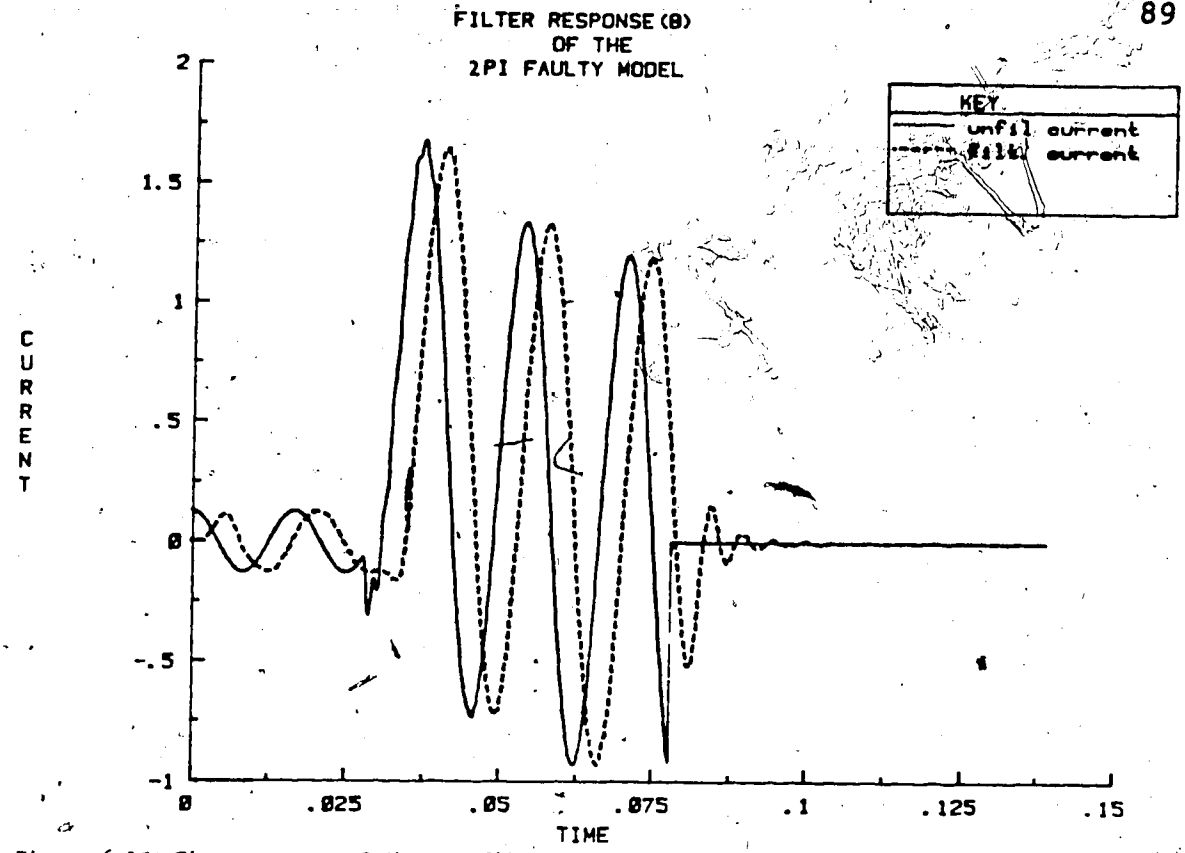

Figure 6.15 Time response of the pre-filtered and post-filtered current signal using 8th order filter - two pi faulted model.

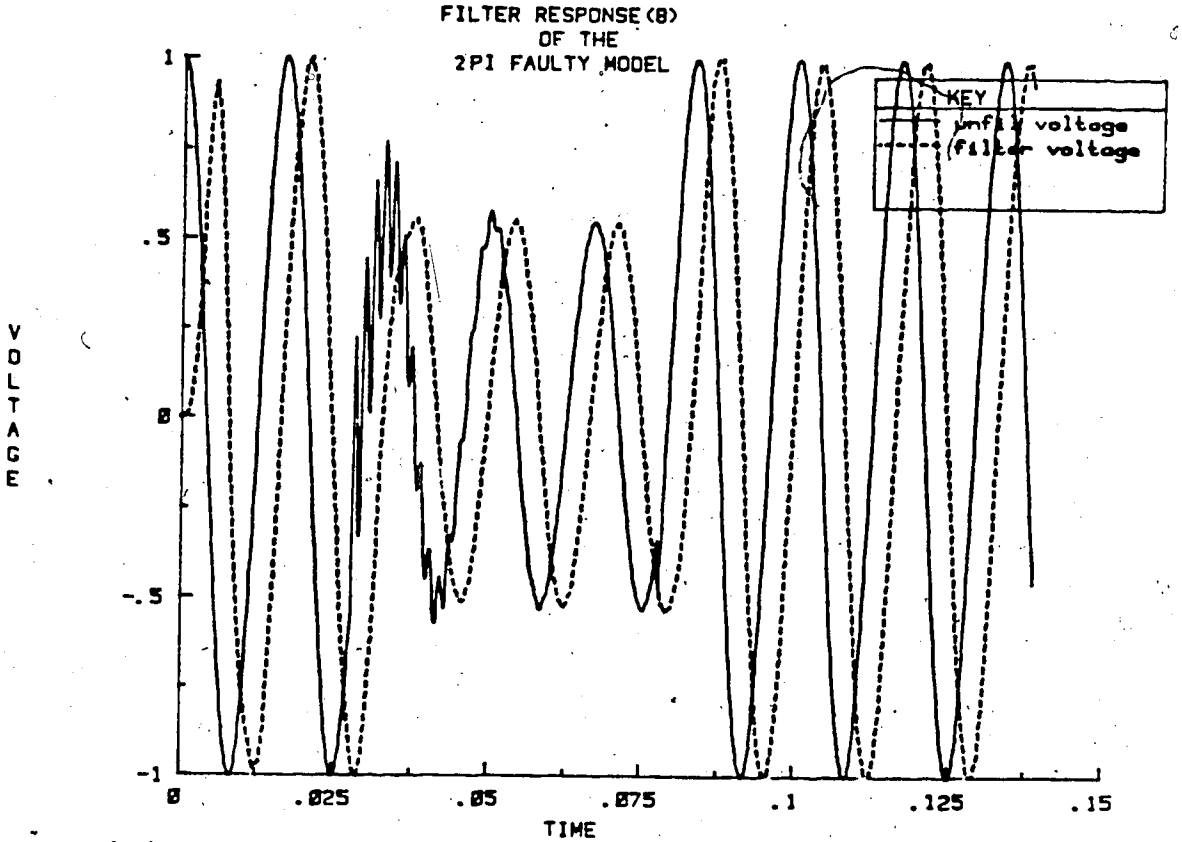

Figure 6.16 Time response of the pre-filtered and post-filtered voltage signal using 8th order filter - two pi faulted model.

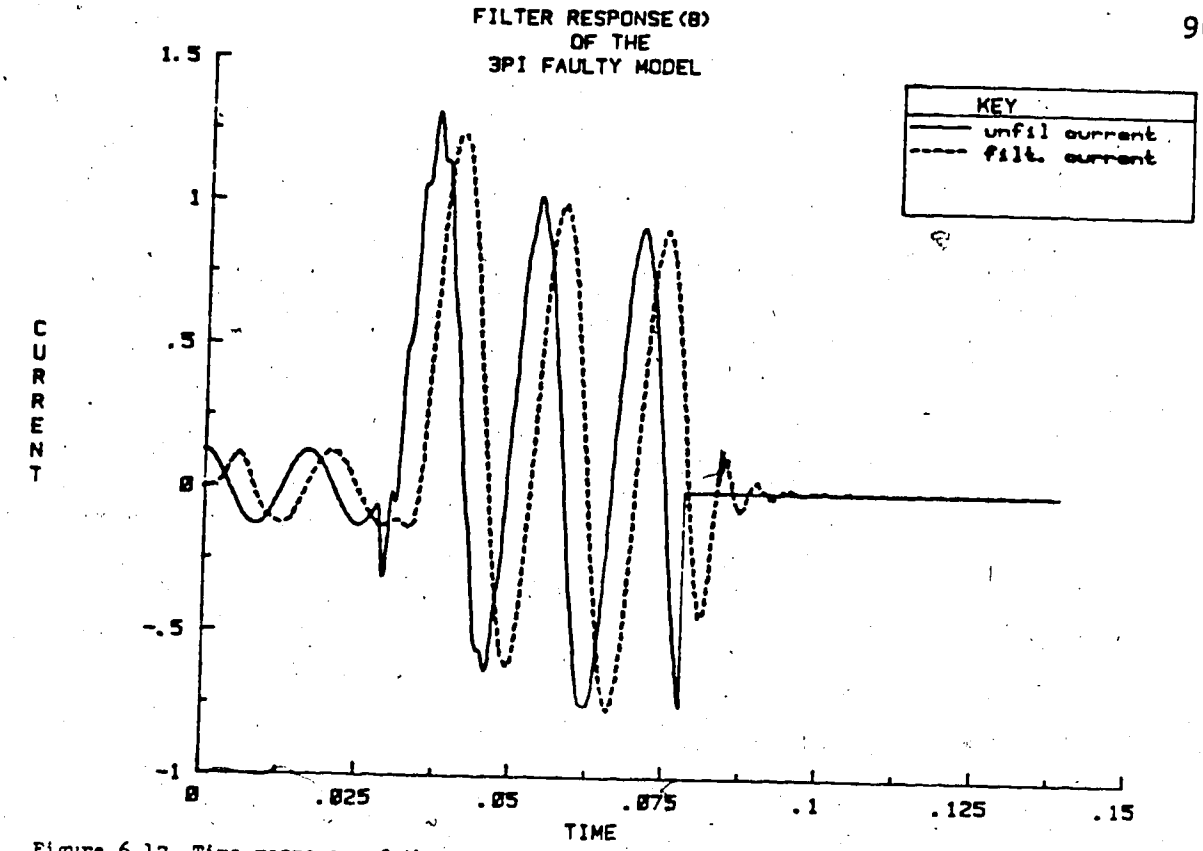

Figure 6.17 Time response of the pre-filtered and post-filtered current signal using 8th order filter - three pi faulted model.

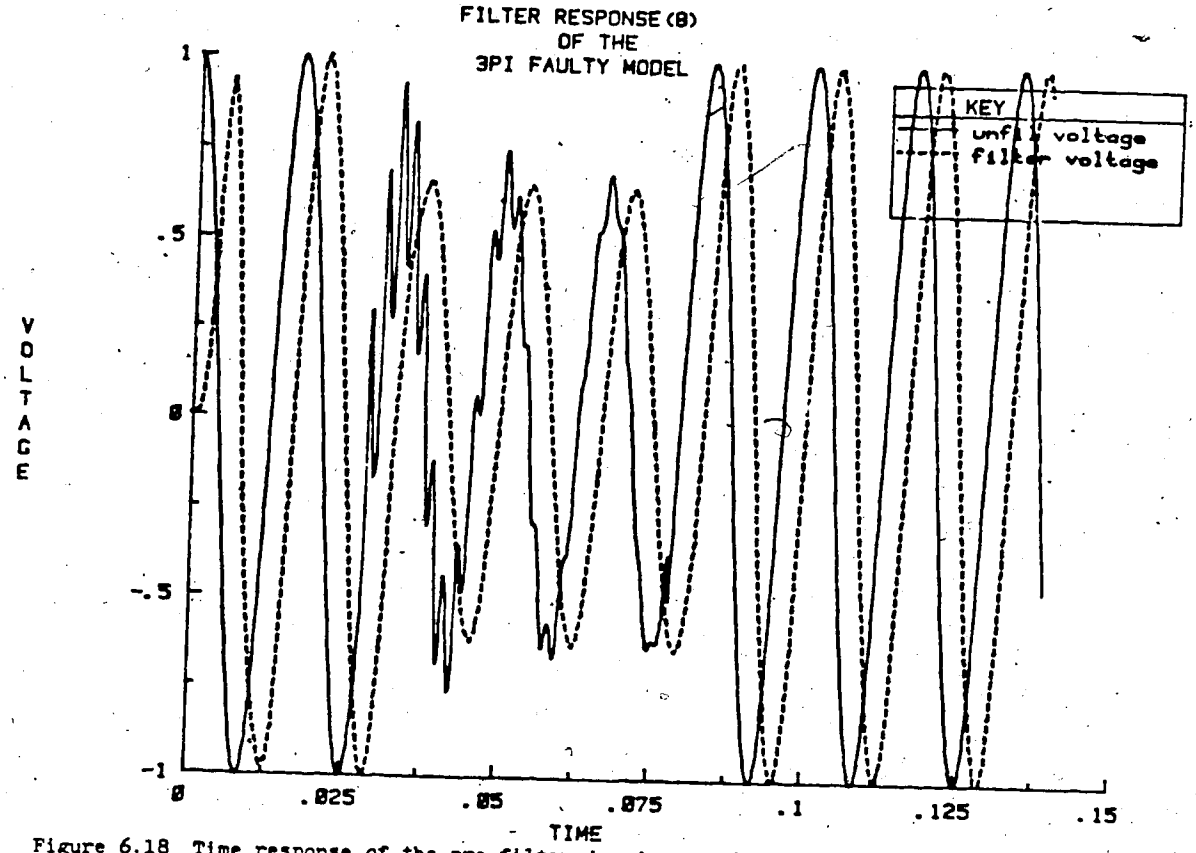

Figure 6.18 Time response of the pre-filtered and post-filtered voltage signal using 8th order filter - three pi faulted model.

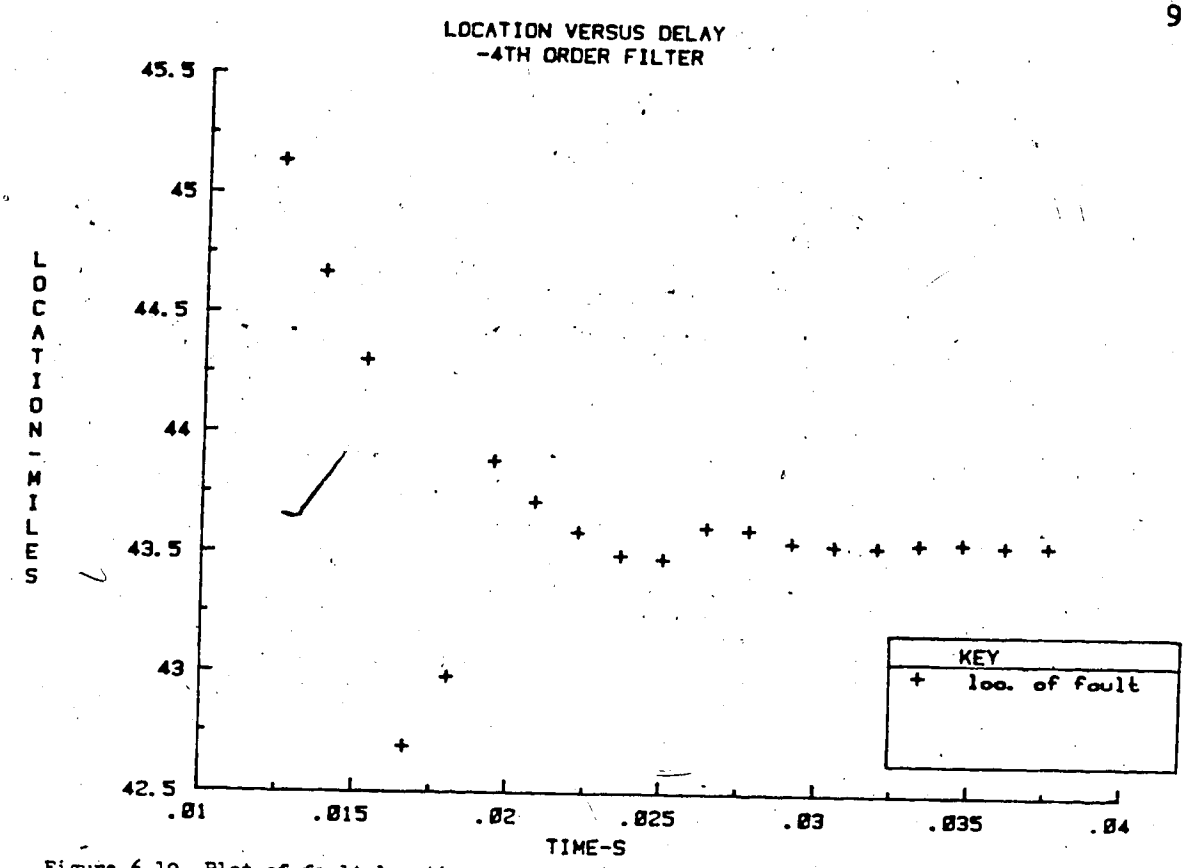

Figure 6.19 Plot of fault location versus delay - one pi faulted model and 4th order filter.

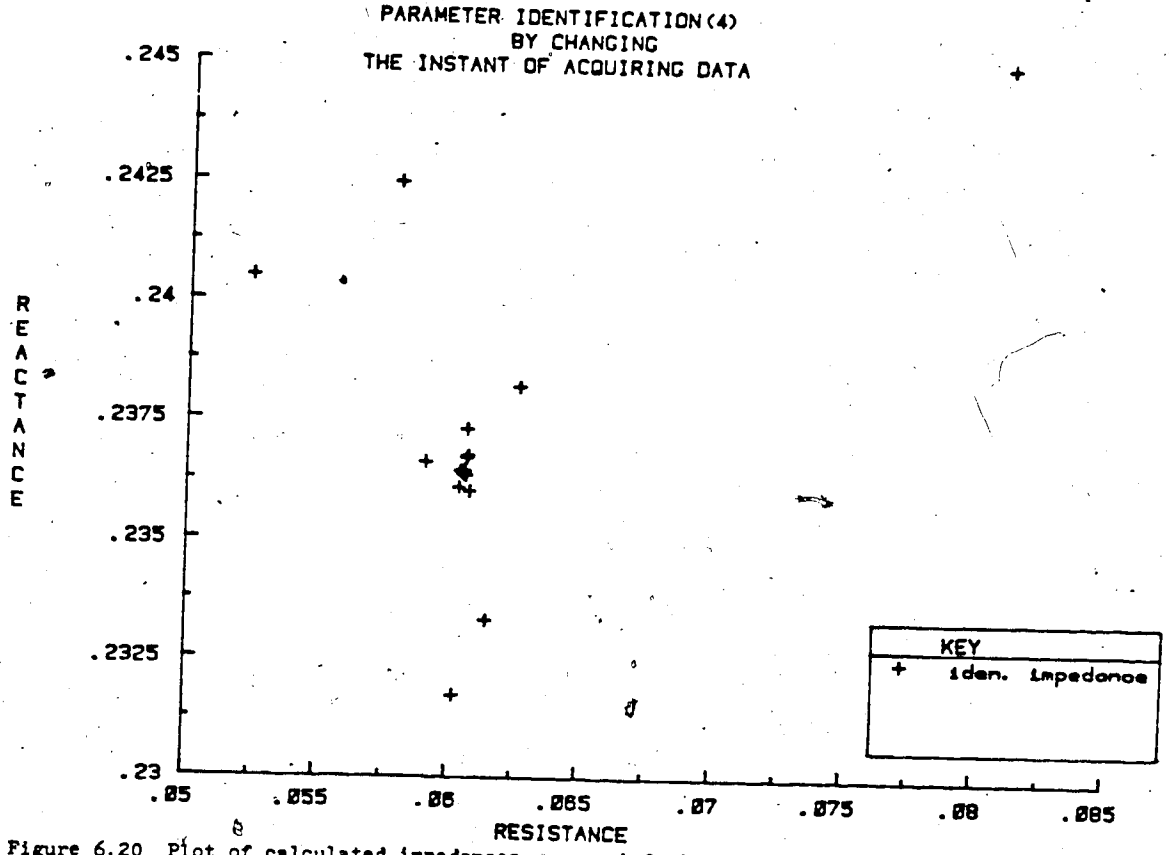

Figure 6.20 Plot of calculated impedances - one pi faulted model and 4th order filter.

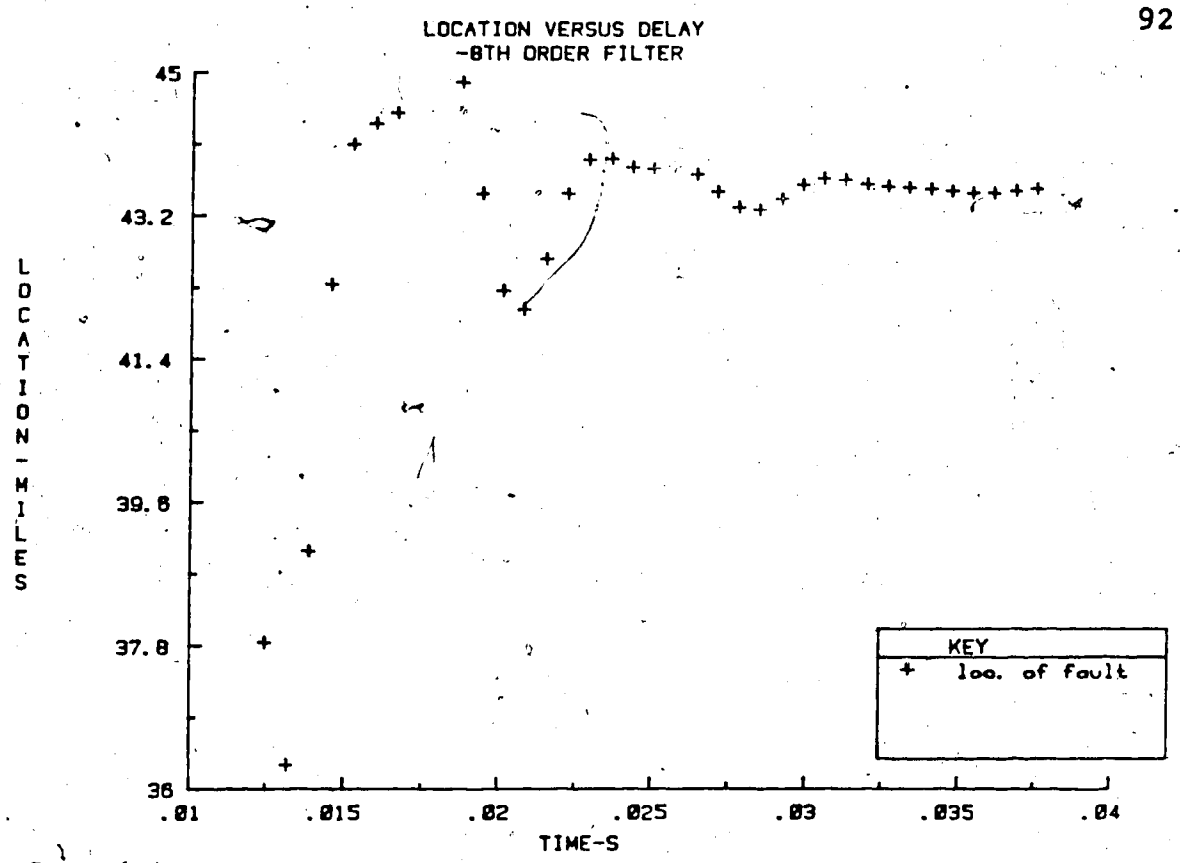

Figure 6.21 Plot of fault location versus delay - one pi faulted model and 8th order filter.

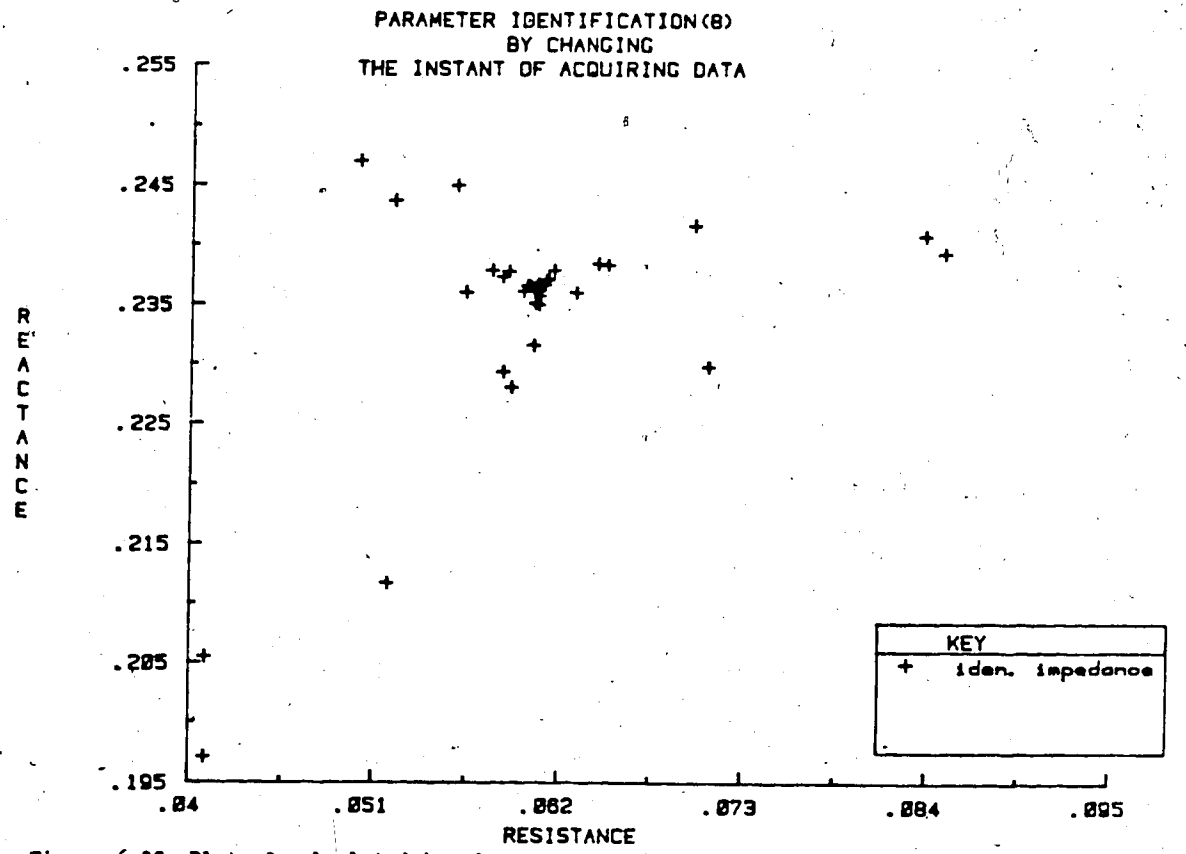

Figure 6.22 Plot of calculated impedances - one pi faulted model and 8th order filter.

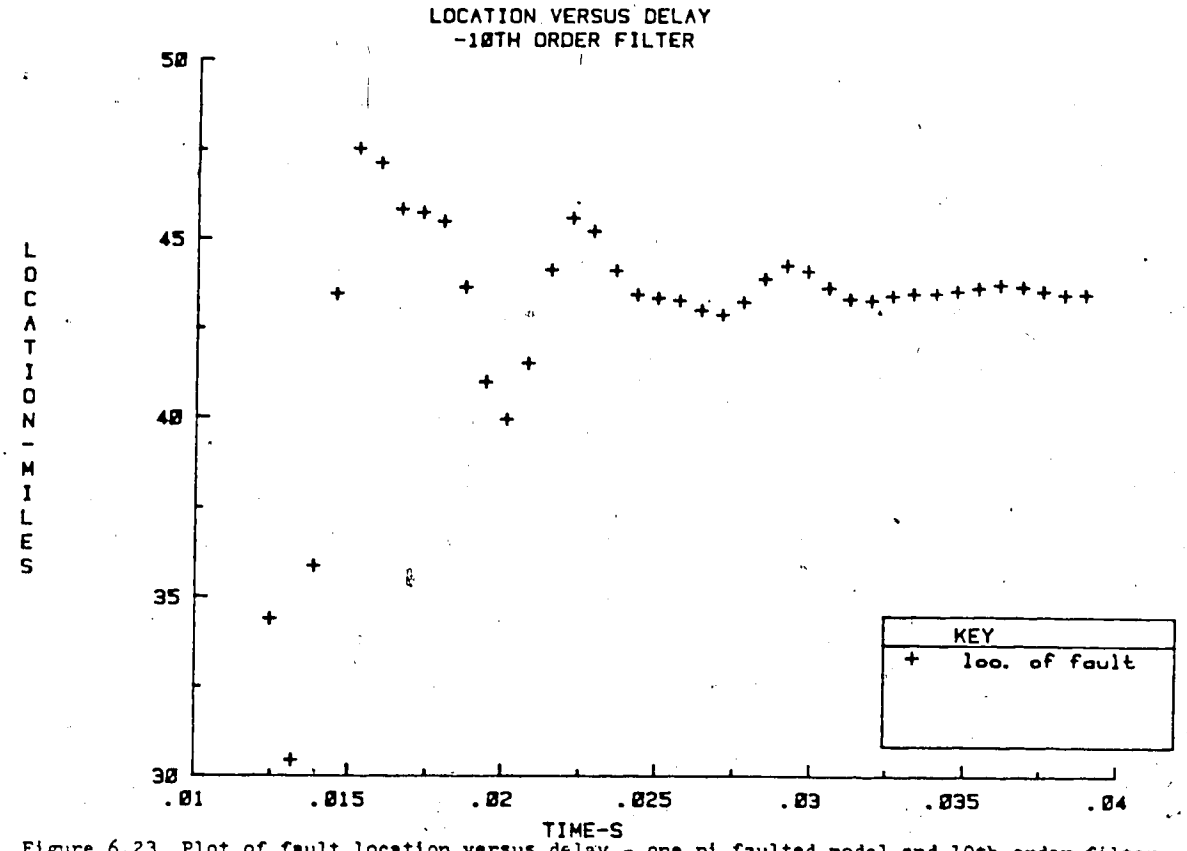

Figure 6.23 Plot of fault location versus delay - one pi faulted model and 10th order filter.

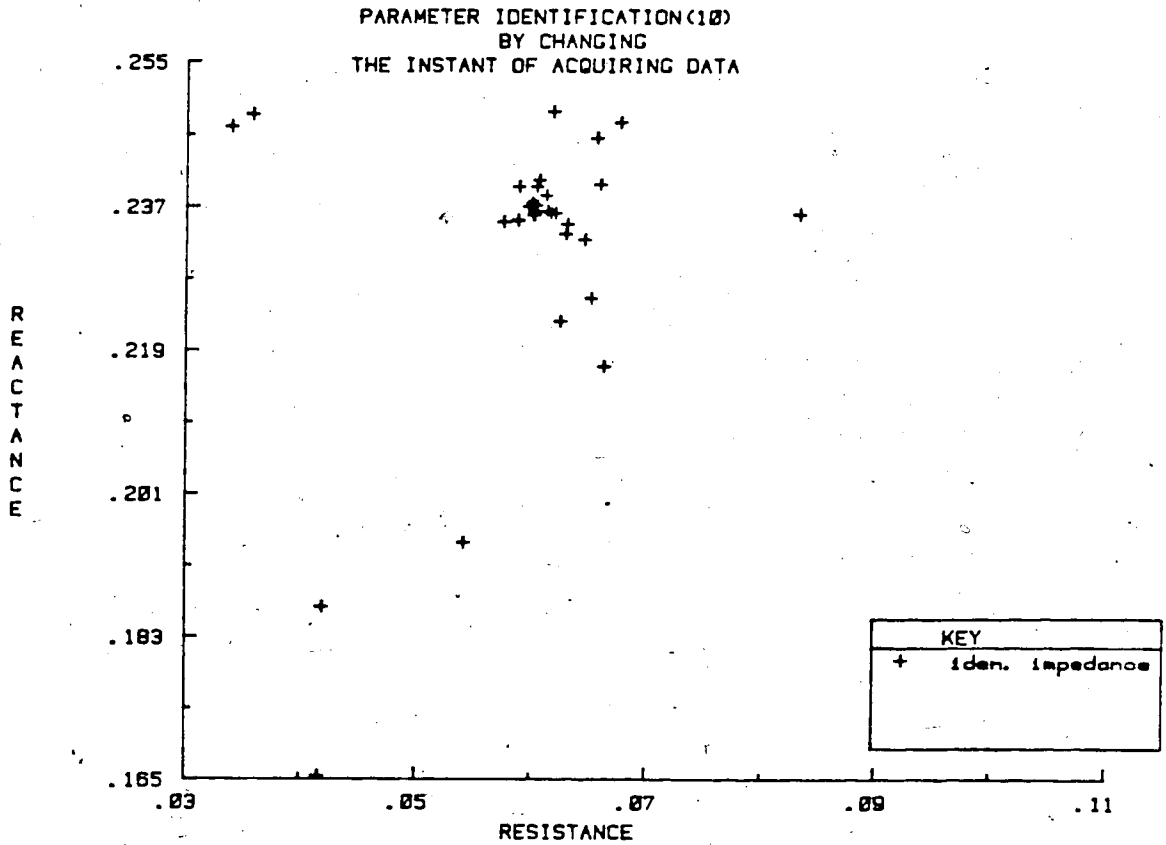

Figure 6.24 Plot of calculated impedances - one pi faulted model and 10th order filter.

impedances as seen in Figures 6.20, 6.22 and 6.24. As seen from Figures 6.19, 6.21 and 6.23, a minimum delay is necessary in order to have the calculated distance converge to a reasonable accuracy. This minimum delay varies between different ordered filters and is longer for higher ordered filters.

The results of the fault location and impedance calculation shown in Figures 6.25 through 6.30 are for the case where a fault occurs at a distance 89 miles from the generating terminal. The computed locations and impedances are within the desired accuracy when compared to the true values. Among the three filters, the 10^{th} order filter gives the highest accuracy in locating a fault although a longer delay is needed to have the final result converge.

Figures 6.31 through 6.36 illustrate the performance of the algorithm if a fault is present at the receiving end of the simulated line. The performance is acceptable for both the 8^{th} order filter case and 10^{th} order filter case as shown in Figures 6.33 through 6.36. Both the fault location and calculated impedance converge to the desired values. However, the final result of the 4^{th} order filter case is not satisfactory. The calculated impedances scatter all over the R-X plane and the computed locations do not converge to the true value. One possible explanation to this undesired effect is that the high frequency components present in the post-fault waveforms are not completely eliminated by the

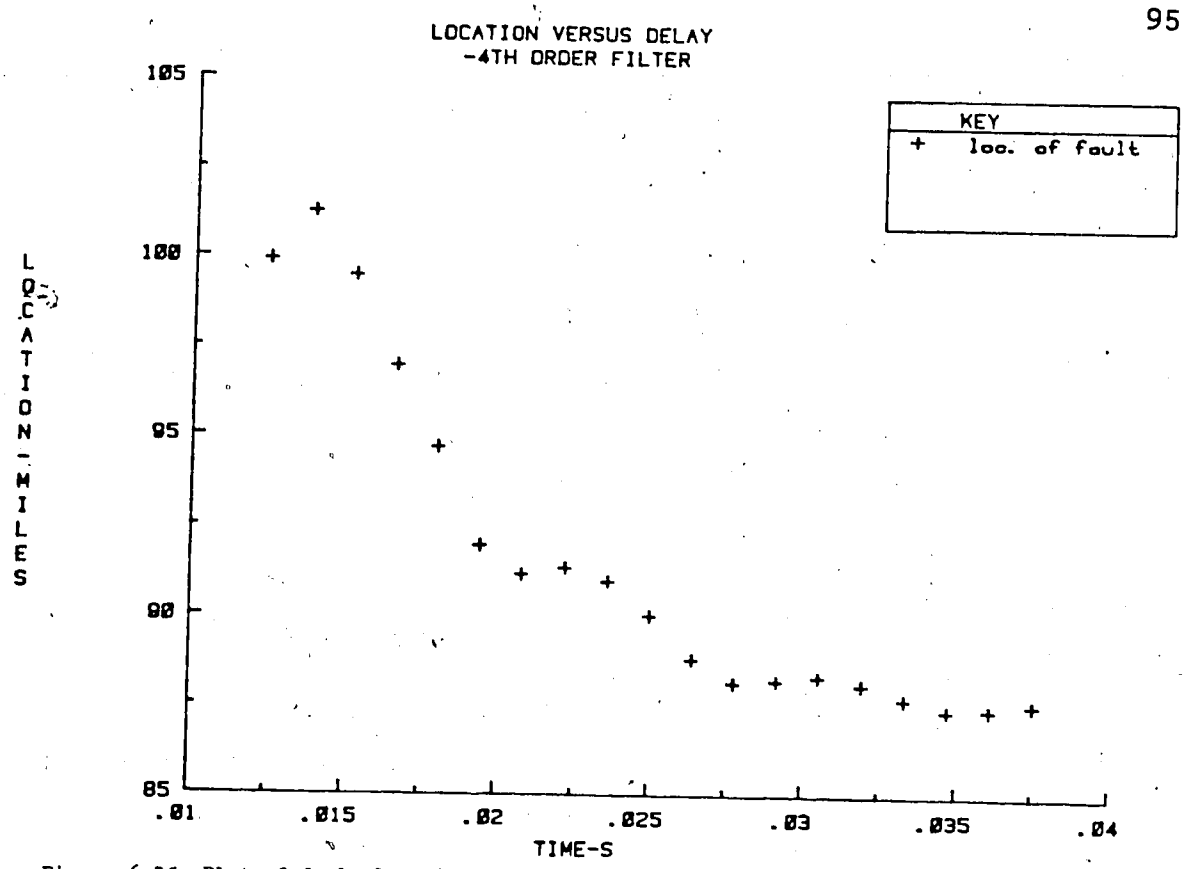

Figure 6.25 Plot of fault location versus delay - two pi faulted model and 4th order filter.

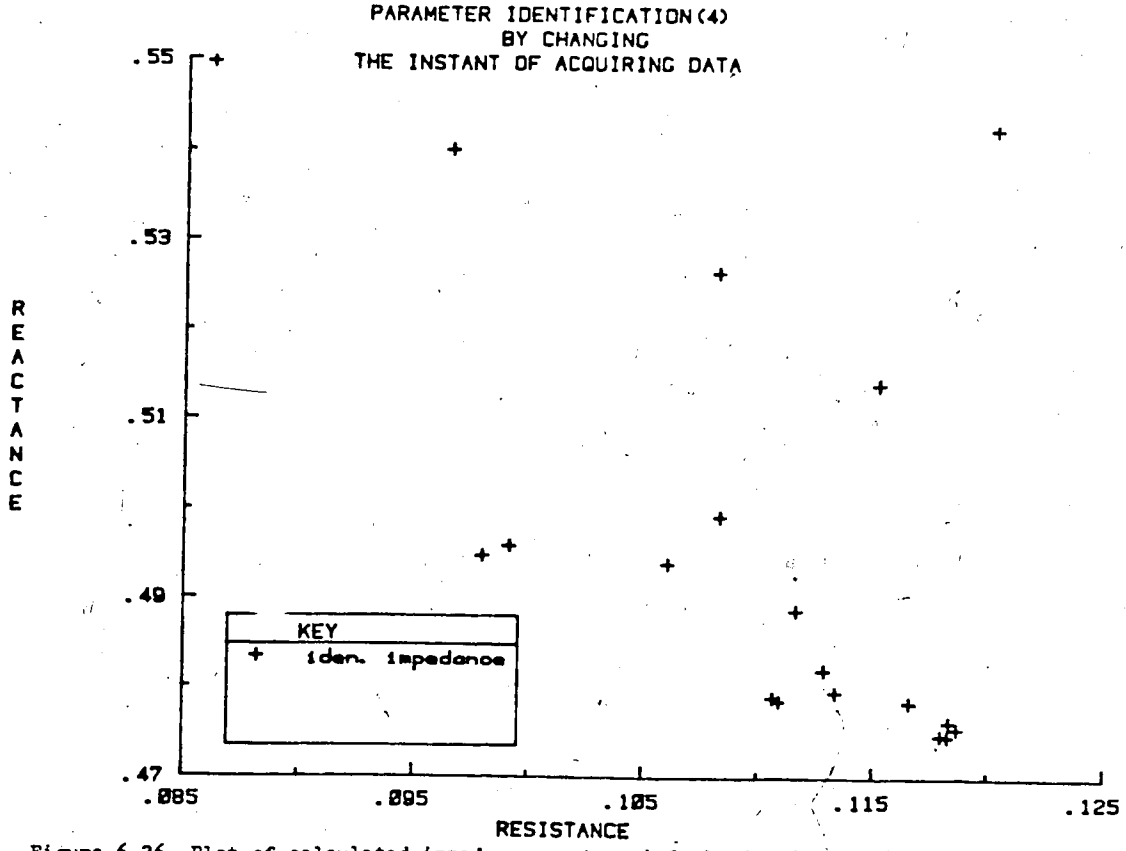

Figure 6.26 Plot of calculated impedances - two pi faulted model and 4th order filter.

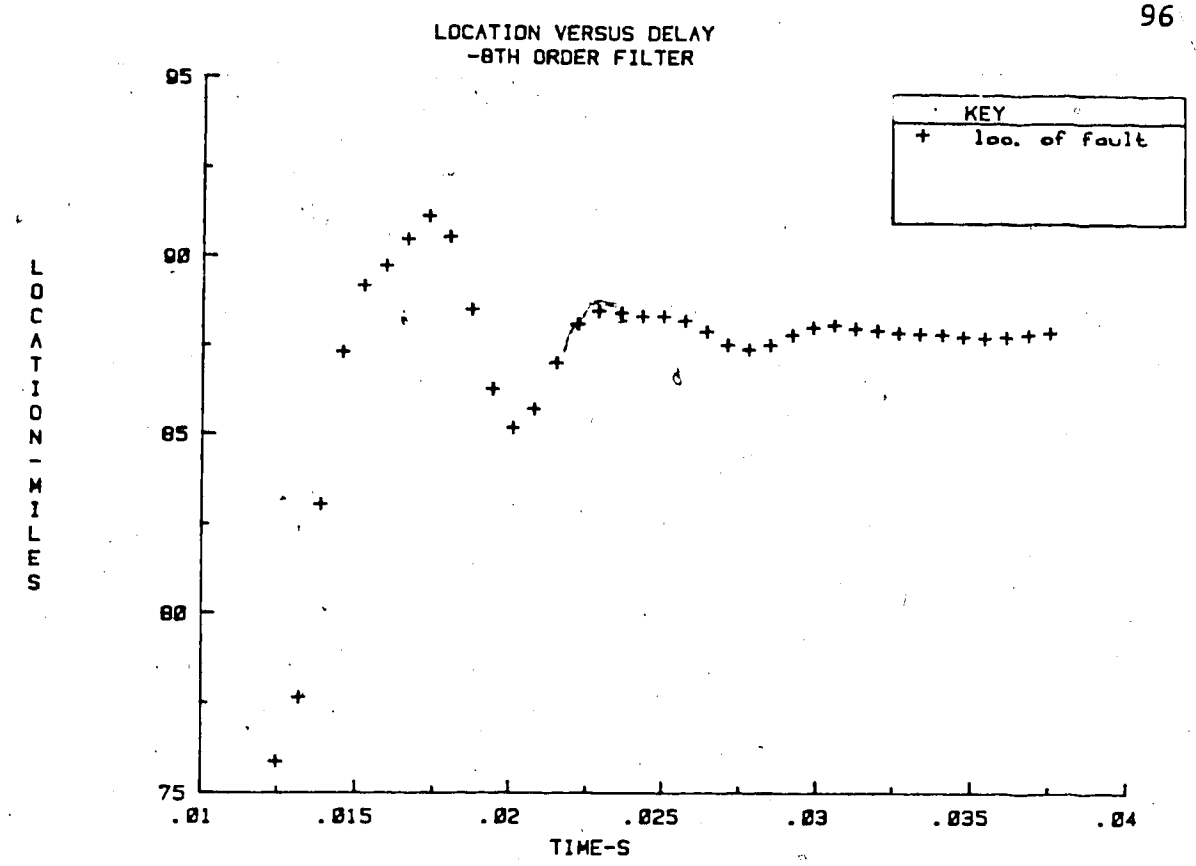

Figure 6.27 Plot of fault location versus delay - two pi faulted model and 8th order filter.

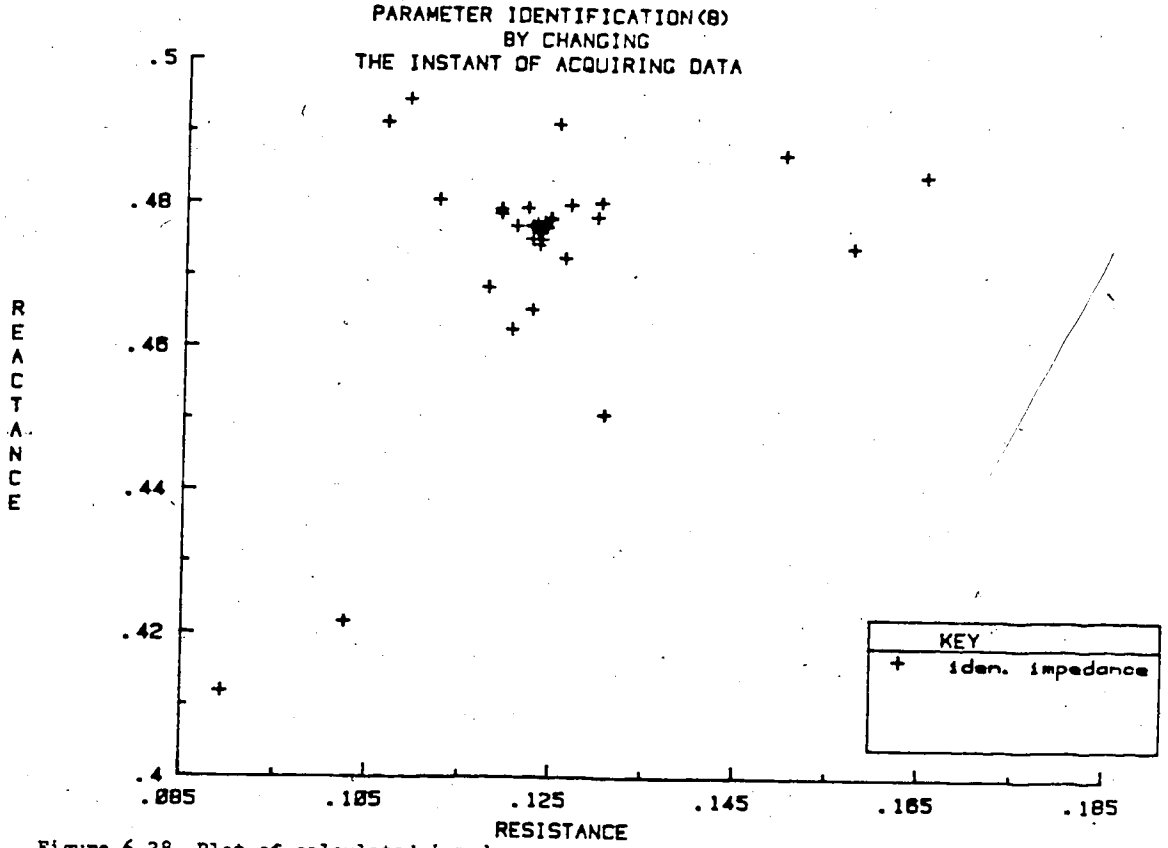

Figure 6.28 Plot of calculated impedances - two pi faulted model and 8th order filter.

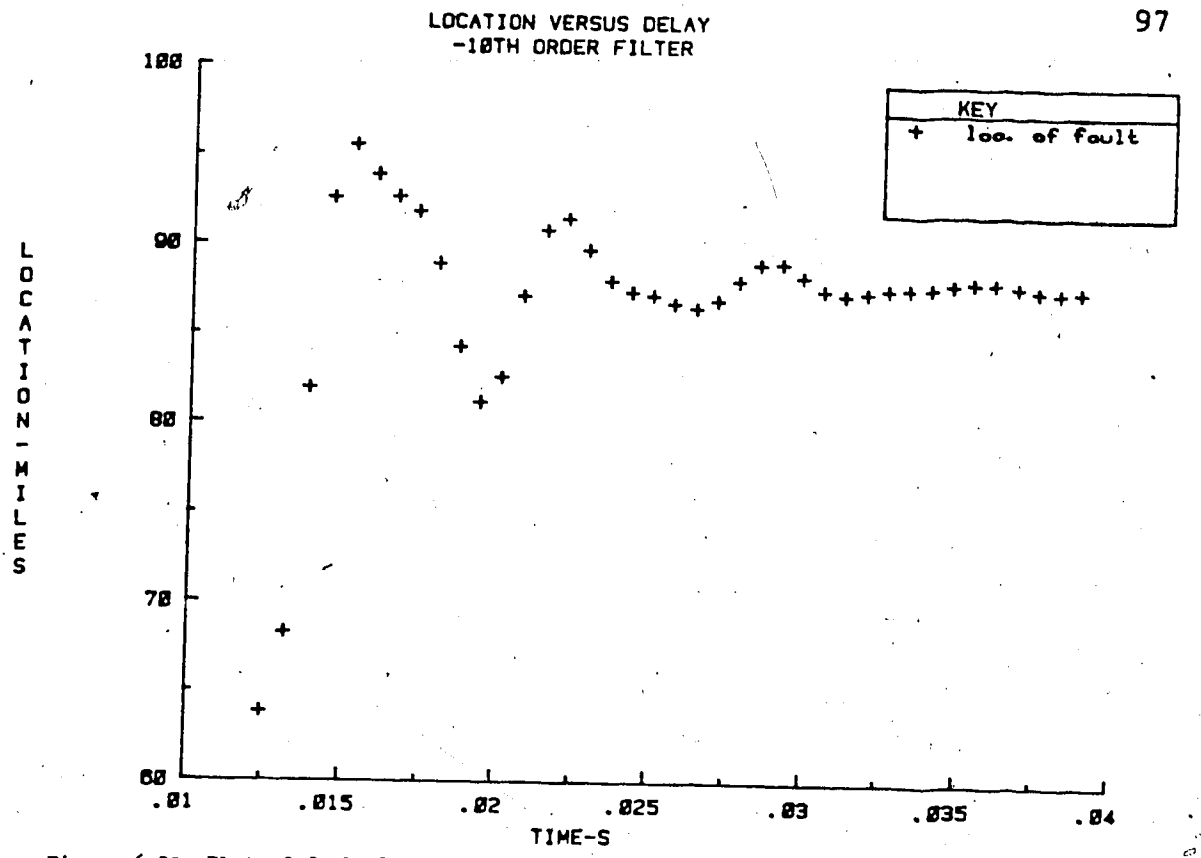

Figure 6.29 Plot of fault location versus delay - two pi faulted model and 10th order filter.

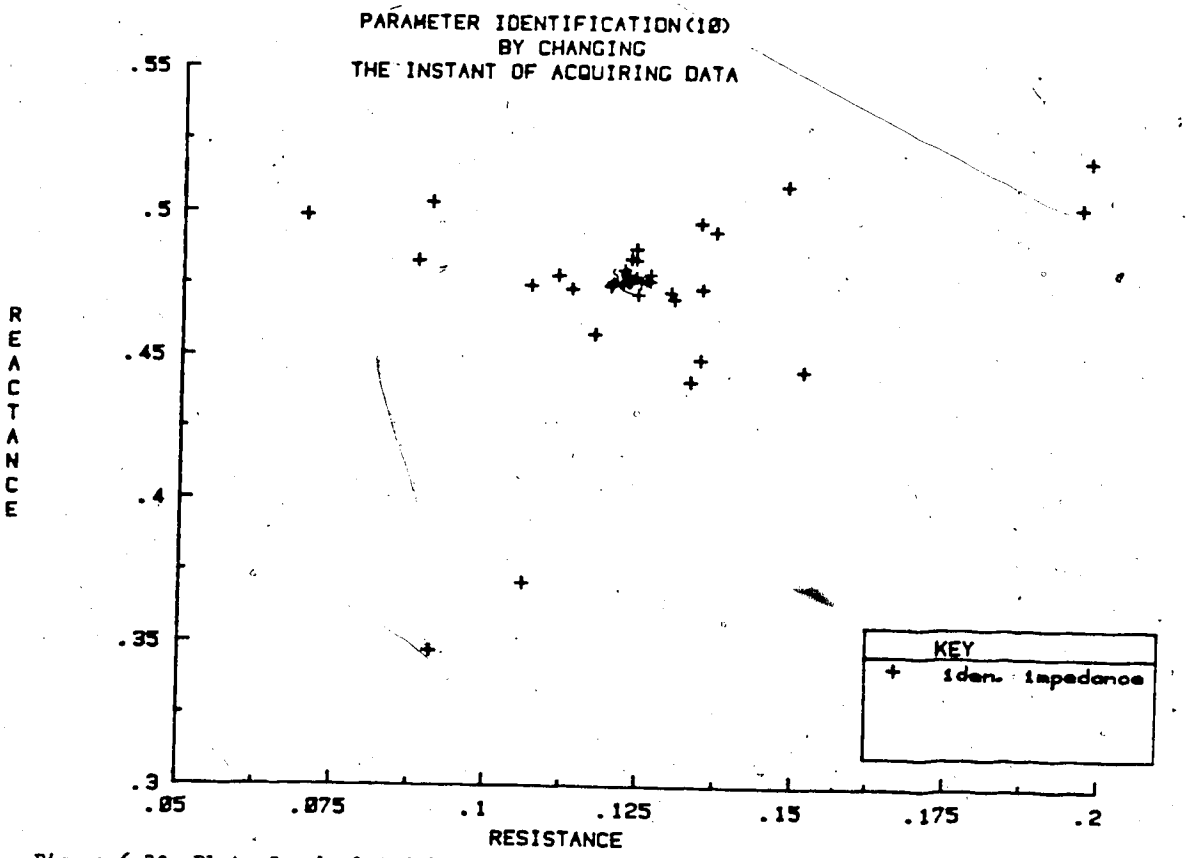

Figure 6.30 Plot of calculated impedances - two pi faulted model and 10th order filter.

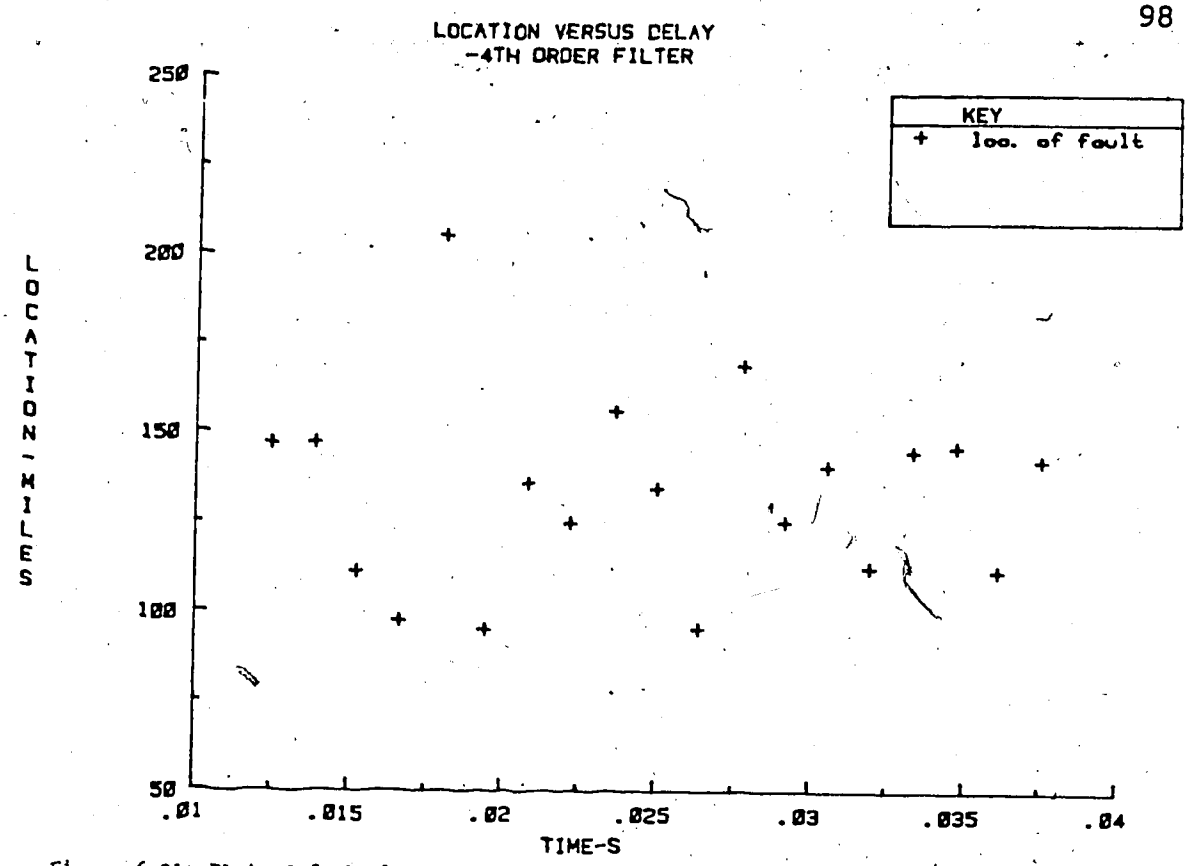

Figure 6.31 Plot of fault location versus delay - three pi faulted model and 4th order filter.

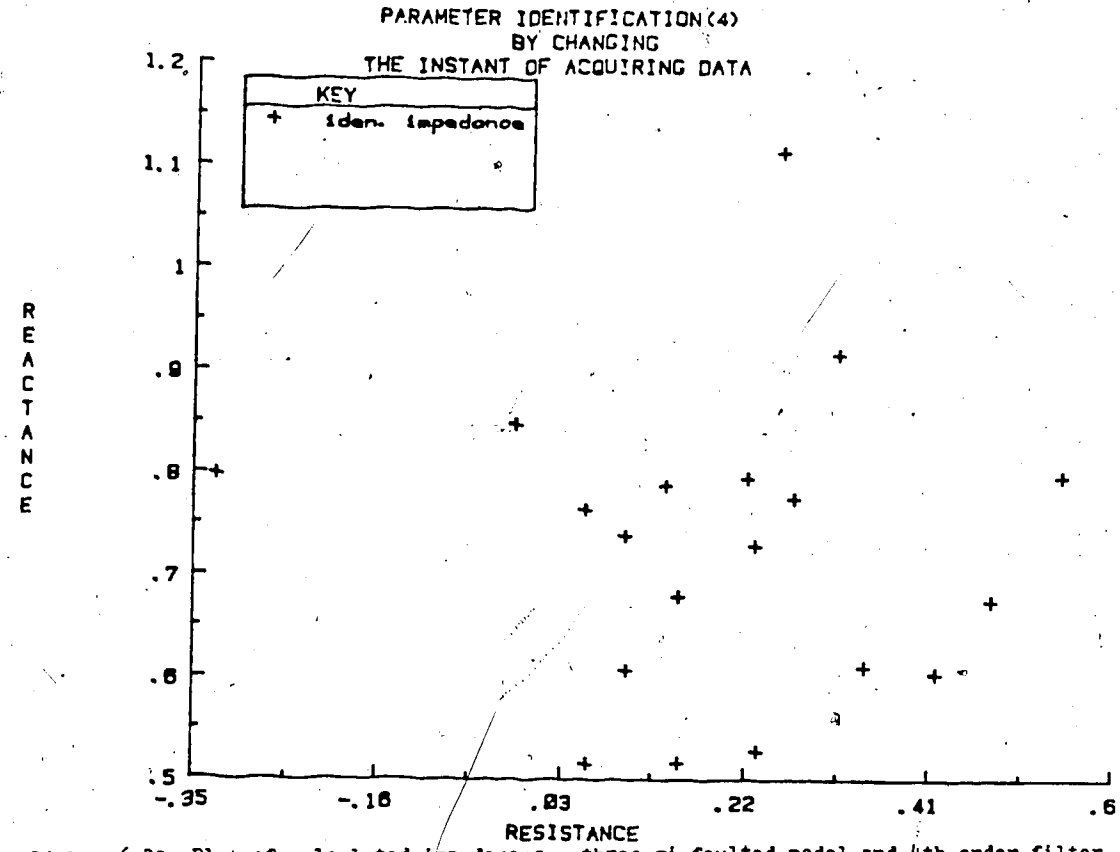

Figure 6.32 Plot of calculated impedances - three pi faulted model and 4th order filter.

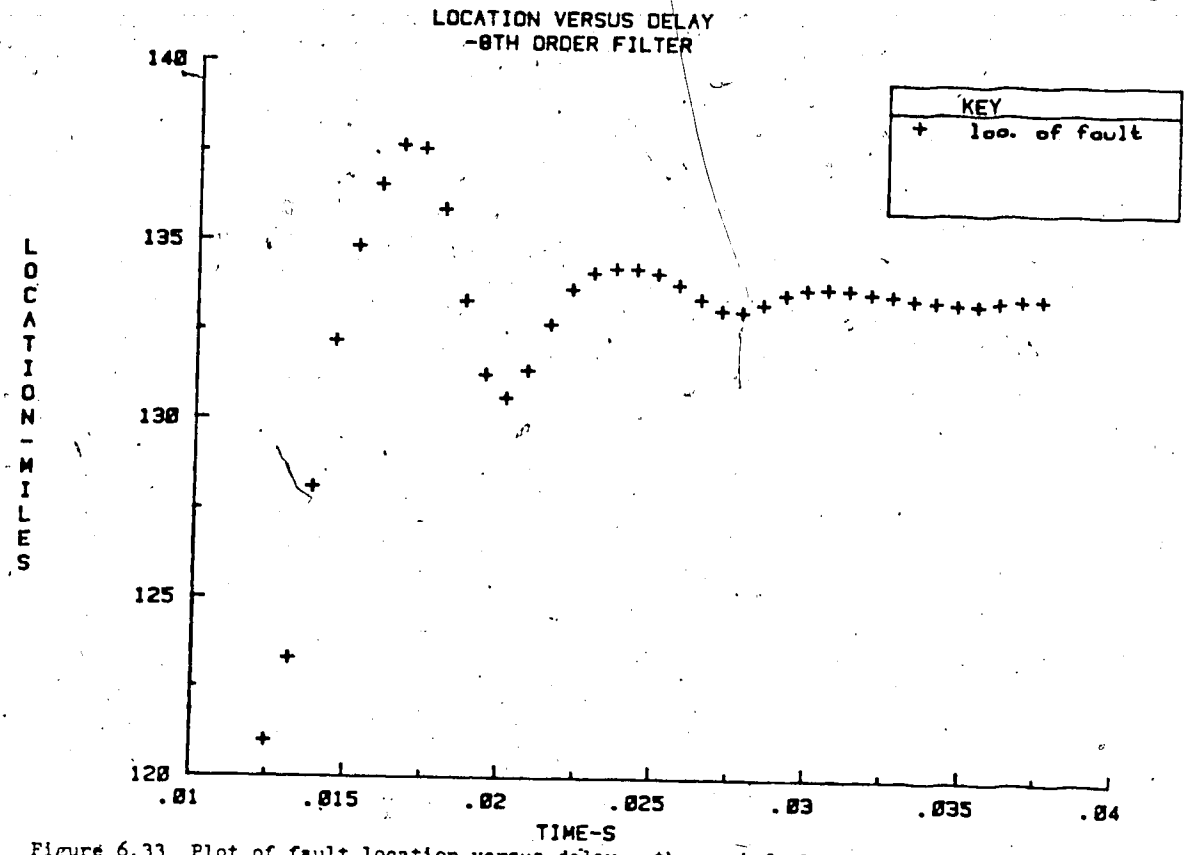

Figure 6.33 Plot of fault location versus delay - three pi faulted model and 8th order filter.

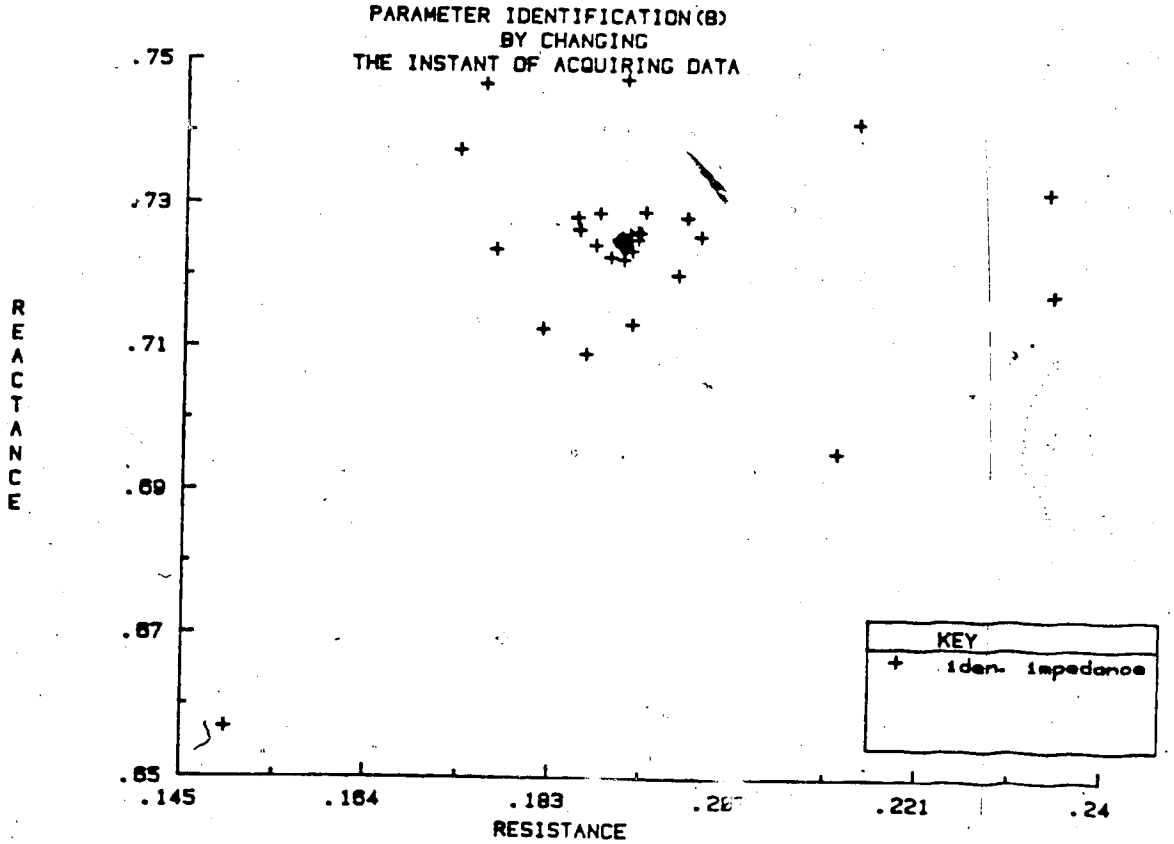

Figure 6.34 Plot of calculated impedances - three pi faulted model and 8th order filter.

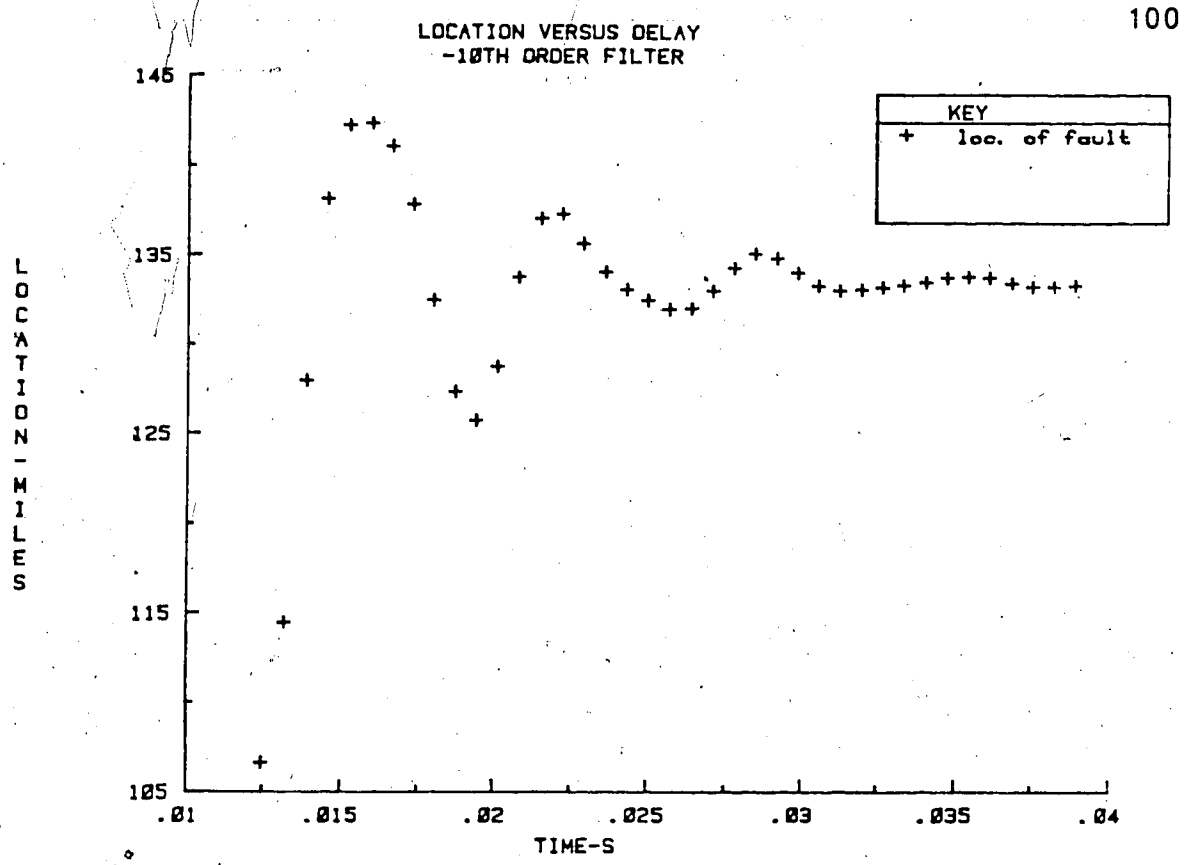

Figure 6.35 Plot of fault location versus delay - three pi faulted model and 10th order filter.

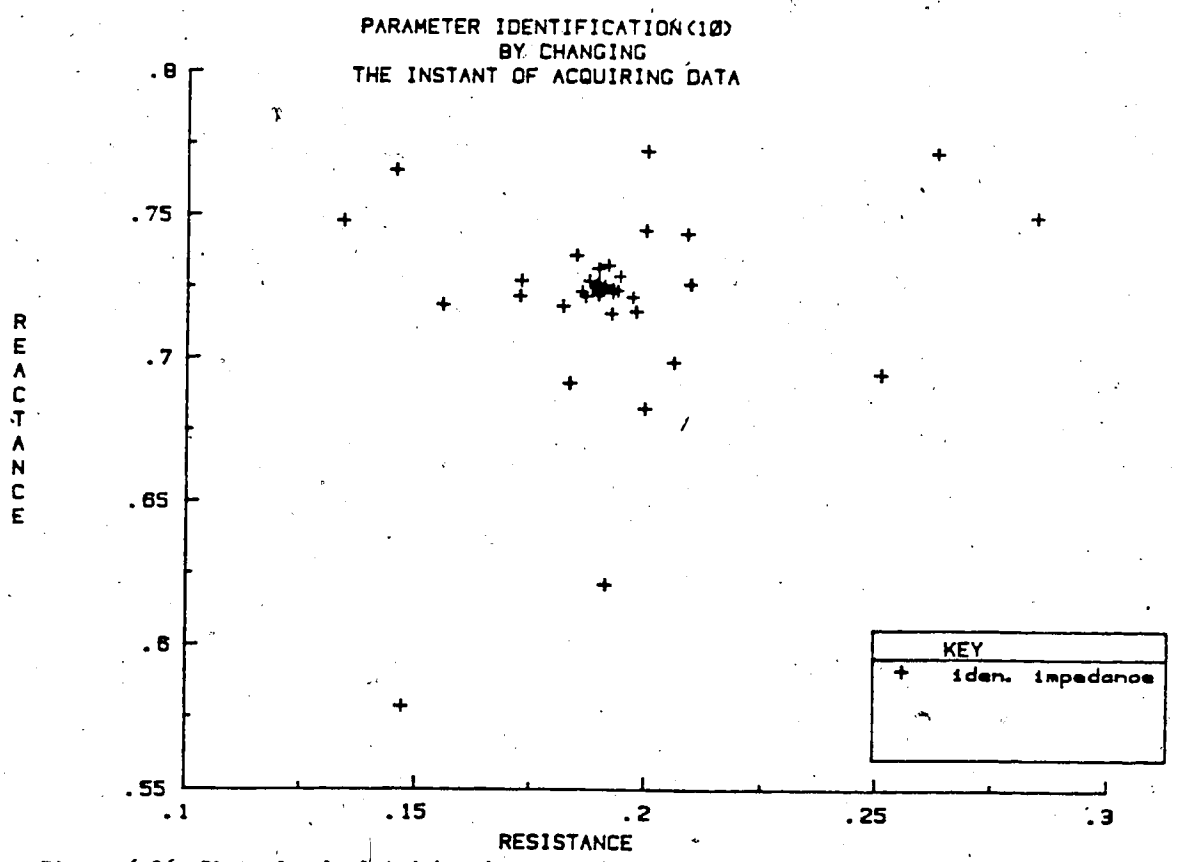

Figure 6.36 Plot of calculated impedances - three pi faulted model and 10th order filter.

filter, and these unwanted components cause an aliasing effect on the digitized signals since the sampling rate of the digital filter is only 720 Hz.

In order to study the error introduced by the presence of fault resistance, the algorithm is applied to a line subject to non-zero resistance ground fault occurring at a location 44.5 miles from the sending terminal. The resistances used are 0.063, 0.126 and 0.189 pu respectively. Figure 6.37 gives the plots of location versus delay for the three different values of fault resistance. The plots are all based on employing an 8th order filter to suppress undesired harmonics. The three curves converge to three different values which are quite close to the true fault location (44.5 miles) as shown in Figure 6.37. Accuracy in locating a fault is higher if the fault involves a smaller resistance. This effect is illustrated by the three graphs (Figure 6.37).

6.4 Conclusion and General Discussion

The performance of the proposed fault location algorithm has been studied in this chapter. From these tests, it can be concluded that the algorithm is able to locate faults with very good accuracy even in the presence of fault resistance and line shunt capacitance. The low-pass filter, which is required by the algorithm to eliminate high undesirable harmonics, causes a time delay in

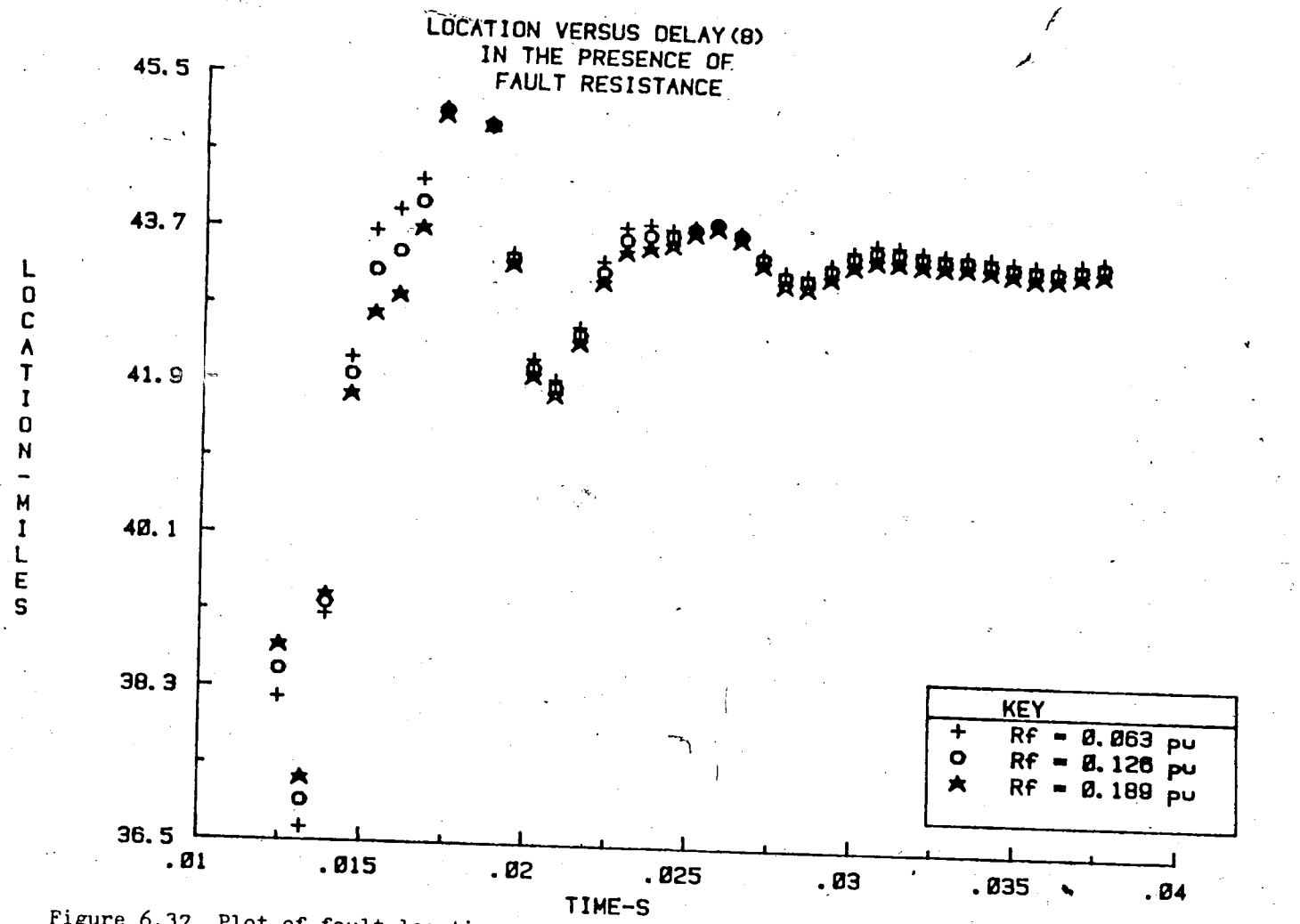

Figure 6.37 Plot of fault location versus delay in the presence of different fault resistance - one pi faulted model and 8th order filter.

locating fault. This delay has to be minimized in order to increase the availability of power transfer. A low order filter is suitable in shortening delay times but the accuracy in fault location is not as high compared to situations where a higher order filter is used. As a result, the choice of filter is a compromise between speed and accuracy. Since all tests are based on data obtained from digitally simulated simple models, it is always desirable to test the algorithm utilizing off-line field data.

One possible future project is to evaluate the performance of the proposed algorithm for on-line applications. The microcomputer system, which is available in the Power Research Laboratory, is well suited for this purpose. The system consists of an LSI 11/2 microprocessor with a lot of useful built-in components designed for on-line and real-time applications. This complete system is known as SNORKEL[28]. The programs, which are outlined in Chapter 5, can be easily modified in order to be executed in the SNORKEL environment for on-line testing. The modified programs together with the SNORKEL system can result in a useful on-line fault locating tool.

CHAPTER VII

Summary and Conclusion

A fast and accurate location of faults for power transmission lines is essential to minimize the down-time of an electrical power system. The availability and security of the system is increased and maintenance costs associated with locating faults by manual methods are reduced. A short-circuit fault location can be determined either by manual, visual inspection or by making electrical measurements from some monitoring points on the lines. It has been shown that in terms of speed, the latter method is more favorable than the former. This is especially true if the lines are long and run through inaccessible areas. The latter approach is gaining acceptance due to the advantages offered by recent progress in both the analog and digital technologies. The cost and flexibility of microprocessor-based monitors are factors influencing the acceptance of automated fault location.

The method of using electrical measurements in locating faults involves either the modelling of transmission lines using wave equations or by lumped-parameter representation. The wave theory describes a complex phenomenon and is difficult to analyse even with the aid of digital computer. Among the various fault location approaches based on lumped-parameter representation, it has been shown that the one which employs the calculation of complex impedance is

the least complex in terms of computational burden. No iterations are required by this method and thus it is well-suited for on-line applications. However, one of the common drawbacks of this algorithm is that it ignores the fault resistance, decaying dc components present in the transients, line shunt capacitance or any combination of these factors. These factors all contribute to the loss of accuracy in the final fault distance measurements.

An impedance calculating algorithm, proposed by Sachdev and Baribeau, is a promising one which is readily implemented into a computer program. In this algorithm, the current and voltage phasors are obtained using curve fitting technique. From these phasors, the impedance seen in the direction of fault from the sending terminal of the faulted line is calculated. Hence, the location of the fault is determined by assuming that the line reactance is proportional to line length. One of the special features of this algorithm is that the decaying dc component has been taken into consideration during the development of the algorithm. The effect of fault resistance on the fault distance determination is minimized due to the fact that the fault is located on the basis of reactance ratio.

Mathematical considerations have shown that the fault locating problem can be formulated into a rectangular matrix form by suitable choices of data window and sampling rate. The problem is then solved by a least error squares curve

fitting technique in which the pseudoinverse of the resulting matrix provides the solution.

Mathematical models of two simple test systems working under both normal and faulty conditions have been derived in this project. These models are essential in supplying both pre-fault and post-fault data to test the fault location algorithm. In addition to this, low-pass digital filters, which suppress undesirable high frequency components and noise, have been developed. These filters are necessary for the evaluation of the performance of the algorithm.

Computer programs were developed to implement the proposed fault location algorithm in an off-line mode. It has been demonstrated in this thesis that the proposed algorithm satisfactorily locates faults for the simulated transmission lines. The performance of the algorithm is acceptable even in the presence of fault resistance and line shunt capacitance. However, the algorithm loses its accuracy if the post-fault load current cannot be neglected. Further studies on the proposed fault location algorithm using both off-line and on-line field data are necessary with particular attention placed on testing the algorithm subject to different fault types.

References

[1] C.A.Gross, "Power System Analysis", John Wiley & Sons, New York, 1979.

[2] T.W.Stringfield, D.J.Marihart and R.F.Stevens, "Fault Location Methods for Overhead Lines", AIEE Transactions, Vol.76, August 1957, pp.518-529.

[3] M.Vitins, "A Correlation Method for Transmission Line Protection", IEEE Transactions on Power Apparatus and Systems, Vol.PAS-97, No.5, Sept./Oct. 1978, pp.1607-1615.

[4] J.Kohlas, "Estimation of Fault Locations on Power Lines", Proceedings of the third IFAC Symposium, the Hague/Delft, the Netherlands, 12-15 June 1973, pp.393-402.

[5] G.G.Richards and O.T.Tan, "An Accurate Fault Location Estimator for Transmission Lines", IEEE Transactions on Power Apparatus and Systems, Vol.PAS-101, No.4, April 1982, pp.945-949.

[6] M.S.Sachdev and M.A.Baribeau, "A New Algorithm for Digital Impedance Relays", IEEE Transactions on Power Apparatus and Systems, Vol.PAS-98, No.6, Nov./Dec. 1979, pp.2232-2238.

[7] G.Ziegler, "Fault Location in H.V. Power Systems", IFAC Symposium on Automatic Control in Power Generation, Distribution and Protection, 15-19 Sept. 1980, pp.121-129.

[8] M.T.Sant and Y.G.Paithankar, "Online Digital Fault Locator for Overhead Transmission Line", Proc. IEE, Vol.126, No.11, Nov. 1979, pp.1181-1185.

[9] W.D.Stevenson,Jr., "Elements of Power System Analysis", Fourth Edition, McGraw-Hill Book Company, New York, 1982.

[10] S.E.Westlin and J.A.Bubenko, "Newton-Raphson Technique Applied to the Fault Location", Paper No.A 76 334-3, IEEE PES Summer Meeting, Portland, 18-23 July 1976.

[11] T.Takagi, Y.Yamakoshi, J.Baba, K.Uemura and T.Sakaguchi, "A New Algorithm of an Accurate Fault Location for EHV/UHV Transmission Lines : Part I Fourier Transformation Method", IEEE Transactions on Power Apparatus and Systems, Vol.PAS-100, No.3, March 1981, pp.1316-1322.

[12] G.G.Richards and O.T.Tan, "Fault Location for Transmission Lines with Current-Transformer Saturation", IEE Proc., Vol.130, Pt.C, No.1, January 1983, pp.22-27.

[13] B.J.Mann and I.F.Morrison, "Digital Calculation of Impedance for Transmission Line Protection", IEEE Transactions on Power Apparatus and Systems, Vol.PAS-90, No.1, Jan./Feb. 1971, pp.270-276.

[14] G.B.Gilcrest, G.D.Rockefeller and E.A.Urden, "High-Speed Distance Relaying Using a Digital Computer : 1-System Description and 2-Test Results", IEEE Transactions on Power Apparatus and Systems, Vol.PAS-91, No.3, May/June 1972, pp.1235-1252.

[15] A.G.Phadka, T.Hlibka and M.Ibrahim, " Digital Computer System for EHV Substation; Analysis and Field Tests", IEEE Transactions on Power Apparatus and Systems, Vol.PAS-95, No.1, Jan./Feb. 1976, pp.291-301.

[16] W.D.Breingan, M.M.Chen and T.F.Gallen, "The Laboratory Investigation of a Digital System for the Protection of Transmission Lines", IEEE Transactions on Power Apparatus and Systems, Vol.PAS-98, No.2, March/April 1979, pp.350-358.

[17] S.J.Leon, "Linear algebra with applications", Macmillan Publishing Company, Inc., New York, 1980.

[18] A.S.Deif, "Advanced Matrix Theory for Scientists and Engineers", Abacus Press, Kent, 1982.

[19] D.Beeman, "Industrial Power Systems Handbook", McGraw-Hill Book Company, New York, 1955.

[20] J.Zaborszky and J.W.Rittenhouse, "Electric Power Transmission", The Ronald Press Company, New York, 1954.

[21] E.A.Robinson and M.T.Silvia, "Digital Signal Processing and Time Series Analysis", Holden-Day, Inc., San Francisco, 1980.

[22] R.E.Bogner and A.G.Constantinides, "Introduction to Digital Filtering", John Wiley and Sons, London, 1975.

[23] A.Antoniou, "Digital Filters : Analysis and Design", McGraw-Hill Book Company, New York, 1979.

[24] E.B.Davison and A.Wright, "Some Factors affecting the Accuracy of Distance-Type Protective Equipment under Earth-Fault Conditions", Proc. IEE, Vol.110, No.9, Sept 1963, pp.1678-1688.

[25] B.W.Kernighan and D.M.Ritchie, "The C Programming Language", Prentice-Hall, Inc., Englewood Cliffs, New Jersey, 1978.

[26] "Unix Programmer's Manual", Seventh Edition, Bell Laboratories, Murray Hill, New Jersey, 1979.

[27] S.R.Bourne, "The Unix System", Addison-Wesley Publishing Company, London, 1983.

[28] "LSI-11 Software Development System Documentation", Advanced Digital Engineering Corporation, Saskatoon, 1981.

Appendix A

Power System Parameters

Data for the system given in Figure 4.1 is outlined in this appendix. This data is given in References 19 and 20, and is given here for ease of reference.

(i) Generator G1:

105 MW capacity at 0.9 pf, rated at 22 KV

18.1 percent reactance on 105/0.9 MVA

(ii) Short-circuiting limiting reactor:

X1 = 0.237 Ω

(iii) Transformer T1:

Transformation ratio 142/22

Load carrying capacity of 60 MVA

8.2 percent reactance on 60 MVA base at 142 KV tap setting

(iv) Transmission line li1:

30 mile-long overhead aluminium-cable-steel-reinforced conductor

Series resistance of 0.5438 Ω/mile

Series reactance of 0.5650 Ω/mile

(v) Transformer T2:

Transformation ratio 126/33

Load carrying capacity of 20 MVA

11 percent reactance on 20 MVA base at 126 KV tap

setting

(vi) Transmission line li2:

5 mile-long overhead copper conductor line

Total series resistance of 1.5 Ω

Total series reactance of 3.3 Ω

(vii) Load L1:

Real power of 15 MW

Reactive power of 8 MVA

Terminal voltage of 31.5 KV

Appendix B

Synthesizing Digital Filters

Three low-pass recursive digital filters were designed and employed in the testing of the proposed fault location algorithm. The design specifications for the filters are given in Section 4.3. The design of the recursive filters are based on the "direct" method outlined in Reference 22. The synthesis technique for each filter that was used in this project is briefly outlined in this appendix.

B.1 4th order filter

The cutoff (fc), transition (f1) and sampling (fs) frequencies of the filter are all given in the design specifications. Hence, the sampling interval is given by:

$$T = \frac{1}{fs}$$

$$= \frac{1}{720} \text{ s}$$

and,

$$\tan\left(\frac{\omega_1 T}{2}\right) = \tan\left(\frac{285 \times 2\pi}{2 \times 720}\right)$$

$$= \tan\left(\frac{285\pi}{720}\right)$$

$$= 2.945905$$

and,

$$\tan\left(\frac{\omega_c T}{2}\right) = \tan\left(\frac{205\pi}{720}\right)$$

$$= 1.223939$$

At the transition frequency, the following equation is

obtained by considering the amplitude characteristic:

$$\log\left[1 + \left(\frac{\tan\left(\frac{\omega_1 T}{2}\right)}{\tan\left(\frac{\omega_c T}{2}\right)}\right)^{2n}\right] = 30$$

i.e.

$$2n = \frac{2.999565}{\log\left(\frac{2.945905}{1.223939}\right)}$$

i.e.

$$n = 3.9317 \simeq 4$$

where n is the order of the required filter.

Using the calculated value of $\tan(\omega_c T/2)$, it can be shown that the poles, which lie on the z^{-1}-plane, have the following x and y coordinates:

x	y
-0.104637	±0.196817
-0.144995	±0.658432
-0.318989	±1.448533
-2.105975	±3.961229

It is noted that four poles lie inside the unit circle of the z^{-1}-plane and the other four lie outside the unit circle. Therefore, the four poles which yield a stable function are:

$$-0.318989 \pm j1.448533$$

and

$$-2.105975 \pm j3.961229$$

The corresponding polynomial due to the stable poles is given by:

$$A(z^{-1}) = (z^{-1} + 0.31899 + j1.44853)(z^{-1} + 0.31899 - j1.44853)$$
$$\times (z^{-1} + 2.10598 + j3.96123)(z^{-1} + 2.10598 - j3.96123)$$
$$= (z^{-2} + 0.6380z^{-1} + 2.20)(z^{-2} + 4.2120z^{-1} + 20.1265)$$

Thus, the required transfer function is:

$$G(z^{-1}) = K\frac{(1 + z^{-1})^4}{A(z^{-1})}$$

where K is a gain constant and is given by:

$$1 = K\frac{2^4}{(3.83798)(25.33842)}$$

i.e. $$K = 6.07802$$

B.2 8th order filter

The sampling interval T is given by:

$$T = \frac{1}{fs}$$
$$= \frac{1}{1440}\ s$$

and,
$$\tan\left(\frac{\omega_1 T}{2}\right) = \tan\left(\frac{295\pi}{1440}\right)$$
$$= 0.75014$$

and,
$$\tan\left(\frac{\omega_c T}{2}\right) = \tan\left(\frac{200\pi}{1440}\right)$$
$$= 0.46631$$

n is obtained from,

$$2n = \frac{2.999565}{\log\left(\frac{0.75014}{0.46631}\right)}$$

i.e. $$n = 7.26 \simeq 8$$

Using the calculated value of $\tan(\omega_c T/2)$, it can be shown that the x and y coordinates of the poles which lie on the z^{-1}-plane are:

x	y
0.367027	±0.085336
0.392673	±0.259994
0.450890	±0.446794
0.559212	±0.653643
0.755727	±0.883342
1.119040	±1.108873
1.770487	±1.172254
2.584865	±0.600985

The eight poles which yield a stable function are:

$$0.755727 \pm j0.883342$$
$$1.119040 \pm j1.108873$$
$$1.770487 \pm j1.172254$$
$$2.584865 \pm j0.600985$$

Therefore, the polynomial in terms of z^{-1} which corresponds to the stable poles is:

$$A(z^{-1}) = (z^{-2} - 1.5115z^{-1} + 1.3542)(z^{-2} - 2.2381z^{-1} + 2.4819)$$
$$\times (z^{-2} - 3.5410z^{-1} + 4.5088)(z^{-2} - 5.1697z^{-1} + 7.0427)$$

Hence, the required transfer function is given by:

$$G(z^{-1}) = K\frac{(1 + z^{-1})^8}{A(z^{-1})}$$

where K is calculated from:

$$1 = K\frac{2^8}{(0.83996)(1.24377)(1.96783)(2.87298)}$$

i.e. $K = 0.02307$

B.3 10th order filter

From the design specifications, the sampling interval is given by:

$$T = \frac{1}{fs}$$

$$= \frac{1}{1440}\,s$$

and,

$$\tan\left(\frac{\omega_1 T}{2}\right) = \tan\left(\frac{290\pi}{1440}\right)$$

$$= 0.73323$$

and,

$$\tan\left(\frac{\omega_c T}{2}\right) = \tan\left(\frac{218\pi}{1440}\right)$$

$$= 0.51503$$

Hence, n is calculated from:

$$2n = \frac{2.999565}{\log\left(\frac{0.73323}{0.51503}\right)}$$

i.e. $n = 9.78 \simeq 10$

Using the calculated value of $\tan(\omega_c T/2)$, x and y coordinates of the poles are shown to be:

x	y
0.321884	±0.070592
0.336568	±0.214214
0.368548	±0.365347
0.423998	±0.529629
0.515107	±0.713253
0.665457	±0.921438
0.921173	±1.150664
1.368509	±1.356622
2.114579	±1.345853
2.964173	±0.650062

The ten poles which yield a stable transfer function are:

$0.665457 \pm j0.921432$

$0.921173 \pm j1.150664$

$1.368509 \pm j1.356622$

$2.114579 \pm j1.345853$

$2.964173 \pm j0.650062$

Therefore, the corresponding polynomial due to the stable poles is given by;

$$A(z^{-1}) = (z^{-2} - 1.3309z^{-1} + 1.2919)(z^{-2} - 1.8423z^{-1} + 2.1726) \times (z^{-2} - 2.7370z^{-1} + 3.7132)(z^{-2} - 4.2292z^{-1} + 6.2828) \times (z^{-2} - 5.9283z^{-1} + 9.2087)$$

Hence, the required transfer function is:

$$G(z^{-1}) = K\frac{(1 + z^{-1})^{10}}{A(z^{-1})}$$

where K is given by:

$$1 = K\frac{2^{10}}{(0.96097)(1.33024)(1.97622)(3.05361)(4.28042)}$$

i.e. $K = 0.032246$